ACIDIZING HIGH-TEMPERATURE CARBONATE FORMATIONS USING METHANESULFONIC ACID

A Dissertation

by

ALEXIS ORTEGA

Submitted to the Office of Graduate and Professional Studies of
Texas A&M University
in partial fulfillment of the requirements for the degree of

DOCTOR OF PHILOSOPHY

Chair of Committee,	Hisham A.Nasr-El-Din
Committee Members,	Stephen A. Holditch
	Jerome Schubert
	Mahmoud El-Halwagi
Head of Department,	A. Daniel Hill

May 2015

Major Subject: Petroleum Engineering

ABSTRACT

Hydrochloric acid (HCl) is the most commonly used stimulation fluid for high-temperature wells drilled in carbonate reservoirs due to its high dissolving power and low cost. However, the high corrosion rate of HCl on well tubulars could make its use in deep wells non-viable. The current study introduces the novel application of methanesulfonic acid (MSA), a strong organic acid, to increase the permeability of carbonate formations, specifically at temperatures above 200°F. The objective of the experimental study is to evaluate the performance of MSA as stand-alone stimulation fluid for high-temperature limestone and dolomite formations.

Coreflood studies were conducted at temperature up to 320°F using limestone and dolomite cores and diluted MSA aqueous solutions. A constant injection rate, ranging from 1 to 25 cm^3/min, was maintained during the coreflood tests and the differential pressure through the core was measured until acid breakthrough. Samples of the effluent fluids were collected and analyzed using Inductively Coupled Plasma (ICP) to measure the calcium and magnesium concentrations, and a computed tomography (CT) scan of each core was performed after the acid injection to study the characteristics of the generated wormholes.

MSA was found effective in creating wormholes in carbonate cores at the temperatures tested. At low injection rates, face dissolution and conical channels were observed in the cores. At intermediate injection rates, the tendency was to create a few dominant wormholes. At high injection rates, ramified wormhole structures were found,

with increased branching for increased flow rates. For each condition tested, an optimum flow rate was identified. Additionally, analysis of the coreflood effluent samples showed no sign of methanesulfonate salts precipitation.

Demonstration of the effectiveness of MSA in propagating wormholes in carbonate cores will offer the petroleum industry with another alternative strong acid to HCl for stimulating high-temperature carbonate formations. MSA's high acidity, solubility of its salts, and thermal stability, along with its readily biodegradable composition provide a beneficial use for MSA as a stimulation fluid in carbonate acidizing techniques. MSA also has a more favorable corrosion profile on metals, such as high chromium alloys, than usual mineral acids employed in well stimulation.

DEDICATION

To **God** who has given me **WISDOM** to achieve this goal.

To my wife, **Sindy**, and daughters, **Isabella** and **Alexa**, who have given me great **JOY** through this journey.

To my mother, **Jasmin**, and sisters, **Tatiana** and **Stephanie**, who have given me **HOPE** to overcome adversity.

To my grandmother, **Margarita**, who has given me a vivid example of the power of **FAITH**.

ACKNOWLEDGEMENTS

I would like to thank my committee chair, Dr. Nasr-El-Din, and my committee members, Dr. Holditch, Dr. Schubert, and Dr. El-Halwagi, for their direction and advice during the development of this research.

Thanks to BASF for funding this project. I want especially to extend my deepest gratitude to Dr. Shawn Rimassa for her continuous support and coaching throughout the course of this study.

TABLE OF CONTENTS

Page

LIST OF FIGURES

Page

LIST OF TABLES

Page

CHAPTER I

INTRODUCTION*

Literature Review

Carbonate matrix acidizing is a technique in which an acidic solution is injected into a carbonate formation (limestone or dolomite) at a pressure less than the pressure at which a fracture can be opened. The goal of carbonate acidizing is to dissolve some of the formation minerals present to increase the apparent permeability in the near-wellbore region (Hill and Schechter 2000). In carbonates, mass transfer often limits the overall reaction rate leading to highly non-uniform dissolution patterns. Often, a few large channels, called wormholes, are created. This wormholing process makes it possible to stimulate to a sufficient radial penetration that even treating undamaged wells can be beneficial. Furthermore, a prediction of the effect of acidizing on the skin effect is possible if the depth of penetration of wormholes in dolomite rock can be described (Hill et al. 2012).

Carbonate rocks, by definition, contain more than 50% carbonate minerals (Robert and Crowe 2000). Reservoir carbonate rock composition is almost only calcite (limestone, $CaCO_3$) or dolomite (dolostone, $CaMg(CO_3)_2$) or a mixture of the two minerals. Those rocks, together, constitute about 90% of all naturally occurring

*Part of this chapter is reprinted with permission from "Acidizing High Temperature Carbonate Reservoirs Using Methanesulfonic Acid: A Coreflood Study" by A. Ortega, H.A. Nasr-El-Din and S. Rimassa, 2014. 2014 AADE Fluids Technical Conference and Exhibition, AADE-14-FTCE-3, Copyright 2014 by AADE.

carbonates (Reeder 1983). Carbonate rocks are typically classified by the calcite/dolomite ratio, and those with a ratio lower than 50% are generally known as the rock dolomite (Schechter 1992). Carbonate rocks present singular characteristics that distinguish them from siliciclastic (Ham and Pray 1962), for example: (1) carbonates form locally, within the basin of deposition; (2) carbonates are almost exclusively composed of biological constituents; and (3) carbonates are highly susceptible to diagenesis. As a result, carbonate pore systems are usually heterogeneous and may feature attributes such as double porosity or high permeability contrasts. Moreover, in carbonates, measured porosity values do not always correlate with permeability because of the dependence of these rock properties on a collection of diagenetic episodes, and on stress-field related fracture patterns (Ahr 2008). However, in general, dolostones are known to be more permeable reservoir rocks than limestones with the same porosity (Wardlaw 1979).

Hydrochloric acid (HCl) is generally employed in carbonate acidizing because it reacts promptly with carbonate minerals producing soluble reaction products, and is available in large quantities at a moderate cost. The main disadvantage of HCl is its high corrosivity on wellbore tubular goods, especially at temperatures above 250°F (Williams et al. 1979). Another limitation of the use of HCl is its negative environmental impact. HCl is toxic to aquatic life by lowering the pH and is not expected to biodegrade when it is released into the soil.

There are numerous problems associated with the high corrosion rate of HCl at high temperatures. First, well tubulars are often made of low-carbon steel, but in certain

applications the well completion may include aluminum- or chromium-plated components (i.e., 13% chromium tubulars suitable for applications involving CO_2 rich environments) that become easily damaged upon contact with HCl solutions (Nasr-El-Din et al. 2003). In addition, HCl will dissolve any rust present in the tubulars and produce great quantities of iron (Fe^{+3}), which will precipitate as $Fe(OH)_3$ (Crowe 1985; Taylor et al. 1999) or, if H_2S is present, as iron sulfide (Nasr-El-Din et al. 2002), potentially causing formation damage.

Various additives, such as corrosion inhibitors and inhibitor aids, are used to reduce corrosion by HCl at high temperatures. The cost of these additives, however, may result in the treatment being uneconomical (Fredd 1997). Also, the use of corrosion inhibitors in high concentrations may result in undesired wettability changes of the formation as the inhibitor may adsorb on the rock surface (Schechter 1992). These drawbacks make organic acids attractive for stimulating high-temperature wells.

Organic acids are typically used as an alternative to HCl in high-temperature formations (Chatelain et al. 1976; Van Domelen and Jennings 1995; Fredd and Fogler 1998a; Huang et al. 2000; Nasr-El-Din et al. 2001; Al-Katheeri et al. 2002; Buijse et al. 2004; Alkhaldi et al. 2009; Al-Douri et al. 2013). These acids are less corrosive and spend slower in carbonate rock than HCl, thus providing deeper penetration and improved stimulation. Therefore, they are preferred when the treating temperature prevents efficient protection against corrosion and/or when the treatments are limited to low injection rates to avoid fracturing the formation. In contrast to these advantages, Chang et al. (2008) listed some limitations associated with the use of weak organic

acids: they cannot be used at high acid concentrations, they have a low dissociation constant, their degree of hydrogen ion generation decreases with an increase in temperature, and their cost is significantly higher than that of HCl for an equivalent mass of rock dissolved.

Some methods, including the use of sulfonic acids, have been tried in an effort to overcome the drawbacks for both mineral and conventional organic acid systems used in carbonate stimulation. Sulfonic acids, which have the formula RSO_3H, are described as a group of organic acids that contain one or more sulfonic, $–SO_3H$, groups (Tully 2000). Although the R-group may be derived from many different sources, typical R-groups are alkane, alkene, alkyne, and arene. Sulfonic acids are such strong acids (as strong as sulfuric acid) that they dissociate completely in water (King 1991). The obtained pK_a value for MSA is -1.92 (Covington and Thompson 1974). Sulfonic acids are stronger than conventional organic acids but not as strong as HCl (Fuller 2010). Because of their unique chemical and physical properties, sulfonic acids have found wide application in the chemical and pharmaceutical industries, and more recently in the oilfield.

Background on Optimum Injection Rate

Wormholes are deep, highly ramified dissolution channels formed by the reaction of acid with porous carbonate rocks. The control of the formation of these channels, which are an order of magnitude larger in diameter than the naturally occurring pores, is important for the success of stimulation treatments (Hill and Schechter 2000). When evaluating the performance of a newly proposed acid system or comparing its properties to commonly used acids, the characterization of these dissolution patterns is required.

In order to understand the wormholing process, many theoretical models have been developed (Buijse and Glasbergen 2005; Daccord et al. 1989; Hill et al. 2012; Furui et al. 2012a, 2012b; Hoefner and Fogler 1988; Hung et al. 1989; Pichler et al. 1992). One of the main challenges of these models is the determination of the dissolution pattern as a function of acid injection rate. Daccord et al. (1989), for example, defined three domains of dissolution patterns as functions of flow rate: compact (stable) dissolution at low flow rates, wormhole (unstable) domain at intermediate flow rates, and uniform dissolution (homogeneous etching) at high flow rates.

In addition to the theoretical models, numerous laboratory studies have shown a dependency of the efficiency of acidizing treatments on the generated dissolution pattern. This observation has resulted in the concept of an "optimum injection rate" (Fredd and Fogler 1998a; Hoefner and Fogler 1989; Wang et al. 1993).

The optimum flow rate is defined as the acid injection rate corresponding to the minimum volume of acid required for wormhole breakthrough. This optimum rate has been found to be determined by the dissolution pattern created by the acid reaction, and therefore is a function of rock composition, acid concentration, reaction temperature, core length, and formation permeability (Bazin 2001; Fredd and Fogler 1999; Wang et al. 1993).

Identifying the optimum injection rate for a given rock/acid system is critical for the comprehension of the wormholing mechanisms. This is a base parameter for the design (selection of acid concentration, acid volume, and injection rate) of acid

treatments. Therefore, it is necessary to determine the optimum injection rate for the new stimulation fluid (MSA) in carbonate rocks.

Background on Methanesulfonic Acid (MSA)

Methanesulfonic acid (MSA, **Fig. 1**) is a strong acid, which is almost completely ionized at 0.1 M in aqueous solution (Telfah 2008). MSA dissociation in water can be written as in **Eq. 1**:

$$CH_3SO_3H + H_2O \rightleftharpoons CH_3SO_3^- + H_3O^+ \quad \cdots\cdots\cdots\cdots\cdots (1)$$

The most reliable pK_a value of methanesulfonic acid in water reported is -1.92 at 25°C (Covington and Thompson 1974). The acidity of MSA in aqueous solutions is substantially greater than that of phosphoric or carboxylic acids (Guthrie 1978).

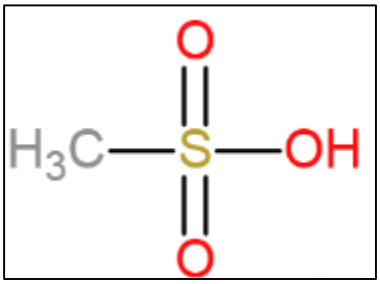

Fig. 1–Structural formula of methanesulfonic acid (MSA).

Methanesulfonic acid has many useful chemical and physical properties. For instance, a 70 wt% MSA aqueous solution has a melting point around -55°C and a high thermal stability, which makes it applicable as a liquid over a wide temperature range.

An aqueous MSA solution under normal atmospheric conditions is odor-free due to the very low vapor pressure (Finšgar and Milošev 2010).

Methanesulfonic acid is more effective at dissolving calcium carbonate scale than many other acids. Because methanesulfonate salts are highly soluble, methanesulfonic acid is very effective for keeping cations in solution, which ensures efficient cleaning (Hauthal 2007). The saturation solubilities of calcium methanesulfonate and magnesium methanesulfonate at room temperature are 2.92 and 1.40 mol•dm^{-3}, respectively (Gernon et al. 1999).

Environmental Advantages

Methanesulfonic acid (MSA) is considered an environmentally improved acid based on its favorable biodegradation profile and low volatile organic compounds (VOC) content. MSA is readily biodegradable by the OECD 301 (aerobe biodegradability in fresh water), 306 (aerobe biodegradability in sea water), and 311 (anaerobe biodegradability) test methods and has NSF/ANSI 60 (for drinking water applications) and Cefas (for marine applications, North Sea) registrations.

MSA has no established OSHA PEL (permissible exposure limit), because MSA aqueous solutions do not evolve any dangerous volatile chemicals, making it safe to handle under normal conditions (Gernon et al. 1999). Therefore, unlike carboxylic acids such as acetic acid, MSA is virtually free of volatile organic compounds (VOC).

Corrosion Behavior

MSA is less corrosive than the usual mineral acids employed in diverse industrial processes (Finšgar and Milošev 2010). If similar quantities are used, the surface removal

rates of MSA are normally less than those of HCl solutions. Also, because of the low vapor pressure, there is no gas phase corrosion with MSA under normal conditions, by contrast with hydrochloric, formic, or nitric acid.

The corrosion rate of L-80 (low-carbon steel) and 22Cr (stainless steel) when they were exposed to 10 wt% MSA for 6 hours were measured at 120 and 160°C. The corrosion rates for un-inhibited acid were 0.20732 and 0.20904 lb/ft^2, for the L80 samples at 120 and 160°C, respectively. These values were well above the acceptable corrosion rate of 0.05 lb/ft^2. Same tests using inhibited acid solutions (including corrosion inhibitor intensifier, KI) resulted in corrosion rates of 0.00119 and 0.00367 lb/ft^2, for the L80 samples at 120 and 160°C, respectively, which are below the acceptable corrosion rate limit. On the other hand, the corresponding corrosion rates for the 22Cr samples (non-inhibited 10 wt% MSA solution) were 0.00004 and 0.01341 lb/ft^2 at 120 and 160°C, respectively. It was observed that in the case of MSA and higher alloy steels such as 22Cr corrosion inhibitor was not needed (Finšgar and Jackson 2014).

Research Objectives

The drawbacks of conventional systems, previously exposed, motivate the study of alternative technologies for application in carbonate acidizing. Due to its beneficial properties, methanesulfonic acid has potential for application as a high-performance, environmentally friendly stimulation fluid. However, the wormholing characteristics of sulfonic acids, when injected into high-temperature carbonate reservoirs, have not been studied thoroughly.

The objectives of this study are to: (1) evaluate the ability of MSA to create and propagate wormholes, and enhance the permeability of carbonate cores, (2) determine the optimum injection rate of MSA in carbonate cores, (3) study the effect of various factors on the acidizing efficiency of MSA: injection rate, temperature, acid concentration, core permeability, core lithology, and (4) determine the potential for formation damage when MSA is used to stimulate carbonate cores at high temperatures.

CHAPTER II

EXPERIMENTAL PROCEDURES

Laboratory coreflood experiments were conducted with Indiana limestone and Silurian dolomite core samples and 5, 10, and 20 wt% aqueous MSA solutions. The experiments were performed at temperatures of 80, 250 and 320°F. An overburden pressure of 1,800 psi was applied to the core cell by means of a manual hydraulic pump connected to the coreflood setup. A new core was used for each experiment.

The acid was injected into the cores at a constant flow rate until breakthrough was observed. A minimum pressure of 1,100 psi was maintained in the core by a backpressure regulator downstream of the core. This pressure was required to keep most of CO_2 in solution. During acid injection, samples of the core effluent were collected and analyzed for pH, calcium concentration, and acid concentration. An Orion PrepHecT Ross Electrode was used to measure the pH value of the samples. The calcium concentration and final acid concentration in the core effluent samples were determined by using the inductively coupled plasma (ICP) and the Titrando 907 equipment, respectively. Finally, after the acid injection, computed tomography (CT) scans of the core samples were performed to characterize the generated wormholes.

Materials

Acid Preparation

The MSA acid solutions used during coreflood injections were prepared by diluting a stock MSA solution (70 wt% MSA) to the desired acid concentration.

Deionized water obtained from a purification water system, with a resistivity of 18.2 MΩ•cm at room temperature, was used to prepare the acid and for all water requirements during the experiments. Corrosion inhibitor, composed of methanol (30 – 60%) and propynol ethoxylate (15 – 40%), was added to the diluted acid blend at a concentration of 1 vol%. For quality control purposes, the prepared solutions were titrated using the Titrando 907 equipment and a 0.1 N potassium hydroxide solution.

The titration procedure described below was followed: 0.7 g of the acid sample were weighed out into a 150 ml beaker and mixed with 100 ml of distilled water. Subsequently, titration with KOH solution (0.1 N) was performed until equivalent point was observed (potentiometric determination). Next, an arithmetic formula (**Eq. 2**) was used to calculate of the weight percent concentration of the MSA solution.

$$\frac{V_1 \times c_1 \times t_1 \times M_1 \times 100}{E} = Conc.of\ MSA\ (wt\%).\cdots\cdots\cdots\ (2)$$

Where,

V_1 = KOH consumption (L)

E = Amount of acid sample (g)

c_1 = Concentration of KOH solution (0.1 mol/L)

t_1 = Titre of KOH solution, 1

M_1 = Molar mass of methanesulfonic acid (96.11 g/mol)

Core Preparation

Core samples, from blocks of Indiana limestone and Silurian dolomite, were cut into cylinders (plugs) of 1.5-in. diameter and 6-in. length. A saturation method was used to measure the porosity of the core plugs. The samples were dried in an oven at a temperature of 250°F for 8 hours and then weighed. After this, the samples were saturated in water under vacuum for 24 hours and weighed. From the difference in weight of the dry and saturated core samples, the porosity was calculated and found to be in the range of 14 to 17 vol% for the limestone cores and 11 to 14 vol%, for the dolomite cores.

Before the acid injection, the core samples were placed inside the core holder and deionized water was injected at different flow rates (i.e., 5, 10, and 20 cm^3/min). The pressure drop across the cores at each flow rate was recorded, and Darcy's law was used to determine the absolute permeability of the cores.

Equipment

Coreflood Setup

The coreflood setup shown in **Fig. 2** was used to simulate a matrix stimulation treatment with MSA. The main experiments in this project were conducted in this unit. Core plugs of 6-in. length and 1.5-in. diameter of different rock type/characteristics (carbonates) were exposed to MSA and heterogeneous chemical reactions occurred inside this unit. The whole system was kept under temperature up to 320°F. The main components of the coreflood setup are described below.

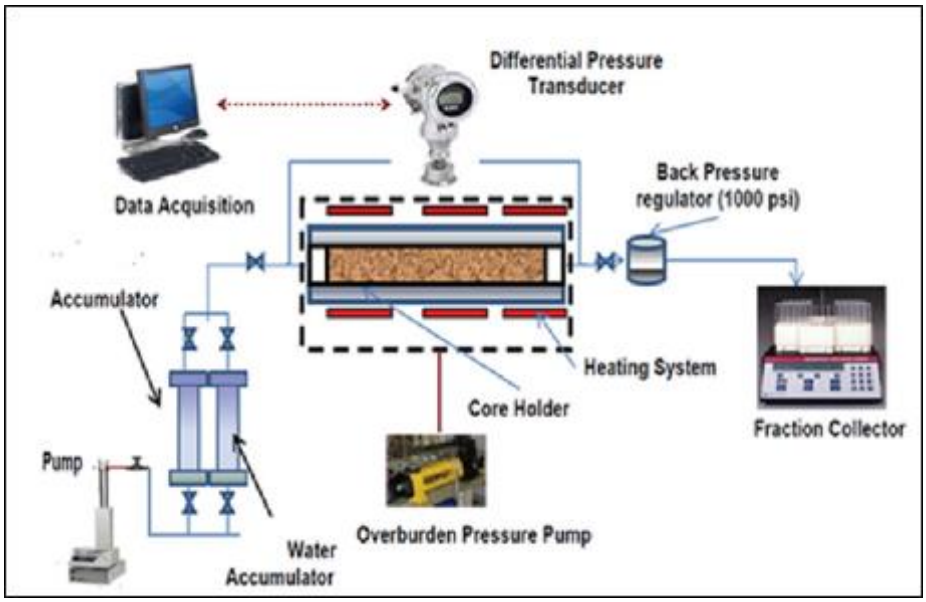

Fig. 2–Coreflood setup used to simulate matrix stimulation treatments.

Syringe Pump

A Teledyne ISCO D-series D1000 precision syringe pump with a maximum allowable working pressure of 2,000 psi was used to inject the acid system into the core.

Core Holder

A core holder with a pressure capacity of 3,000 psi was used to handle cores of 1.5-in. diameter and 6-in length.

To heat the cores to the required test temperature, a heat jacket was placed around the core holder. The temperature was controlled by a compact bench top CSC32 series with a 4-digit display and a 0.1° resolution with an accuracy of ±0.25% full scale ±1°C. It uses a type-K thermocouple and two outputs (5 A 120 Vac SSR). Water was injected at 2 cm^3/min during the heating period.

Pressure Transducer

A digital pressure transducer, connected to a computer with LabView® software installed, was used to monitor and record the pressure drop across the core during the experiments.

Sample Collector

During acid injection, samples of the core effluent were collected and analyzed for pH, calcium concentration, and acid concentration.

X-Ray CT-Scanner

Fig. 3–CT-scanner used to characterize the dissolution structures created by MSA in dolomite cores.

A state of the art Toshiba Aquilion RXL CT Scanner (**Fig. 3**) with 3D advanced visualization software was used to characterize the dissolution structures created by MSA in the dolomite cores. This equipment has a 16-detector row 32 slice computerized tomography system that delivers high speed iterative image reconstruction of 0.5 mm data sets at up to 16 images per second. The scanner has a 72 cm gantry opening with +/- 30 degrees tilt with an accurate 0.5 mm x 16-row high-resolution detector. Also, the CT-Scanner has a low contrast resolution of 2 mm at 0.3%.

Inductively Coupled Plasma Optical Emission Spectrometry (ICP-OES)

The Optima 7000 DV ICP-OES machine (**Fig. 4**) was used to determine the concentration of various multivalent ions in the core effluent samples obtained from the different coreflood experiments performed. Commonly measured ions included Ca^{++}, Mg^{++}, and Fe^{+++}.

Fig. 4–Inductively Coupled Plasma Optical Emission Spectrometry (ICP-OES).

X-Ray Fluorescence (XRF)

X-ray fluorescence (XRF) is the emission of characteristic "secondary" (or fluorescent) X-rays from a material that has been excited by bombarding with high-energy X-rays or gamma rays. It is elemental analysis and chemical analysis for the rock samples. During this project a S2 Ranger X-Ray Fluorescence (XRF) machine (**Fig. 5**) was used for routine, non-destructive chemical analyses of carbonate rock samples.

Fig. 5–S2 Ranger X-Ray Fluorescence (XRF).

Scanning Electron Microscope (SEM)

An Evex Mini-Scanning Electron Microscope (SEM) was used during the current study to image a mineral sample by scanning it with a high-energy beam of electrons in a raster scan pattern (**Fig. 6**). The electrons interact with the atoms that make up the sample producing signals that contain information about the sample's surface topography and composition.

Fig. 6–Evex Mini-Scanning Electron Microscope (SEM).

CHAPTER III

ACIDIZING HIGH-TEMPERATURE LIMESTONE FORMATIONS WITH METHANESULFONIC ACID[†]

Introduction

One of the first references of the potential use of alkanesulfonic acids for the treatment of oilfield wells is found in a patent filed by Tate (1982), who disclosed a method for improving the recovery of hydrocarbons in sandstone formations. More recently, Fu (2010) proposed the injection of an aqueous mixture for the treatment of sandstone formations, which consisted of a surfactant, an inorganic acid (for example HCl), and an organic acid (such as formic acid, acetic acid, citric acid, or MSA). In a similar application, Fuller (2010) presented a method for treating sandstone formations, which consisted of injecting a blend of an aqueous liquid, a fluoride source, and an effective amount of an alkane sulfonic acid, preferably MSA. The stimulation of carbonate formations using alkanesulfonic acids, and in particular MSA, was first disclosed by Heidenfelder et al. (2009). On the same line of research, Bertkau and Steidl (2012) disclosed an innovative method comprising the use of alkanesulfonic acid (MSA) microcapsules as an additive for carbonate acidizing applications. None of the previous

[†]Part of the data reported in this chapter is reprinted with permission from "Acidizing High Temperature Carbonate Reservoirs Using Methanesulfonic Acid: A Coreflood Study" by A. Ortega, H.A. Nasr-El-Din and S. Rimassa, 2014. 2014 AADE Fluids Technical Conference and Exhibition, AADE-14-FTCE-3, Copyright 2014 by AADE.

studies included a description of the wormholing characteristics of sulfonic acids (and specifically, MSA) when they are injected through carbonate cores at high temperatures.

The current study expands on the results obtained for the injection of MSA in carbonate cores (Ortega et al. 2014) by performing coreflood tests at different temperatures so the effect of temperature on the wormholing characteristics could be evaluated. Also, since this is the first study to thoroughly examine the fate and propagation of MSA in coreflood experiments, benchmark tests using HCl were performed at the same reservoir conditions. The coreflood analysis showed a comparable reactivity of MSA to HCl for molar-equivalent solutions at 250°F.

Coreflood Study

Twelve coreflood runs were performed using 10 wt% MSA, at injection rates of 1 to 25 cm^3/min. These runs were done to determine the effect of the injection rate on MSA performance, specifically, the acid volume to breakthrough, and the resulting wormhole characteristics. These first set of experiments were conducted at a temperature of 250°F. **Table 1** presents a summary of the results obtained for each of the core samples used. During coreflood injection, the pressure drop across the core was plotted using the LabView® software. Samples of the coreflood effluent were collected and analyzed for calcium concentration, pH, and acid concentration.

The analyses performed for Core #4 are provided as an example of the complete coreflood procedure. **Fig. 7** shows the behavior of the pressure drop across the core during the injection of the 10 wt% MSA system at a rate of 10 cm^3/min. The differential pressure, which initially stabilized at 15 psi during the injection of water, started to

decrease shortly after the acid injection began. This decrease in pressure indicates the reaction of the acid with the carbonate rock, and the creation of dissolution patterns (wormholes) as the acid front was moving along the core length. The differential pressure continued to decrease with time until acid breakthrough occurred.

TABLE 1—PROPERTIES OF LIMESTONE CORES USED WITH 10 WT% MSA AT 250°F AND SUMMARY OF COREFLOOD RESULTS

Core No.	Pore Volume, cm^3	Porosity, vol%	Injection Rate, cm^3/min	Acid Vol. to Breakthrough, PV
32	24.6	14.2	1.0	9.18
7	25.1	14.4	1.5	4.56
10	28.0	16.1	3.0	3.33
41	24.9	14.3	4.0	3.28
1	29.1	16.7	5.0	3.27
12	28.5	16.4	6.0	2.91
3	29.0	16.7	7.5	3.00
4	29.6	17.0	10.0	4.25
39	25.9	14.9	12.0	4.83
28	25.7	14.8	15.0	5.44
8	23.9	13.8	20.0	6.48
9	29.4	16.9	25.0	6.51
Average Porosity = 15 vol% / Average Permeability = 160 md				

The volume of acid to breakthrough is defined as the volume of acid needed to propagate the wormhole through the length of the core. When breakthrough was achieved, a low and constant pressure drop was recorded from the coreflood apparatus,

indicating that the fluid was flowing through the created wormhole structures. For the current case, 4.25 pore volumes (PV) of acid were needed to achieve breakthrough.

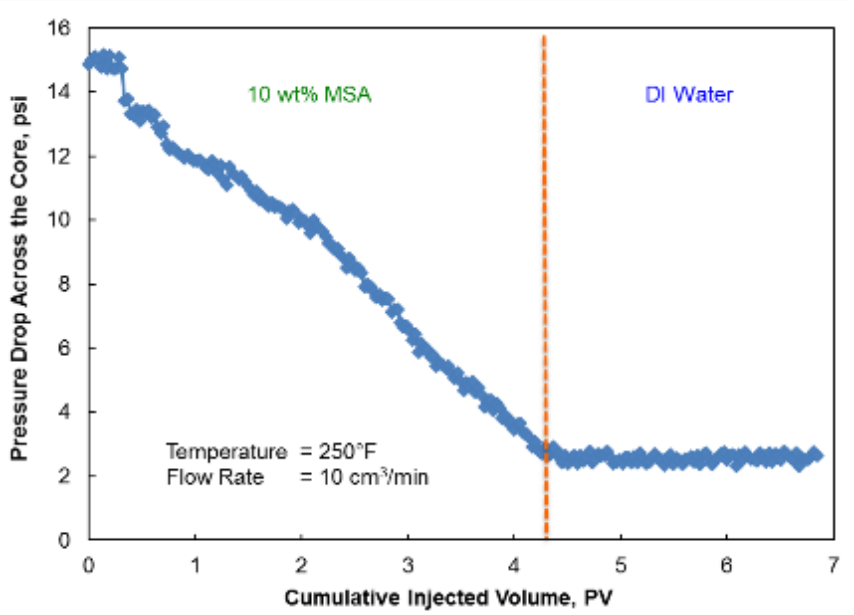

Fig. 7–Pressure drop across Core #4 during the injection of 10 wt% MSA at a rate of 10 cm^3/min.

As MSA reacted with the carbonate rock creating dissolution channels along the core, the calcium concentration in the effluent samples started to increase. **Fig. 8** shows the calcium concentration in the core effluent samples. It shows that the total ICP's measured calcium concentration reached a maximum value of 21,460 mg/l ± 4%.

Fig. 9 shows the pH and acid concentration of the coreflood effluent samples for the same experiment. The pH was nearly 7.5 at the start of the injection (water). Then, it decreased with the injection of acid to a value of 1.06 (after acid breakthrough) and increased again as the injection of water resumed. As expected, an opposite trend was

found for the final acid concentration in the effluent samples, which achieved a maximum value of 1.31 wt% MSA after breakthrough, indicating that acid was spent.

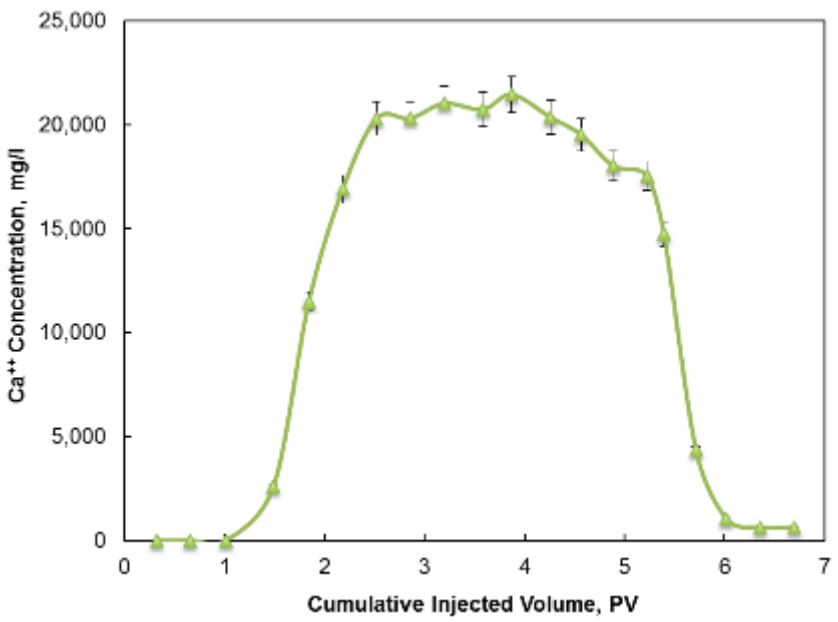

Fig. 8–Calcium concentration in the core effluent samples of Core 4. Error bars represent relative standard deviation (RSD) from the measurements.

A procedure similar to the one explained above for Core #4 was followed for all the other core samples used in the study. **Fig. 10** shows the behavior of the pressure drop across the core during the injection of the 10 wt% MSA system at injection rates of 1, 6, 10, and 25 cm^3/min. As described above for Core #4, at each injection rate the differential pressure reached a stabilized value during the initial water injection, and started to decrease with the volume of acid injected due to the reaction of the acid with the calcite rock, and the creation of wormholes. The pressure decreased until acid breakthrough was achieved.

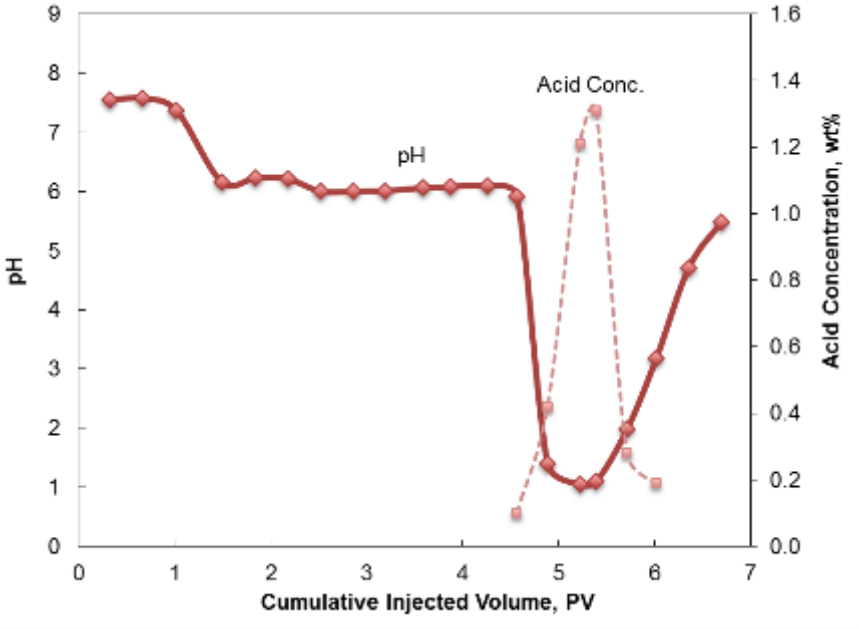

Fig. 9–pH and acid concentration in the core effluent samples of Core #4.

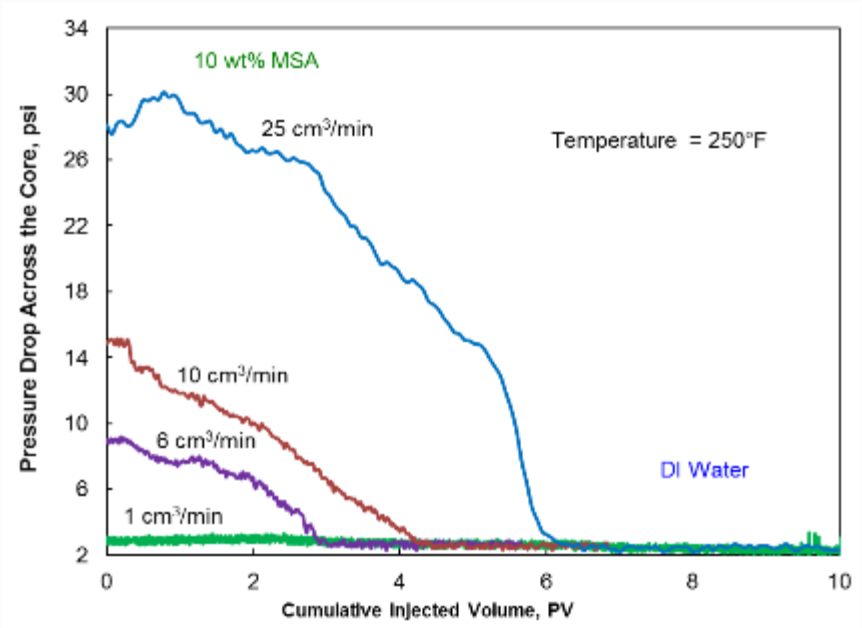

Fig. 10–Pressure drop across different cores during the injection of the 10 wt% MSA system at injection rates of 1, 6, 10, and 25 cm^3/min.

Fig. 11 presents the calcium concentration in the coreflood effluent samples, collected for some of the experiments at different injection rates. As in the case of Core #4 (Fig. 8), the calcium concentration increased with the injection of acid, reaching a maximum value, then decreased when the injection fluid was switched back to water.

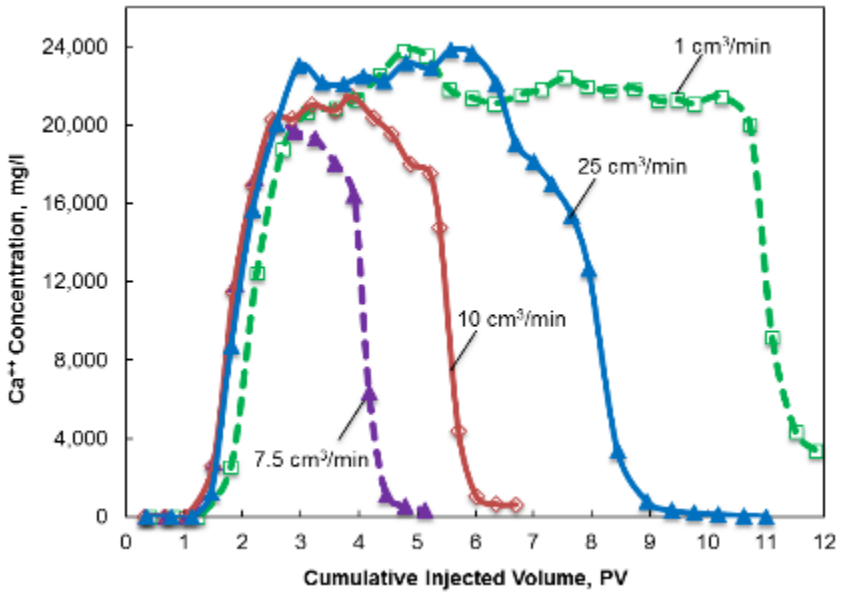

Fig. 11–Calcium concentration in the core effluent samples, collected for the various experiments with MSA at different injection rates (± 4%, relative standard deviation).

The calcium concentration plotted in Fig. 11 indicates the amount of carbonate rock dissolved by the acid at each injection rate, and is a function of the acid/rock contact time and contact area. Both, the contact time and contact area, are minimized when the acid is injected at conditions close to the optimal. As a result, the lowest peaks for calcium concentration (Fig. 11) were observed for injection rates between 5 and 7.5 cm^3/min (the most optimal cases). By contrast, the highest peaks for calcium

concentration were observed when the acid was injected at conditions far from the optimal, for example, at 1 and 25 cm^3/min, corresponding to the cases with the highest contact time and contact area, respectively.

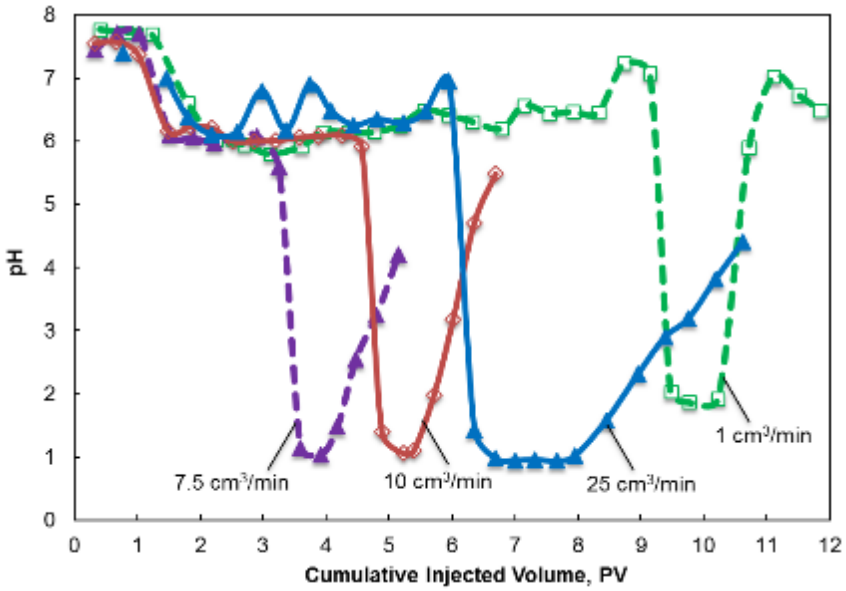

Fig. 12–pH of the core effluent samples, collected for the various experiments with MSA at different injection rates.

Similarly, the change in pH and acid concentration can be compared for all the cases tested. Since these two variables are inversely related (the higher the acid concentration, the lower the pH), they both can be used to confirm the breakthrough determined from the analysis of the pressure drop. For example, the decrease in pH measurements to a minimum value indicates acid breakthrough (**Fig. 12**). This minimum value of pH varied in the range of 0.96 (Core #9, 25 cm^3/min) to 1.87 (Core #32, 1 cm^3/min).

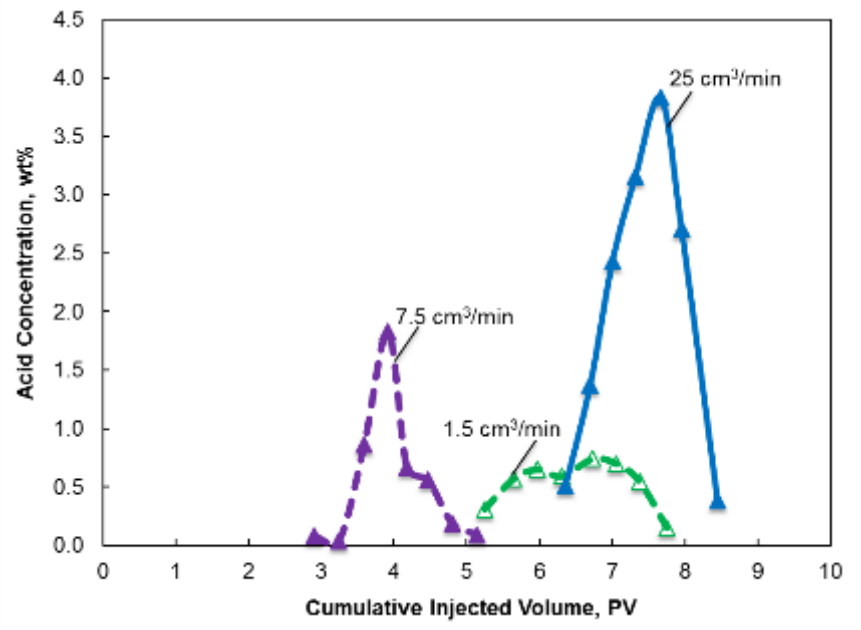

Fig. 13–Acid concentration in the coreflood effluent samples collected for the various experiments with MSA at different injection rates.

On the contrary, the peak (maximum) of the final acid concentration (**Fig. 13**) ranged between 0.7 wt% (Core #7, 1.5 cm^3/min) and 3.8 wt% (Core #9, 25 cm^3/min). The results presented in Figs. 12 and 13 demonstrate the dependency of pH and acid concentration on the injection rate. The higher the acid injection rate, the lower the time the acid has for spending upon contact with the carbonate rock, therefore resulting in a higher acid concentration (and lower pH) of the core effluent samples.

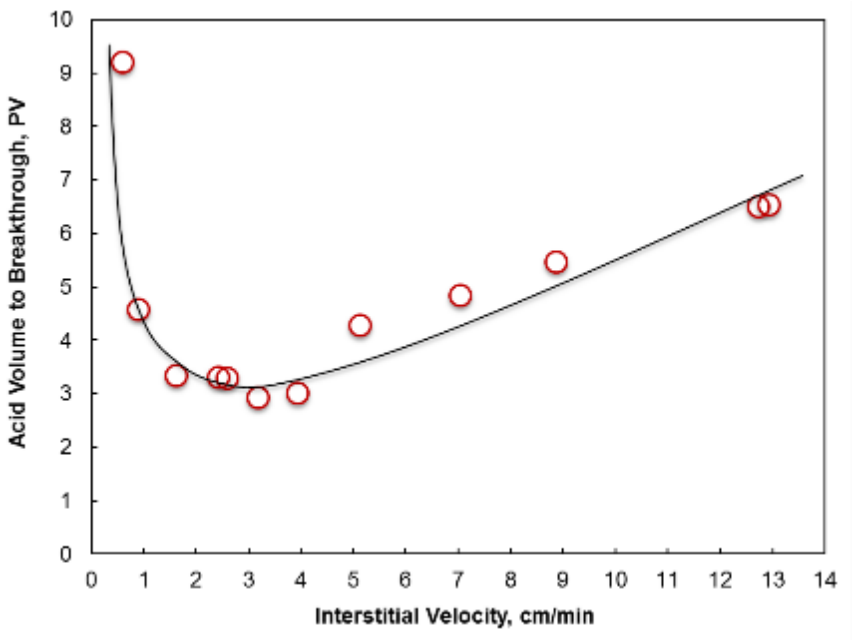

Fig. 14–Optimum injection rate curve for the reaction of MSA with limestone at 250°F.

Optimum Injection Rate

The optimum injection rate is the rate at which the volume of acid required to achieve breakthrough is minimum. The volume of acid to breakthrough as a function of interstitial velocity is shown in **Fig. 14**. For each of the core samples treated, the interstitial velocity was calculated by dividing the superficial velocity (volumetric flow rate over the cross area of the core) by the corresponding core porosity (as reported in Table 1). From this figure, as the injection rate increases, the volume of acid to breakthrough decreases and reaches a minimum at a rate between 5 and 7.5 cm^3/min (2.6 to 3.9 cm/min, interstitial velocity). At injection rates higher than the optimum, the volume of acid to achieve breakthrough increases again. However, the curve is steeper on the left side of the optimum injection rate and relatively flat for rates higher than the

optimum. This fact indicates that the effect of the injection rate is more pronounced at low injection rates, corresponding to a mass-transfer-limited regime. On the other hand, a surface-reaction-limited regime is reached for high injection rates, with the pore volumes to breakthrough being affected less by changes in the injection rate.

The lowest volume of acid to breakthrough is obtained at an injection rate of 6 cm^3/min, and therefore, for the conditions tested, this is considered the optimum injection rate when 10 wt% MSA is used to stimulate limestone cores at a temperature of 250°F.

CT-Scan Images

The dissolution structures that were created at the different flow rates considered in the coreflood study can be characterized by analyzing the 3D scan images of the cores treated with 10 wt% MSA at 250°F. **Fig. 15** presents CT scan images, along with some photographs of the inlet side of the core samples after acid injection, for low-injection rate (1 and 1.5 cm^3/min), intermediate-injection rate (6 and 7.5 cm^3/min), and high-injection rate (20 and 25 cm^3/min), showing the wormholing ability of MSA in the whole range of injection rate tested.

At low-injection rates, dissolution of the inlet face of the core can be observed in the scan images. A conical wormhole is also visible, which caused the core stimulation to be inefficient (sub-optimal). At intermediate-injection rates, or rates close to the optimum injection rate, no face dissolution of the core was observed; additionally, a single dominant wormhole was created, penetrating the total length of the core. The size of the generated wormhole decreased as the acid penetrated deeply into the core, until

acid breakthrough was achieved. This dissolution pattern resulted in an efficient stimulation of the core. At high-injection-rates, again no face dissolution of the core was observed. However, a more ramified/branched dissolution structure was generated as a result of the acid being forced into smaller pores. Consequently, the number of pore volumes to breakthrough increased with respect to the intermediate-rate case (lower acid efficiency).

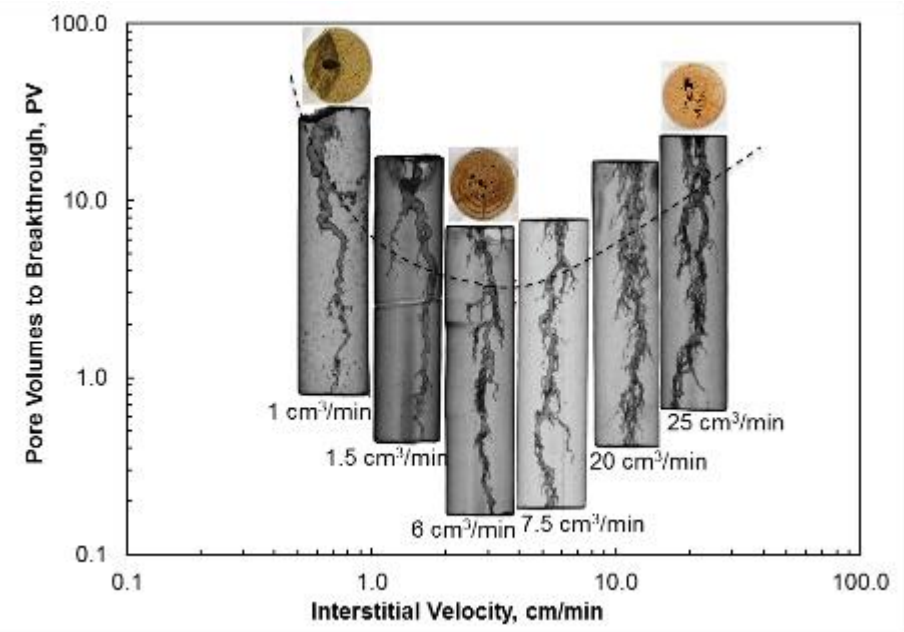

Fig. 15–Low injection (left) leads to face dissolution and conical wormholes. Dominant wormholes are a characteristic of the intermediate rate case (center). High injection results in ramified dissolution structures (right).

Analysis of the 3D scan images provides an explanation for the difference in calcium concentration measured for the range of injection rates tested, as described in a previous section. At a low injection rate (1 cm^3/min), a large volume of MSA is consumed on the inlet face of the core (face dissolution). Also at this rate, the reactant

penetrates into the porous matrix and enlarges flow channels. However, a significant amount of MSA is consumed on the walls of these flow channels, causing the formation of a conical-shaped dissolution channel. From the CT-scan images at 1 cm^3/min, the maximum diameter of the conical wormhole was about 0.46-in (11.7 mm). This conical channel requires the injection of several pore volumes of acid for the channel to break through the porous medium. The combined effect of face dissolution and conical channels results in a high degree of acid reaction with the rock, which in turn generates a high amount of calcium ions in the effluent samples.

On the other hand, at an intermediate injection rate (6 cm^3/min) unconsumed MSA reaches the tip of the growing flow channels. Successive consumption at the tip extends the dissolution channels and leads to the development of a dominant wormhole of reduced size. From the CT-scan images at 6 cm^3/min, the average diameter of the dominant wormhole was about 0.15-in (3.8 mm). This dominant wormhole requires a minimum pore volume of acid to break through the rock matrix. For that reason, the calcium concentration of the effluent samples at this intermediate rate is lower than the corresponding concentration for the low injection rate case.

Lastly, at a high injection rate (20 cm^3/min) a dominant channel rapidly generates and propagates. With continued acid injection, very fine branches around the main wormhole are created, having an effect similar to an increase of the main wormhole diameter. From the CT-scan images at 20 cm^3/min, the maximum diameter of the combined dominant wormhole and ramifications was about 0.37-in (9.4 mm). Since dissolution occurs over a high surface area, a higher degree of acid reactivity results in a

higher amount of calcium ions in the effluent samples than the amount measured for the intermediate injection rate case.

From the study of the 3D scan images it is confirmed that MSA can be used as an effective stimulation fluid at intermediate flow rates, being able to create deep, dominant wormholes without face dissolution and branching. The generation of a dominant wormhole provides a significant increase in permeability, as shown in **Fig. 16**, which describes the permeability enhancement obtained in carbonate cores tested with MSA at different injection rates, after acid breakthrough occurred.

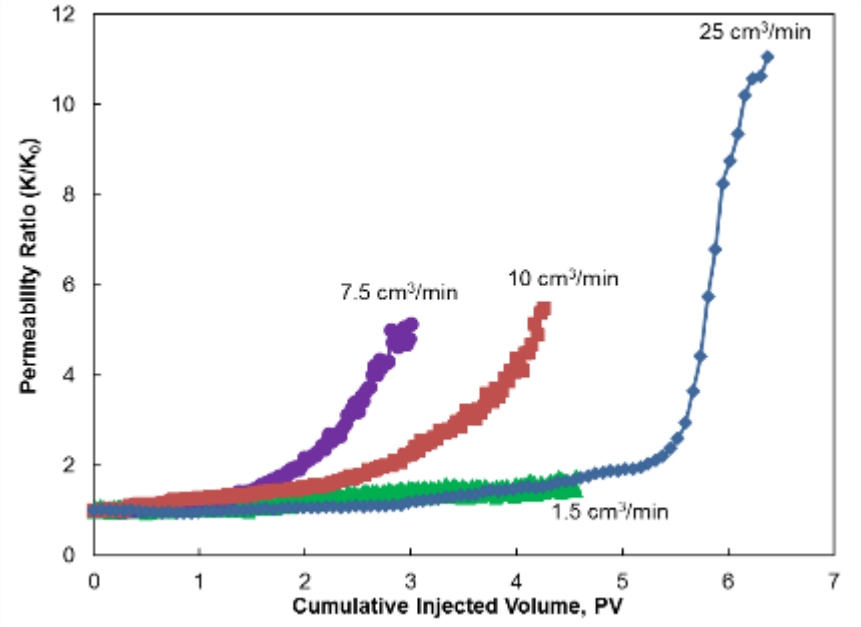

Fig. 16–Permeability enhancement by injection of 10 wt% MSA in carbonate cores.

During coreflood testing, the pressure drop across the rock is measured as dissolution progresses, and the average permeability of the rock is calculated using Darcy's law. It can be observed from results in Fig. 16 that the amount of acid required to increase the average permeability by a certain degree depends on the acid injection

rate. For example, at a very low injection rate (i.e., 1.5 cm^3/min), the average permeability increases slowly with the pore volumes of acid injected. As the acid injection rate is increased, the rate of increase in average permeability increases up to a certain acid injection rate (6 to 7.5 cm^3/min). At this acid-injection rate, the optimum injection rate, permeability increment is steepest as compared with other acid-injection rates. For acid-injection rates (i.e., 25 cm^3/min) higher than the optimum acid-injection rate, the rate of permeability increment decreases with the increase in the injection rate.

Characterization of MSA Dissolution Patterns – Fractal Dimension

The 2D wormhole patterns resulting from the injection of 10 wt% MSA in carbonate rock at 250°F were analyzed to determine their fractal nature with a box-counting method. Box-counting is a sampling process used to find fractal dimensions by laying a series of grids of decreasing caliber over an image and recording data for each successive caliber. The box-counting fractal dimension provides an index of pattern complexity, which indicates the change in pattern detail with a change in scale. Binary images of the wormhole patterns were prepared from the CT-scan images and fractal dimensions of 1.58 ± 0.02, 1.61 ± 0.01, and 1.75 ± 0.02 were determined for the cases of low-injection rate (1 cm^3/min), intermediate rate (6 cm^3/min), and high-injection rate (20 cm^3/min), respectively. The obtained values are in agreement with previously reported fractal dimensions of 1.6 ± 0.1 by Daccord and Lenormand (1987) and 1.4 by Kalia and Balakotaiah (2007). However, it appears to be a slight dependency of the fractal dimension on the injection rate as the fractal dimension increases as the injection rate is increased.

Comparison with HCl Solutions

TABLE 2—PROPERTIES OF LIMESTONE CORES USED WITH 4 WT% HCl AT 250°F AND SUMMARY OF COREFLOOD RESULTS

Core No.	Pore Volume, cm^3	Porosity, vol%	Injection Rate, cm^3/min	Acid Vol. to Breakthrough, PV
HCl2	29.83	17.2	2.0	4.25
HCl42	25.72	14.8	4.0	2.90
HCl38	25.95	14.9	6.0	3.49
HCl1	29.58	17.0	10.0	3.89
HCl33	24.48	14.1	20.0	7.01
Average Porosity = 16 vol%				
Average Permeability = 200 md				

To evaluate MSA as an alternative to conventional mineral acid systems, a comparison of the 10 wt% MSA system coreflood performance was made against a molar equivalent HCl solution (4 wt% HCl), both of which had a molar concentration of 1.1 mol/l (1.1 M). Five coreflood experiments were run with 4 wt% HCl using Indiana limestone cores at 2, 4, 6, 10, and 20 cm^3/min. The properties of the core samples used are presented in **Table 2**. The experiments were performed at a temperature of 250°F. Table 2 also presents a summary of the results obtained for each of the core samples used.

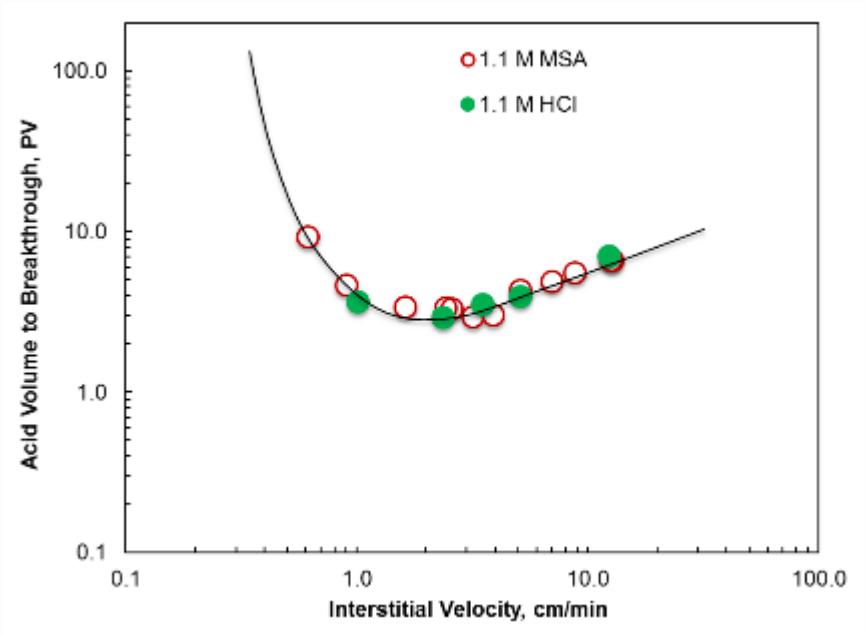

Fig. 17–Acid volume to breakthrough for 4 wt% HCl and 10 wt% MSA at 250°F.

Fig. 17 compares the volume of 4 wt% HCl to achieve breakthrough as a function of acid interstitial velocity, against the results already presented (Fig. 14) for 10 wt% MSA. At each injection rate tested, the acid volume required to breakthrough (Fig. 17) for the molar-equivalent HCl system was comparable with the corresponding acid volume to breakthrough of MSA. Additionally, it can be observed that there is an agreement in the optimum injection rate obtained for the two acid systems (between 4.0 and 6.0 cm^3/min).

A comparison of the dissolution patterns created by each acid system at three of the flow rates tested (2, 6, and 20 cm^3/min) is provided in **Fig. 18**. At rates lower than the optimum rate, for example 2 cm^3/min, both acid systems created conical channels with dissolution of the core face. Also similar to what was explained before for the case

of MSA, HCl tends to create a dominant wormhole when injected at rates close to the optimum rate (i.e., 6 cm^3/min). At injection rates higher than the optimum rate (for example 20 cm^3/min) dominant channels with very fine ramifications were created for the two acids.

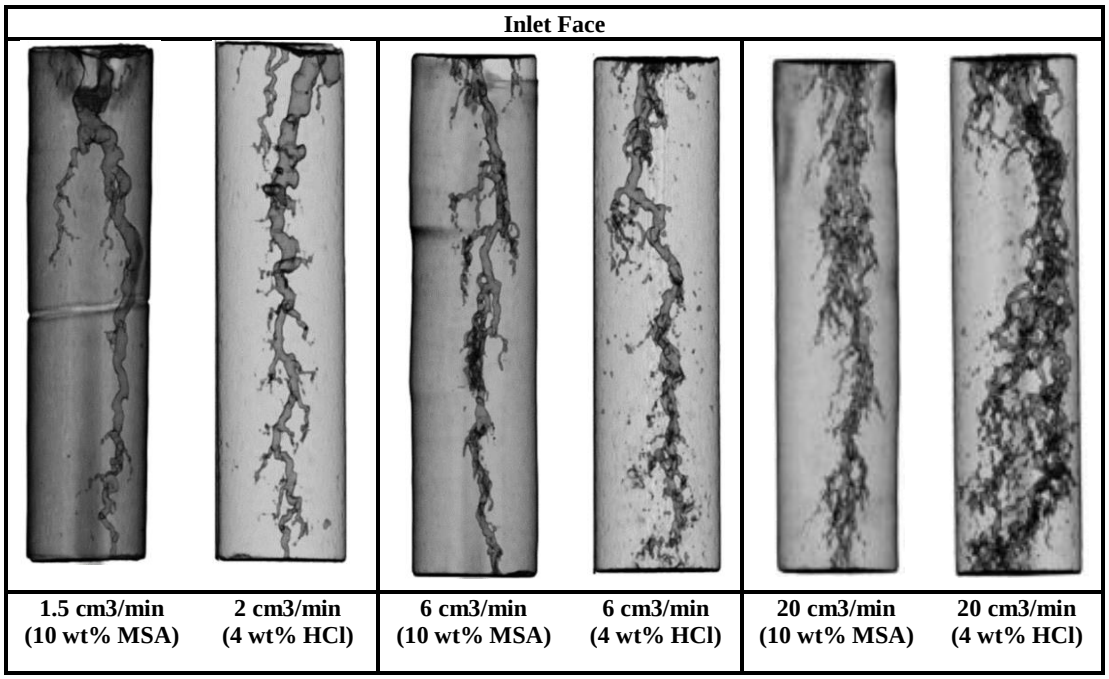

Fig. 18–Dissolution patterns identified from 3D scan images of core samples treated with molar-equivalent MSA and HCl solutions (1.1 M), at 250°F.

The fractal dimension of the wormhole patterns generated by the injection of 4 wt% HCl can be compared with the fractal dimension of the patterns produced by 10 wt% MSA at same temperature conditions. Following the procedure explained above, fractal dimensions of 1.57 ± 0.02, 1.60 ± 0.02, and 1.76 ± 0.01 were determined for the cases of low-injection rate (2 cm^3/min), intermediate rate (6 cm^3/min), and high-injection rate (20 cm^3/min), respectively. It can be observed the similarity in the fractal dimension

values determined for both molar equivalent solutions (10 wt% MSA and 4 wt% HCl). Also, the same trend of increase in the pattern complexity with increase in the injection rate is found for the case of HCl, as noticed previously for MSA.

The calcium concentration, pH, and final acid concentration were compared for the effluent samples collected during the coreflood experiments performed using MSA and HCl at different injection rates. Since the two acid systems tested were both strong acids and the molar-equivalent solutions of such acids were used, the maximum calcium concentrations obtained from ICP analysis were comparable for all the experiments.

Figs. 19 through 21 show the comparison of calcium concentration, pH, and final acid concentration, respectively, of the effluent samples collected for experiments with 10 wt% MSA and 4 wt% HCl at an injection rate of 10 cm^3/min.

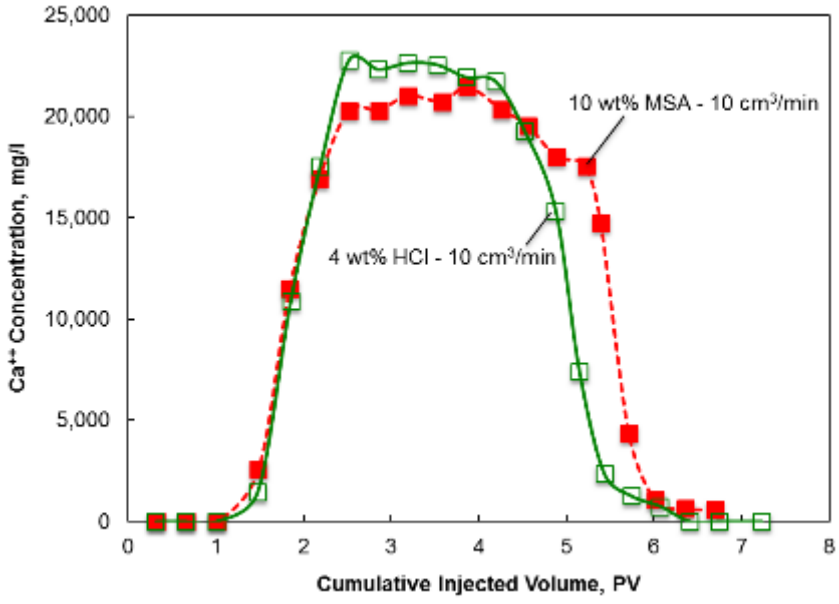

Fig. 19–Calcium concentration in the coreflood effluent samples collected for experiments with MSA and HCl at 10 cm^3/min.

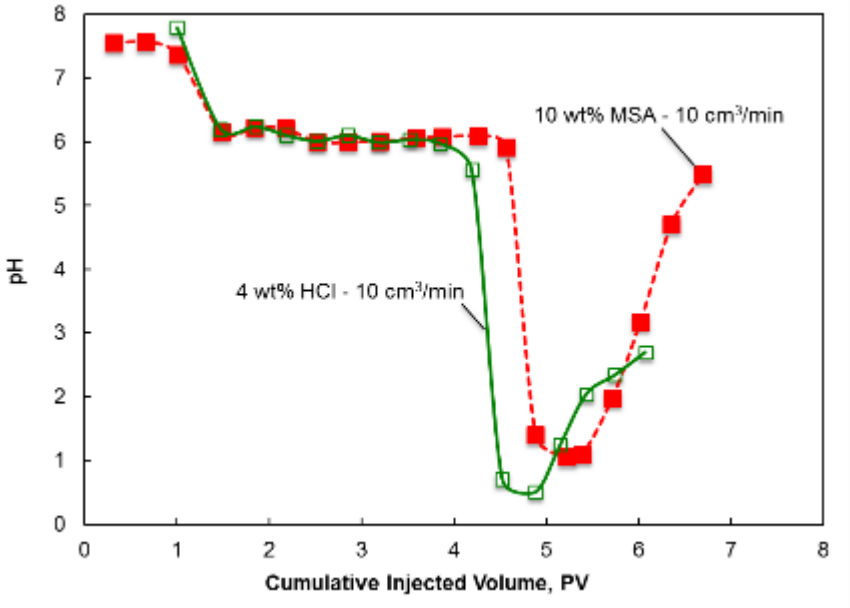

Fig. 20–pH of the coreflood effluent samples collected for experiments with MSA and HCl at 10 cm^3/min.

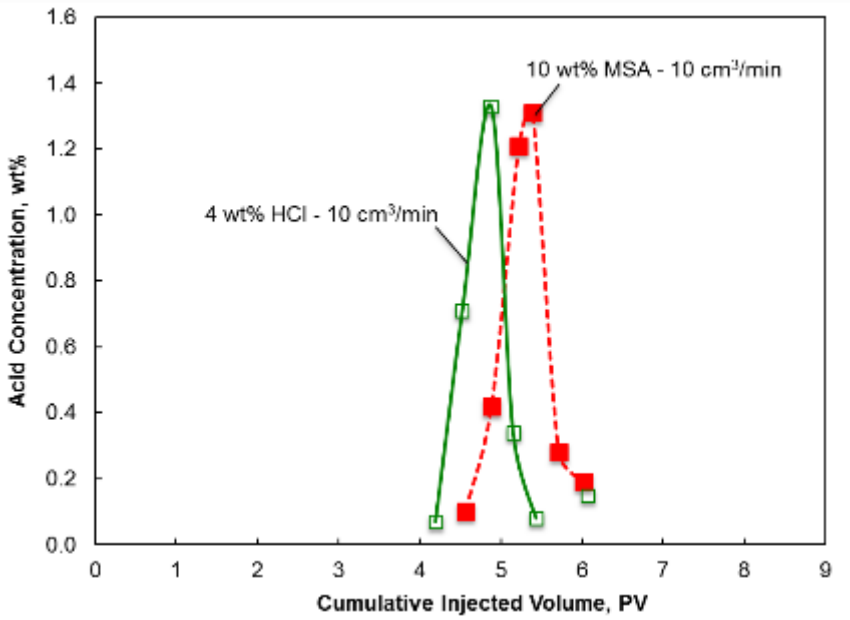

Fig. 21–Acid concentration in the coreflood effluent samples collected for experiments with MSA and HCl at 10 cm^3/min.

The similarity of the results obtained for the two molar equivalent systems tested can be noted. Also, the previous comments for the dependency of pH and final acid concentration on the injection rate also apply for the description of Figs. 20 and 21.

Conclusions

A 10 wt% MSA aqueous acid solution was used to stimulate limestone cores using a coreflood setup. The effect of acid injection rate on the propagation of MSA in carbonate cores were examined in detail. Based on the results obtained, the following conclusions can be drawn:

1. MSA was found to be effective in creating and propagating wormholes in limestone cores at temperatures up to 320°F, providing a significant increase in permeability.
2. For the acid injection rates covered in the current study, an optimum injection rate of 6 cm^3/min was determined when 10 wt% MSA was used to stimulate limestone cores at 250°F.
3. A similar acid efficiency was noted when MSA and HCl at 1.1 M were used to stimulate limestone cores at 250°F.

CHAPTER IV

EFFECT OF VARIOUS PARAMETERS ON THE ACIDIZING EFFICIENCY OF METHANESULFONIC ACID IN LIMESTONE FORMATIONS

Effects of Temperature

TABLE 3—PROPERTIES OF LIMESTONE CORES USED WITH 10 WT% MSA AT 80°F AND SUMMARY OF COREFLOOD RESULTS

Core No.	Pore Volume, cm^3	Porosity, vol%	Injection Rate, cm^3/min	Acid Vol. to Breakthrough, PV
74	23.53	13.5	1.0	3.62
84	21.66	12.5	2.0	2.71
86	25.11	14.5	4.0	2.88
85	25.39	14.6	5.0	3.18
87	25.82	14.9	6.0	3.29
69	25.37	14.6	10.0	4.93
88	25.00	14.4	20.0	6.93
Average Porosity = 14 vol%				
Average Permeability = 178 md				

The effect of temperature on wormhole formation with 10 wt% MSA was investigated by performing additional coreflood tests at temperatures of 80 and 320°F. Seven coreflood experiments were run with 10 wt% MSA, at each temperature, at injection rates from 1 to 20 cm^3/min using Indiana limestone cores. The properties of the

core samples used and the results obtained from coreflood testing are given in **Tables 3 and 4**, at 80 and 320°F respectively.

TABLE 4—PROPERTIES OF LIMESTONE CORES USED WITH 10 WT% MSA AT 320°F AND SUMMARY OF COREFLOOD RESULTS

Core No.	Pore Volume, cm^3	Porosity, vol%	Injection Rate, cm^3/min	Acid Vol. to Breakthrough, PV
45	25.41	14.62	1.5	7.08
46	25.82	14.86	4.0	5.80
48	25.91	14.91	6.0	5.06
44	25.56	14.71	7.0	4.89
51	25.34	14.58	8.0	5.81
50	25.96	14.94	10.0	6.16
47	25.87	14.89	20.0	7.92
Average Porosity = 15 vol%				
Average Permeability = 160 md				

From the coreflood experiments, it was confirmed that MSA can be used as an effective stimulation fluid at 80 and 320°F, showing the wormholing ability of MSA in the whole range of injection rate tested. The dissolution structures that were created by the injection of 10 wt% MSA in limestone cores at 80 and 320°F can be characterized by analyzing the 3D scan images of the treated cores. A similar trend to what was described before for the case of 250°F is observed in both figures, regarding the dependency of dissolution structure on the injection rate; however, some important differences can be noticed, as described below.

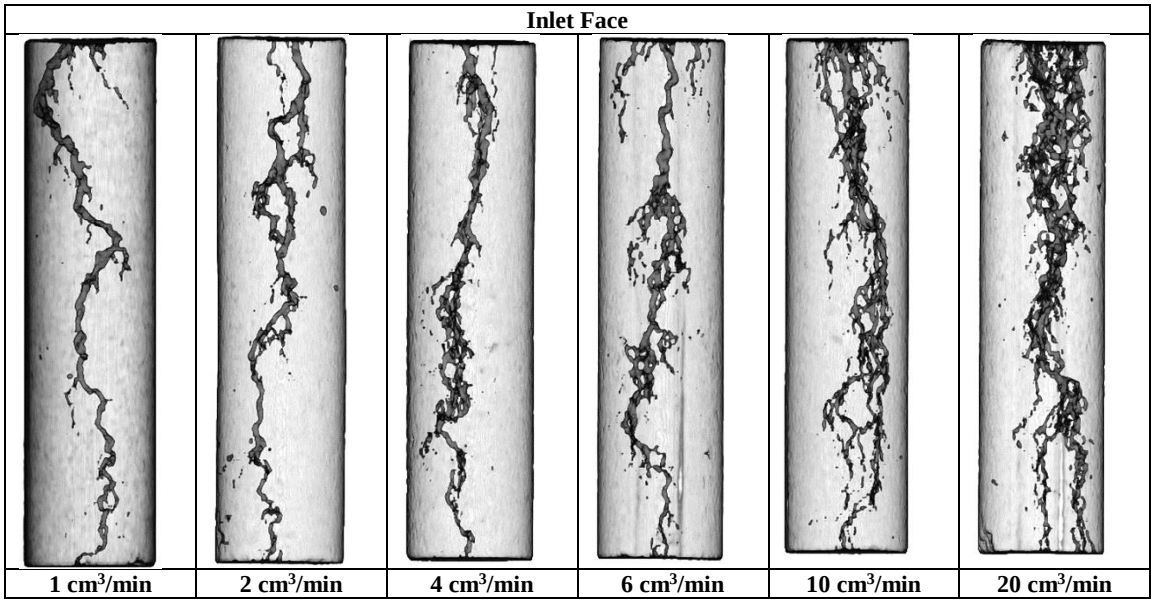

Fig. 22–Dissolution patterns identified from 3D scan images of core samples treated with 10 wt% MSA at 80°F.

By comparing Fig. 15 and **Fig. 22** (250°F vs. 80°F), it can be noticed that for the case of 80°F, lower injection rates were required to have face dissolution and to create conical wormholes. Also, at high injection rates (i.e., 20 cm^3/min), the degree of wormhole ramification was higher for the case of 80°F. Even at injection rates as low as 10 cm^3/min, some degree of branching is observed at 80°F. In general, the size of the wormholes tends to decrease with lower temperatures.

By comparing Fig. 15 and **Fig. 23** (250°F vs. 320°F), it can be noticed that at low injection rates (i.e., 1.5 cm^3/min), the degree of face dissolution was higher for the case of 320°F. Even at injection rates as high as 4 cm^3/min, some degree of face dissolution is observed. Also, higher injection rates were required to achieve same degree of wormhole

ramification. In general, the size of the wormholes tends to increase with higher temperatures.

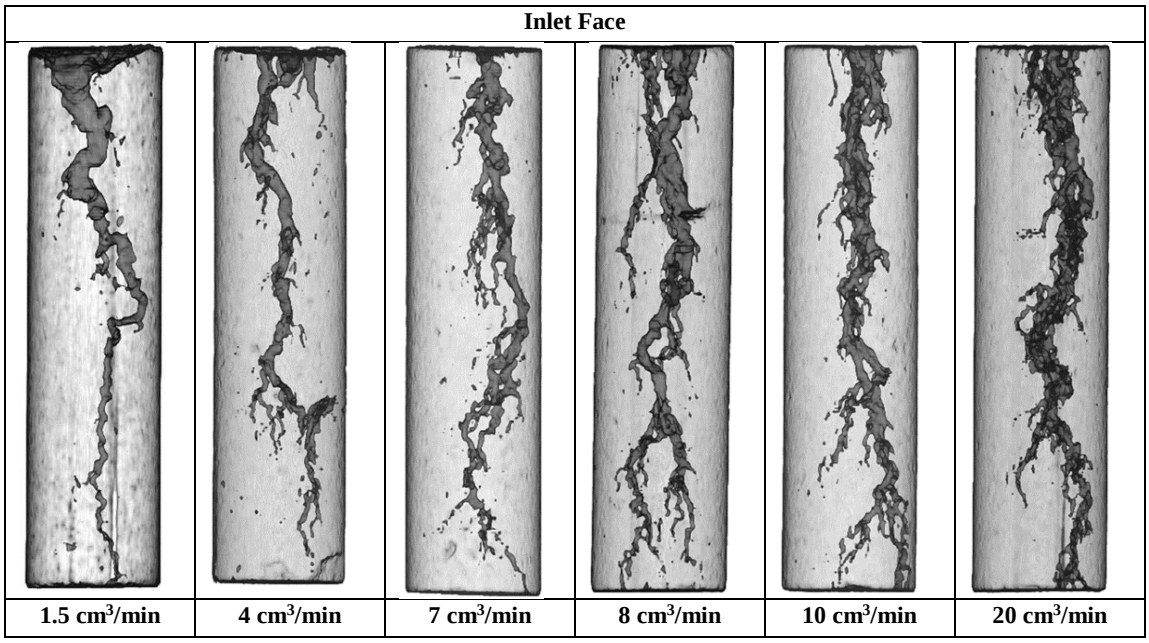

Fig. 23–Dissolution patterns identified from 3D scan images of core samples treated with 10 wt% MSA at 320°F.

Fig. 24 presents the effect of temperature on acid efficiency. This effect is twofold: first, the effect of temperature on the optimum injection rate (an increase in temperature shifted the optimum flow rate to higher values); second, the effect of temperature on the acid volume required to breakthrough (an increase in temperature increased the pore volumes required to breakthrough, decreasing the efficiency for the wormhole formation). The effects of temperature observed with MSA are consistent with those reported for HCl by previous investigators (Wang et al. 1993; Fredd and Fogler 1999; Bazin 2001) .The lowest volumes of acid to breakthrough were obtained at

injection rates of 2 and 7 cm^3/min, and therefore, these are considered the optimum rates when 10 wt% MSA is used to stimulate limestone cores at temperatures of 80 and 320°F, respectively.

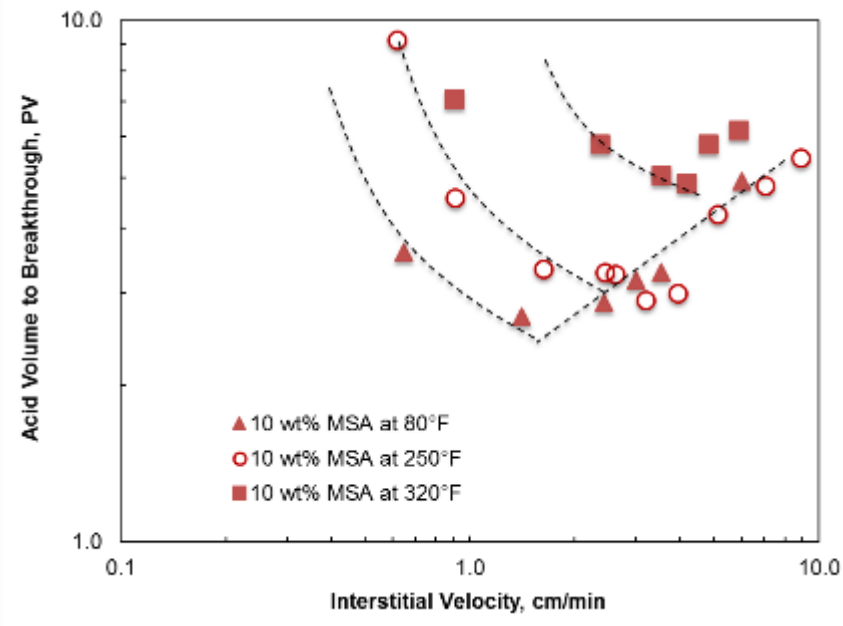

Fig. 24–Effect of temperature on the number of pore volumes to breakthrough with 10 wt% MSA.

The observed increase in the number of pore volumes required to breakthrough (or the decrease in acid efficiency) is a result of the acid becoming more mass-transfer limited as the temperature is increased. Because of a higher acid reactivity at higher temperatures, the acid is significantly consumed on the wormhole walls and in lateral branches, being therefore less effectively transported to the tip of the wormhole. Consequently, the average diameter of the dominant wormhole increased with temperature, as shown in **Fig. 25**. In this figure the wormhole size at optimum injection

rate conditions, is presented. The wormhole average diameter increased from 0.10 in. at 80°F, to 0.15 in. at 250°F, to 0.22 in. at 320°F.

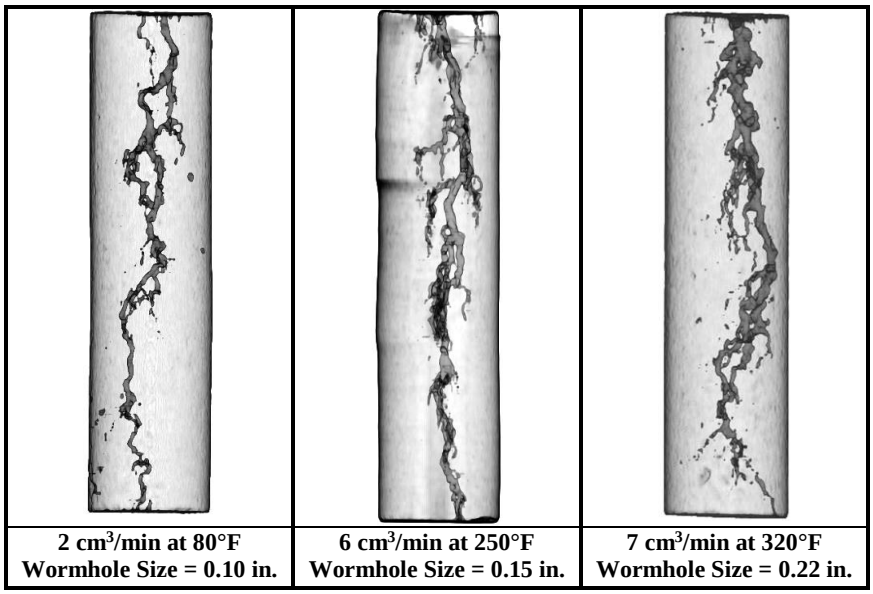

Fig. 25–Effect of temperature on the wormhole size near the optimum injection rates for 10 wt% MSA.

A comparison of the wormhole fractal dimensions provides an additional insight into the effect of temperature on dissolution structure. When the fractal dimension values of the dissolution patterns created at optimum injection rates, for the different temperatures tested, are compared, a trend of increasing pattern complexity with increasing temperature can be observed. For example, a fractal dimension value of 1.56 was computed at optimum rate conditions (2 cm^3/min) for the case of 80°F. This value is lower than the one computed for the case of 250°F, 1.61, also at optimum conditions (6 cm^3/min). For the highest tested temperature (320°F), a maximum fractal dimension value of 1.65 was obtained at optimum rate conditions (7 cm^3/min).

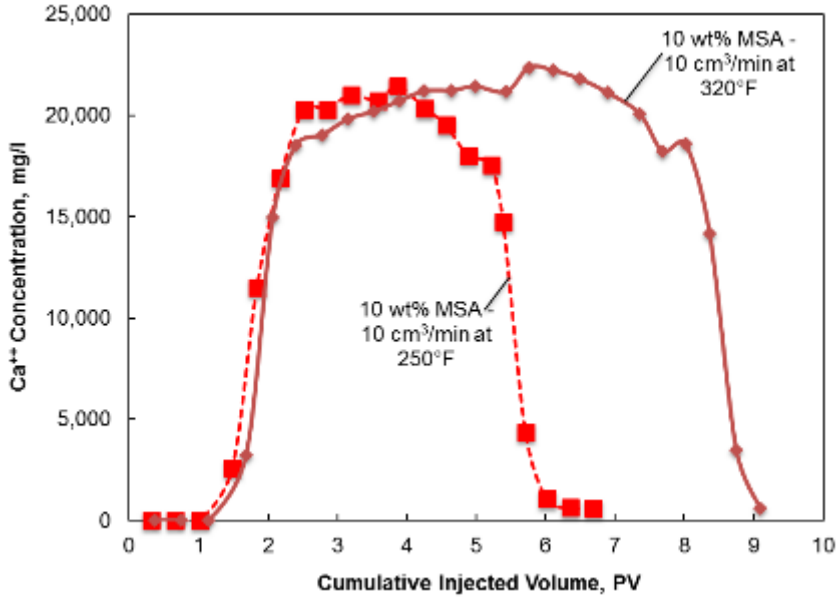

Fig. 26–Calcium concentration in the coreflood effluent samples collected for experiments with MSA at 250°F and 320°F (10 cm^3/min).

Fig. 26 shows the comparison of calcium concentration of the effluent samples collected for experiments with 10 wt% MSA at an injection rate of 10 cm^3/min, at the tested temperatures of 250 and 320°F. As expected, the maximum calcium concentrations obtained from ICP analysis (± 4%, relative standard deviation) were comparable for both the experiments.

Effects of Acid Concentration

The effect of acid concentration on wormhole formation at 250°F was investigated by performing additional coreflood tests using different aqueous MSA solutions (5 and 20 wt%). Coreflood experiments were run for each acid concentration, at injection rates from 1 to 25 cm^3/min, using Indiana limestone cores. The properties of

the core samples used and the results obtained from coreflood testing are given in **Tables 5 and 6**, for 5 and 20 wt% respectively.

TABLE 5—PROPERTIES OF LIMESTONE CORES USED WITH 5 WT% MSA AT 250°F AND SUMMARY OF COREFLOOD RESULTS

Core No.	Pore Volume, cm^3	Porosity, vol%	Injection Rate, cm^3/min	Acid Vol. to Breakthrough, PV
54	25.06	14.4	1.0	18.59
64	26.52	15.3	2.0	10.16
55	25.61	14.7	4.0	10.00
75	23.94	13.8	5.0	9.15
56	26.05	15.0	6.0	10.27
65	25.80	14.8	10.0	10.56
67	25.26	14.5	20.0	15.64

Average Porosity = 15 vol%

Average Permeability = 155 md

Fig. 27 presents the effect of acid concentration on acid efficiency. Decreasing the acid concentration tends to decrease the optimum injection rate. The reduced reaction rates at the lower acid concentrations require a reduced acid flux to achieve the optimum conditions. On the other hand, limestone cores acidized with MSA at a lower concentration (i.e., 5 wt% MSA) exhibit wormholes with more branching than acidizing with a more concentrated MSA aqueous solution (i.e., 20 wt% MSA) at the same injection rate; therefore, a lower live acid penetration is obtained (in other words, more acid volume is required).

TABLE 6—PROPERTIES OF LIMESTONE CORES USED WITH 20 WT% MSA AT 250°F AND SUMMARY OF COREFLOOD RESULTS				
Core No.	Pore Volume, cm^3	Porosity, vol%	Injection Rate, cm^3/min	Acid Vol. to Breakthrough, PV
18	27.63	15.9	1.5	2.22
70	24.54	14.1	3.5	1.31
66	24.50	14.1	6.0	1.29
31	23.04	13.3	10.0	1.90
49	26.39	15.2	25.0	3.16
Average Porosity = 15 vol% Average Permeability = 251 md				

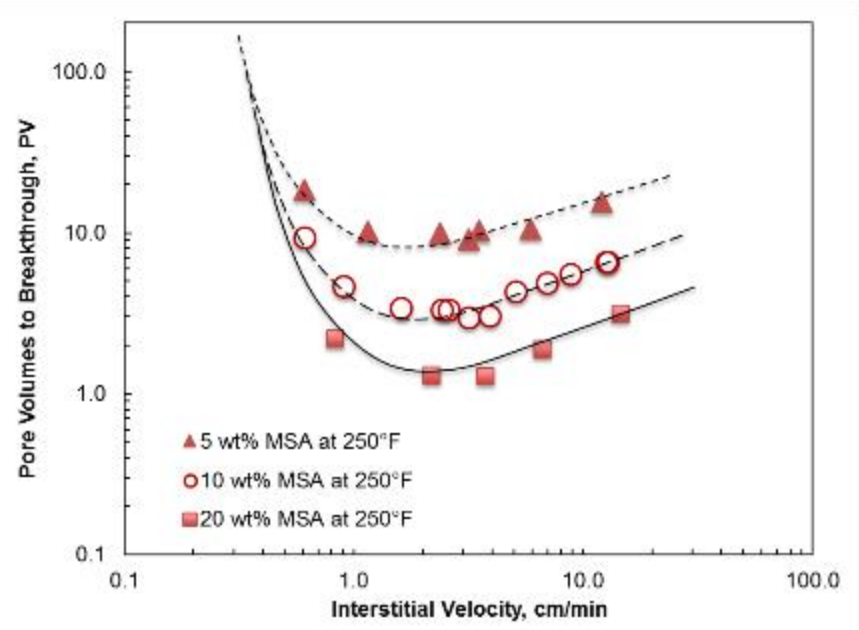

Fig. 27–Effect of acid concentration on the number of pore volumes to breakthrough at 250°F.

The effects of acid concentration observed with MSA are consistent with those reported for the case of HCl by previous investigators (Wang et al. 1993; Bazin 2001). The lowest volumes of acid to breakthrough were obtained at injection rates of 5 and 6 cm^3/min, and therefore, these are considered the optimum rates when 5 and 20 wt% MSA, respectively, are used to stimulate limestone cores at a temperature of 250°F.

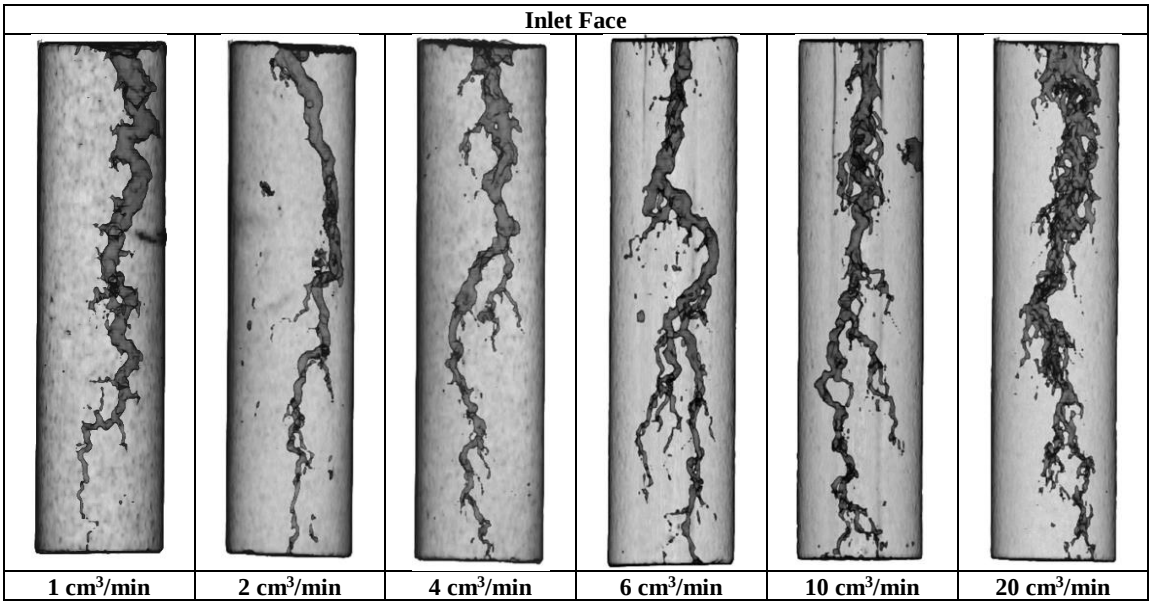

Fig. 28–Dissolution patterns identified from 3D scan images of core samples treated with 5 wt% MSA at 250°F.

The dissolution structures that were created by the injection of MSA in limestone cores at 250°F can be characterized by analyzing the CT-scan images of the treated cores (**Figs. 28 through 30**). Since the effective diffusivity of an aqueous MSA solution decreases with decreasing acid concentration, a lower overall reactivity of the less concentrated MSA systems causes a more homogeneous dissolution pattern (or less dominant wormholing/channeling) since fresh acid can penetrate into more pores. This

behavior is similar to what it has been reported for other less reactive systems such as EDTA and acetic acid (Fredd and Fogler 1998).

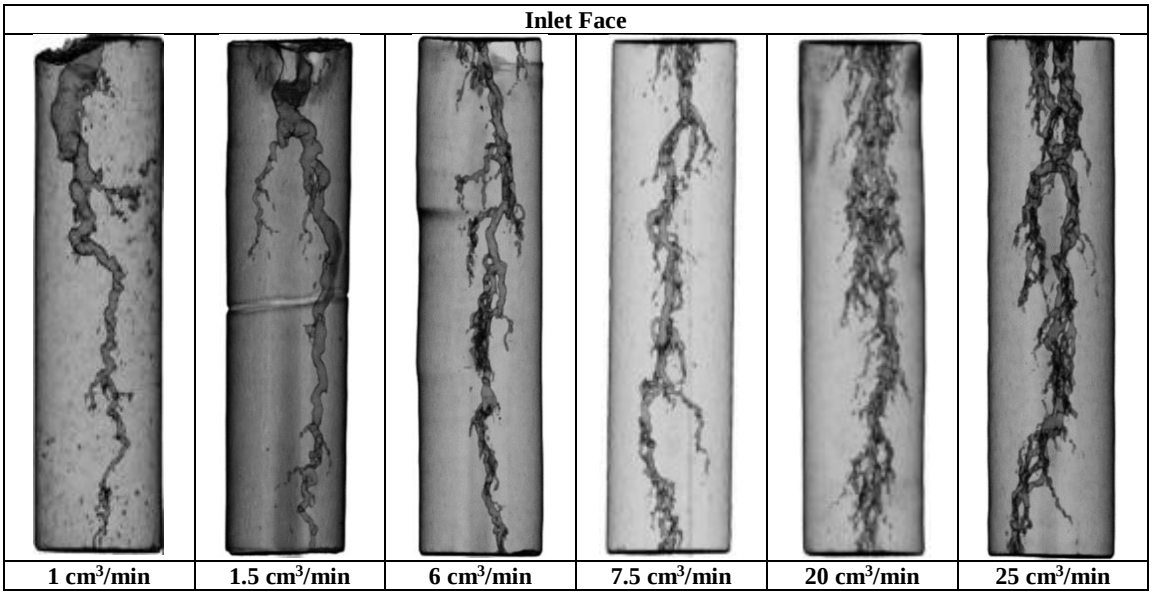

Fig. 29–Dissolution patterns identified from 3D scan images of core samples treated with 10 wt% MSA at 250°F.

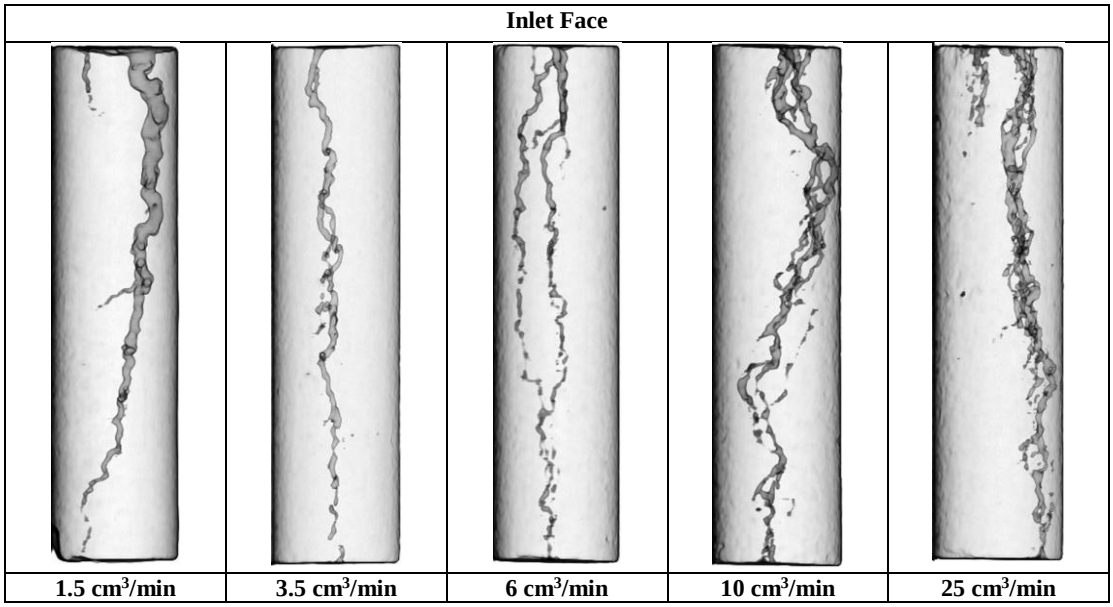

Fig. 30–Dissolution patterns identified from 3D scan images of core samples treated with 20 wt% MSA at 250°F.

By comparing Figs. 28 and 29 (5 wt% vs. 10 wt% MSA), it can be noticed that for the case of 5 wt% MSA, lower injection rates are required to have face dissolution and to create conical wormholes. Also, at intermediate and high injection rates the degree of wormhole ramification was higher. Even at injection rates as low as 6 cm^3/min, some degree of branching was observed when 5 wt% MSA was injected. In general, the size of the wormholes tends to increase at lower concentrations.

By comparing Figs. 29 and 30 (10 wt% vs. 20 wt% MSA), it can be noticed that at low-injection rates the degree of face dissolution was lower at low injection rates for the case of 20 wt% MSA. Even at injection rates as low as 1.5 cm^3/min, almost no face dissolution was observed. Also, higher injection rates are required to achieve same degree of wormhole ramification; however, the generation of competing wormholes was observed. In general, the size of the wormholes tends to decrease at higher concentrations.

The mass of acid consumed at the optimum injection rates for the three different acid concentrations tested is compared in **Table 7**. From the results using limestone, in terms of both acid consumption (mass of acid) and injection time (volume of acid injected), a high MSA concentration was better. These results contradict previous trends with HCl (Wang et al. 1993; Bazin 2001). However, the efficiency of MSA at high acid concentration was considerably improved by the high-temperature conditions (250°F) at which the tests in the present study were conducted (as opposed to room temperature in the previous studies).

TABLE 7—AMOUNT (MASS) OF ACID INJECTED TO PENETRATE THE LIMESTONE CORES AT DIFFERENT ACID CONCENTRATIONS		
Acid Concentration, wt%	Acid Injected, V/VP	Mass of Acid, g
5	9.15	11.1
10	2.91	8.6
20	1.29	6.9

Effects of Core Permeability

The effect of core permeability on wormhole formation with 10 wt% MSA at 250°F was investigated by performing additional coreflood tests using low-permeability limestone cores (14 md, average permeability). Eight low permeability coreflood experiments were run at injection rates from 1 to 10 cm^3/min. The properties of the core samples used and the results obtained from coreflood testing are given in **Table 8**.

The permeability of the carbonate porous media has an effect on wormholing efficiency, especially in the case of mass-transfer limited reactions, such as the reaction of MSA and limestone at high temperatures, where branching is more prominent in higher permeability cores for the same flow rate conditions. Also, as permeability decreases live acid enters new pore space less easily, then increasing the tendency for dissolution channels to become dominant. For example, CT-scan images of the acidized low permeability cores (**Fig. 31**) showed a lower degree of branching, and more dominant wormholes, as compared to the corresponding high permeability cores previously presented in Fig. 29.

An indirect measure of channel branchedness (pattern complexity) can be obtained by computing the fractal dimension of the 2D patterns generated by the reaction of 10 wt% MSA in low and high permeability limestone cores at the same temperature conditions. If the branches are numerous and small in diameter, a high fractal dimension will be obtained from the 2D CT-scan images. On the other hand, single dominant wormholes will result in channels of low fractal dimension. **Fig. 32** shows a general decrease in the fractal dimension value for wormholes propagated in low permeability cores.

TABLE 8—PROPERTIES OF LOW PERMEABILITY LIMESTONE CORES USED WITH 10 WT% MSA AT 250°F AND SUMMARY OF COREFLOOD RESULTS

Core No.	Pore Volume, cm^3	Porosity, vol%	Permeability, md	Injection Rate, cm^3/min	Acid Vol. to Breakthrough, PV
95	24.54	14.1	7	1.0	3.02
15	22.41	12.9	20	2.0	2.17
97	25.36	14.6	5	3.0	2.19
16	22.86	13.2	25	4.0	2.28
94	24.63	14.2	7	5.0	2.51
96	25.19	14.5	7	6.0	2.66
89	27.82	16.0	11	8.0	2.78
17	23.57	13.6	28	10.0	3.29

Average Porosity = 14 vol%

Average Permeability = 14 md

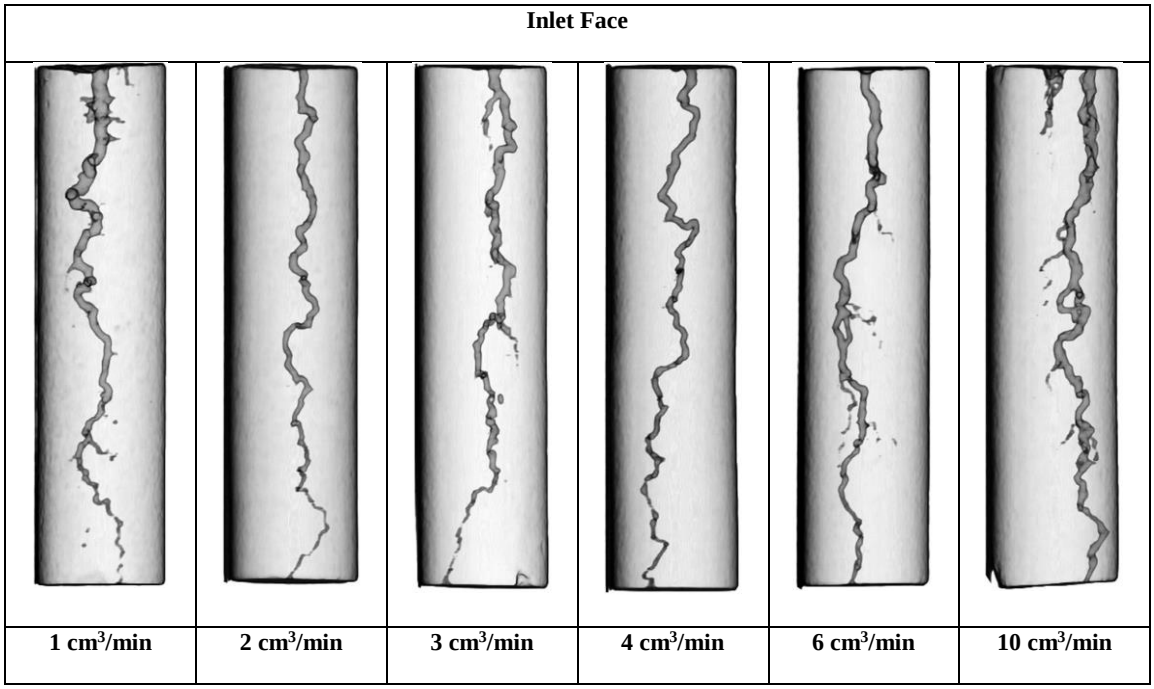

Fig. 31–Dissolution patterns identified from 3D scan images of low permeability core samples treated with 10 wt% MSA at 250°F.

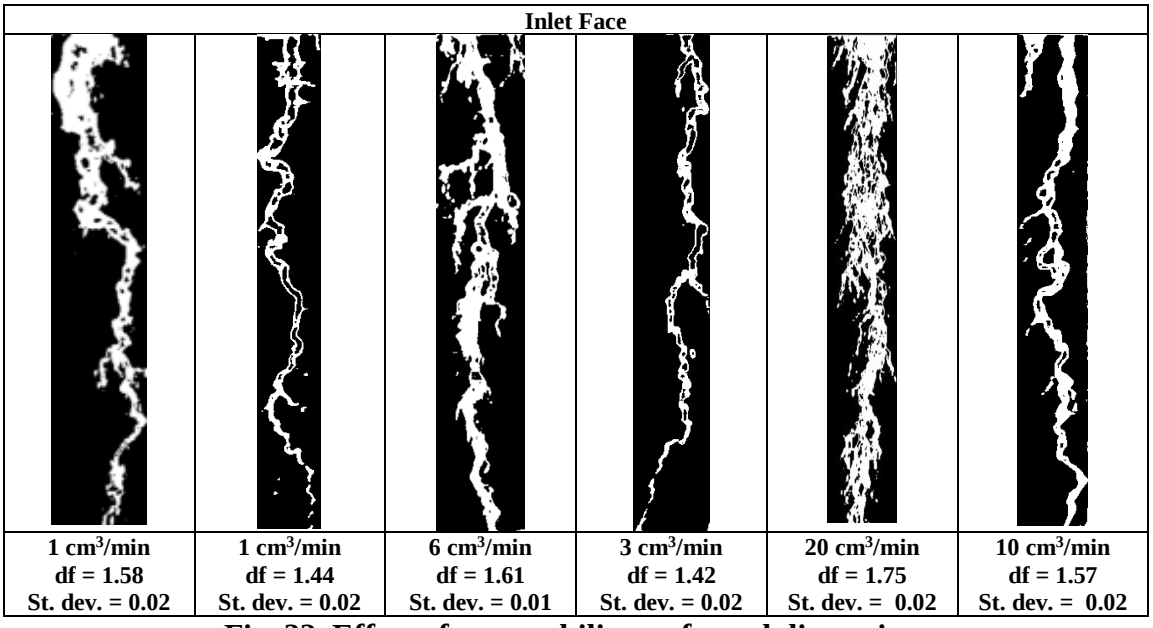

Fig. 32–Effect of permeability on fractal dimension.

The decrease in branching observed in low permeability cores quicken channel propagation. Consequently, lower acid volumes to breakthrough and lower rates at the optimum injection condition were required for the lower permeability materials. **Fig. 33** compares the coreflood data for low (14 md) and high (160 md) permeability Indiana limestone cores acidized with 10 wt% MSA at 250°F. It can be observed that the lower permeability cores required less fluid to stimulate.

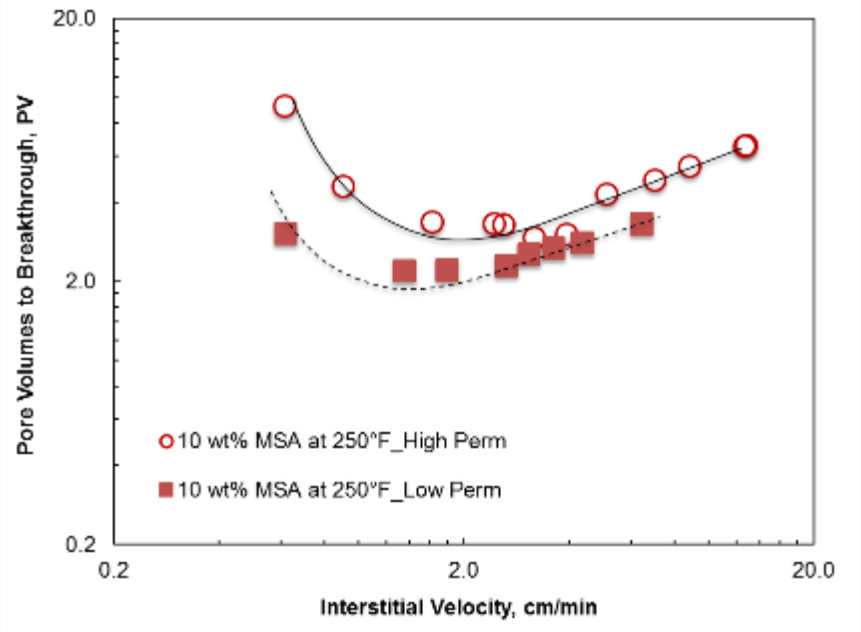

Fig. 33–Effect of core permeability on the number of pore volumes to breakthrough at 250°F, using 10 wt% MSA.

Conclusions

A 10 wt% MSA aqueous acid solution was used to stimulate limestone cores using a coreflood setup. The effect of temperature, acid concentration, and rock

permeability on the propagation of MSA in carbonate cores were examined in detail. Based on the results obtained, the following conclusions can be drawn:

1. The efficiency of the wormhole formation with 10 wt% MSA in limestone cores decreased with increasing temperature. Besides, the optimum flow rate was shifted to higher values.
2. Decreasing the MSA concentration decreased the optimum injection rate. Additionally, at the same injection rates, higher acid volumes were required because more branched dissolution structures were created in limestone cores acidized at lower concentrations (i.e., 5 wt% MSA) than in cores acidized with more concentrated MSA aqueous solutions (i.e., 20 wt% MSA).
3. When acidizing limestone cores at high-temperature conditions, in terms of both mass of acid consumed and volume of acid injected, high MSA concentrations are preferred.
4. Since branching was less prominent in lower permeability cores for the same flow rate conditions, channel propagation was accelerated. Consequently, lower acid volumes to breakthrough and lower rates at the optimum injection condition were required for the lower permeability materials.

CHAPTER V

ACIDIZING HIGH-TEMPERATURE DOLOMITE FORMATIONS WITH METHANESULFONIC ACID

Introduction

Many carbonate rocks contain a significant amount of dolomite. Most dolostones are formed by dolomitization (Zenger and Mazzullo 1982), or the replacement of limestone by dolomite, a process which usually increases porosity but impairs permeability due to precipitation of dolomite crystals. Intercrystalline porosity is common in dolomite replacements of limestone. However, dolomitization may lead to decreased porosity if sustained placement of diagenetic dolomite cements occurs (Lucia and Major 1994), or to increased permeability in cases when the intercrystalline porosity is preserved after total replacement of limestone by dolomite, without precipitation of "excess" dolomite cement (Ahr 2008).

Several studies have looked at the effects of acidizing in dolomite rocks. Lund et al. (1973), for example, examined the reaction rate of pure dolomite marble with HCl using a rotating disk technique. They found that the dissolution of dolomite is reaction rate limited at temperatures less than about 125°F and mass transfer limited at temperatures greater than about 200°F. Between these two temperatures, the dissolution is influenced by both the kinetics of the surface reaction and the rate of mass transfer.

More recent works have focused on determining the effect of rock mineralogy on dolomite reactivity. Anderson (1991), for instance, looked into the reactivity of the San

Andres dolomite using actual formation samples from several fields. The experimental procedure and data analysis techniques employed were the same as those of Lund et al. (1973). However, by comparing the results of the study against the industry-accepted values the author concluded that different dolomites may have different surface kinetics.

Taylor et al. (2004b), on the other hand, measured the acid dissolution rate changes using reservoir rocks which varied from 3 to 100 wt% dolomite. The experimental results showed that, from almost pure calcite to almost pure dolomite, rock dissolution rates varied by more than an order of magnitude due to rock mineralogy. An additional dependence of the reaction rates on the presence of trace minerals, such as clays, was also determined. Other dolomite reaction kinetic studies are described in detail in Herman and White (1985), Gautelier et al. (1999), Nasr-El-Din et al. (2002), and Taylor et al. (2004a).

The acidizing of carbonate rocks has been the subject of numerous technical papers (Bazin et al. 1997; Buijse 1997; Daccord, Lenormand, et al. 1993; Daccord, Liétard, et al. 1993; Daccord et al. 1989; Fredd 2000b; Fredd and Miller 2000; Fredd et al. 1997; Gdanski 1999; Glasbergen et al. 2005; Gong and El-Rabaa 1999; Hung et al. 1989; Panga et al. 2002; Williams et al. 1979) which have exposed the complexity of the wormholing process. Some of these works have focused, in particular, on the characterization of dolomite dissolution by the injection of acid in coreflood experiments. As an example, Hoefner and Fogler (1988) studied the acidization of dolomite cores at room temperature using aqueous HCl. At low temperatures, where the dissolution rate of dolomite is reaction-rate limited and orders of magnitude lower than

that of limestone, they observed an almost uniform (very highly branched) dissolution of the pore space when dolomite was treated with HCl at high injection rates. From the experimental results, the volume of acid required to reach breakthrough in dolomite cores increased with increasing injection rates (or decreasing Damkohler numbers). However, in a later study (Hoefner and Fogler 1989) the authors suggested that at very low rates the volume must again increase, resulting in the existence of an optimum injection rate (or optimum Damkohler number).

Wang et al. (1993) confirmed the results obtained by Hoefner and Fogler (1989) in relation with the injection of HCl in dolomite cores at room temperature. They noted that when the acid injection rate was increased the volume of acid required to penetrate the cores also increased. Moreover, no optimum rate was observed for dolomite cores at room temperature. Additionally, they reported that, compared with the limestone results, the dolomite cores required relatively large volumes of acid to breakthrough. Also, from the observation of the inlet faces of the dolomite cores after acid injection, they described that the dissolution process produced a spongy rock structure instead of single dominant wormholes. Another important contribution of their work was the study of the effect of temperature on the dissolution efficiency of HCl in dolomite rock.

Bazin et al. (1996) characterized the acid (HCl) wormholing in dolomite rock by performing coreflood experiments with X-ray computed tomography visualization (CT scan). From the CT scan observations they reported that, at low temperatures, the low reactivity dolomite produced dissolution structures (wormholes) that were comparable to the structures obtained at low flow rates with limestone. Even more, they found a

similarity in the size of the wormholes obtained in dolomite cores with respect to those produced in limestone cores at low flow rates.

All of the experimental studies mentioned previously used HCl solutions as stimulation fluid for the low-reactive dolomite. In addition, the use of retarded HCl-based systems, such as emulsified acids (Kasza et al. 2006; Laws et al. 2005; Nasr-El-Din et al. 2008; Nasr-El-Din, Solares, et al. 2001; Navarrete et al. 2000) and gelled acids (Nasr-El-Din et al. 2002), in particular in high-temperature acid fracturing applications, has also been recommended. In the same line of research, other authors (Bartko et al. 2003; Harp et al. 1968; Nasr-El-Din, Lynn, et al. 2001) have studied the use of organic acids (i.e., formic or acetic acid) to stimulate wells containing dolomite. Much less work has been published regarding the application of alternative, unconventional, fluid technologies for dolomite acidizing. For instance, preliminary experiments with EDTA at ambient temperature have revealed no significant dolomite dissolution (Fredd 2000a). The application of sulfonic acids, and specifically methanesulfonic acid (MSA), for the matrix acidizing of dolomite formations has not been studied before.

The current study expands on the results obtained for the injection of MSA in limestone cores (Ortega et al. 2014) by performing coreflood experiments with dolomite to evaluate the effect of rock mineralogy on the wormholing process. As expected, the coreflood analysis showed a reduced efficiency of MSA at 250°F when it was used to stimulate dolomite rocks as compared to limestone. An optimum injection condition corresponding to the different parameter tested was identified, with no sign of methanesulfonate salt precipitation.

X-Ray Fluorescence of Dolomite Samples

TABLE 9—ELEMENTAL ANALYSIS OF A DOLOMITE CORE SAMPLE USING THE XRF TECHNIQUE	
Element	Concentration, wt%
Ca	23.5
Mg	10.2
C	12.6
O	51.3
Si	0.08
Fe	0.25
S	0.49
Na	1.16
K	0.14
Cl	0.11
Sr	0.01
Sn	0.01
Mn	0.02

The initial composition of the dolomite cores was obtained by performing X-ray fluorescence (XRF) analysis of a core sample. A disk with a diameter of 1.5-in and a thickness of 0.75-in. was cut and tested using the XRF technique. Results from the analysis (**Table 9**) showed that the dolomite sample contained more than 98 wt% of calcium, magnesium, carbon, and oxygen. **Table 10** presents the average calcium to magnesium molar ratio, which is about 1.4 for the analyzed sample. A molar ratio larger than 1 is indicative of a calcian-rich dolomite.

TABLE 10—CALCIUM TO MAGNESIUM MOLAR RATIO IN DOLOMITE ROCKS USED IN THE STUDY		
Element	Concentration, mol%	Molar Ratio of Ca to Mg
Ca	11.0	1.4
Mg	7.9	

Solubility of Dolomite Cores in MSA

Similar to limestone, calcium magnesium carbonate (dolomite) dissolves in strong acids, releasing carbon dioxide, following the reaction stoichiometry shown in **Eq. 3** (Lund et al. 1973). Also similar to limestone, the dissolution reaction in Eq. 3 is considered irreversible, therefore the influence of mass transfer is attributable to the transport of reactants to the mineral surface.

$$CaMg(CO_3)_2 + 4H^+ \rightarrow Ca^{++} + Mg^{++} + 2H_2O + 2CO_2 \cdots\cdots (3)$$

The solubility of dolomite core samples in 10 wt% MSA was tested by performing tests at static conditions and at room temperature (80°F). Two different core samples were prepared by cutting small pieces of dolomite rock of different sizes (coarse and fine size). Fifteen grams of coarse size sample and 6 grams of fine size sample were poured into a beaker filled with 100 ml and 50 ml of 10 wt% MSA, respectively. The samples were left immersed in acid for period of 4 hours. After reaction, the solid deposits remaining were filtered and washed with deionized water, in order to remove

any acid excess. The deposits were then dried so a SEM/EDX analysis could be performed with the objective of determining their chemical composition.

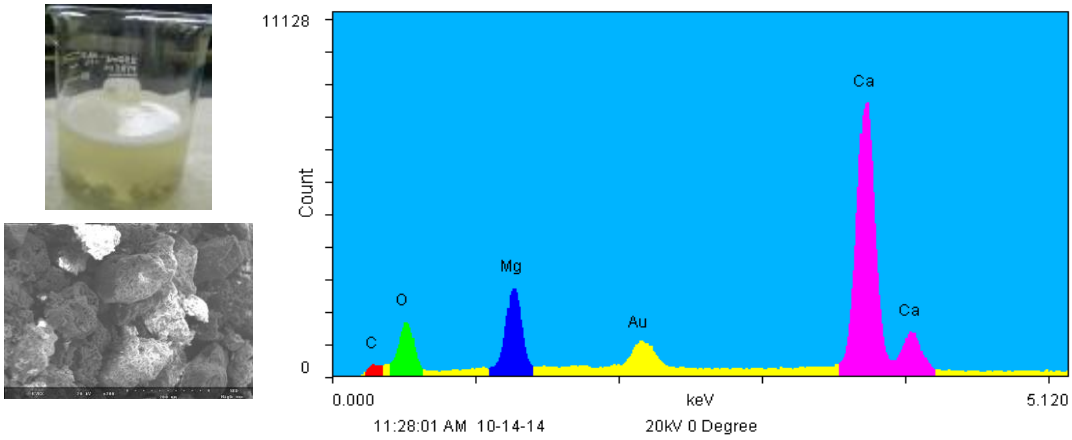

Elements:	WT%	AT%	K_A	K_F	K_Z	Intensity	P/bkg
C K	11.39	17.23	0.199	1	1.032	48.516	1.1
O K	57.17	64.96	0.149	1	1.015	351.719	7.4
MgK	12.08	9.03	0.299	1.001	0.974	612.812	6.4
CaK	19.36	8.78	1	1	0.944	2606.2	29.1

Fig. 34–SEM/EDX analysis of sediment remaining after reaction of coarse size dolomite samples and 10 wt% MSA.

Results from the SEM/EDX analysis of the reaction residue are presented for both of the tested samples and are shown in **Figs. 34 and 35**. These results show no signs of methanesulfonate salt precipitation (i.e., calcium or magnesium methanesulfonate), but instead show a deposit composition corresponding to dolomite rock with a molar calcium to magnesium ratio close to unity. From these static measurements at room temperature, it is evident that the rock under study shows great solubility in a 10 wt% MSA solution. It can be then expected that, at high bottomhole temperatures, the very fast reaction will result in quick acid spending and face dissolution (low treatment efficiency). On the other hand, accurate reaction kinetics data

will require the use of the rotating disk apparatus to simulate dynamic reaction conditions.

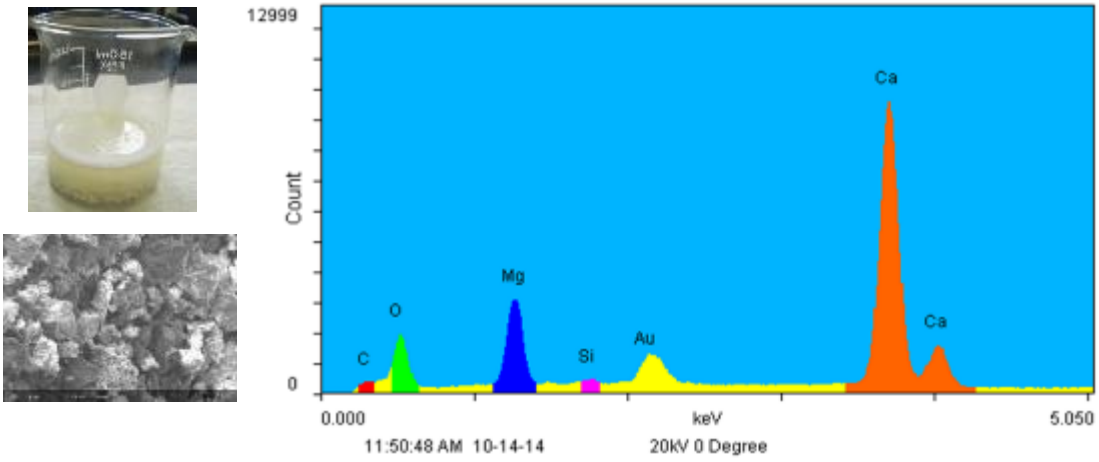

Elements:	WT%	AT%	K_A	K_F	K_Z	Intensity	P/bkg
C K	10.85	16.53	0.195	1	1.033	37.205	0.9
O K	56.91	65.1	0.148	1	1.015	283.227	6.5
MgK	12.15	9.14	0.299	1.001	0.974	503.835	6.2
SiK	0.23	0.15	0.427	1.002	0.973	16.2	0.2
CaK	19.87	9.08	0.998	1	0.944	2186.93	29.1

Fig. 35–SEM/EDX analysis of sediment remaining after reaction of coarse size dolomite samples and 10 wt% MSA.

CT-Scan Study of Fresh Core Samples

Core plugs (1.5-in. diameter and 6-in. length) were cut from a block of Silurian dolomite. Some of these plugs were screened by using a computerized tomography (CT) scanning. The objectives of the screening were to determine the degree of heterogeneity of the core samples, to indicate the possible presence of additional materials in the cores, and to measure core porosity. The porosity measurements were performed by using a two-scan technique, which involved making time-sequenced CT scans at the same physical location in a core at different known fluid saturations (for example, dry and

fluid saturated). Since this method eliminates any rock contribution, information about rock mineralogy becomes unnecessary (Davis et al. 1992).

Computed tomography is used to identify structural characteristics of core material such as core heterogeneity. CT scan images represent discrete X-ray attenuation information of the material scanned (Coles et al. 1995), usually provided in Hounsfield units (HU). In addition to a visual evaluation of the CT images, quantitative information such as porosity can be obtained from CT values with proper processing and calculations. For the case of this study, the porosity at each location in the core was obtained by subtracting the two images (pixel-by-pixel) and dividing by a calibration constant. **Eq. 4** was used to compute the core porosity:

$$\varphi = \frac{CTN_m^f - CTN_m^{vac}}{CTN_f - CTN_{vac}} \cdots\cdots\cdots\cdots\cdots (4)$$

In Eq. 4:

CTN_m^f – the measured CTN of water-filled core

CTN_m^{vac} – the measured CTN of clean, dry evacuated core

CTN_f – the measured CTN of water (defined to be 0 HU)

CTN_{vac} – the measured CTN of air (defined to be - 1,000 HU)

Even though the CT porosity measurements allow to determine the average porosity of a dry core sample, the main usefulness of these measurements is the ability to visualize the distribution of porosity on a small scale. As an example, **Fig.36** shows the

initial porosity distribution on a dolomite core sample (Core #79). Using the dual-scan method, the average initial porosity of the core was calculated as 10.7 ± 1.4 vol%, similar to the one estimated using the saturation method (12.0 vol%). From the same figure, the average fluid saturated CTN measurements and dry evacuated CTN measurements were 2,253 HU and 2,146 HU, respectively.

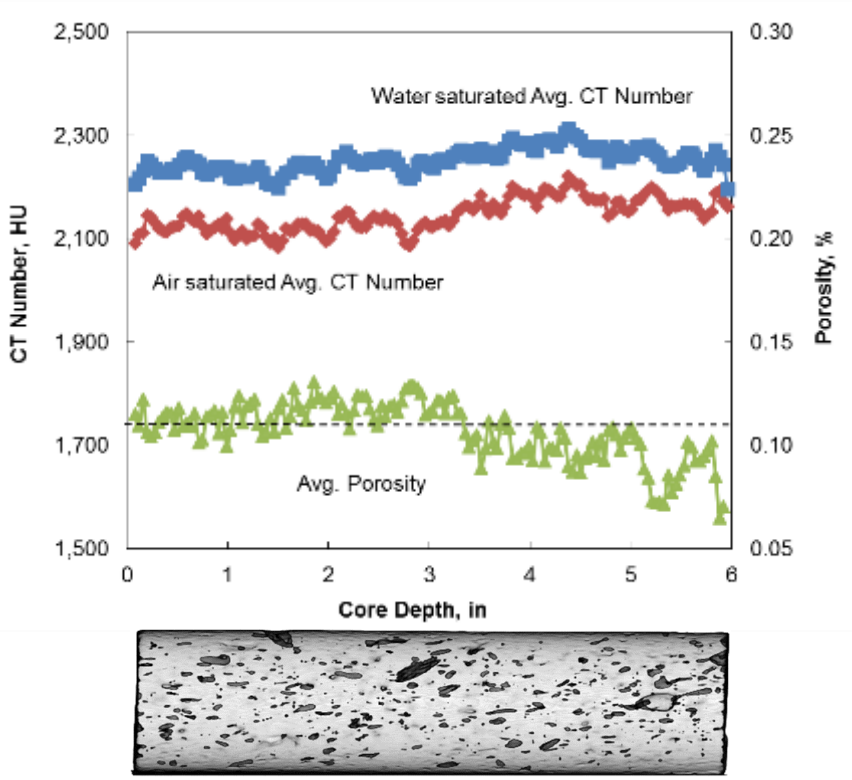

Fig. 36–CT-scan of fresh dolomite core samples (Core #79).

A procedure similar to the one described above (Core #79) was followed for other dolomite core samples used in the study. **Table 11** presents the calculated porosity values using the described method. The range of porosity values for the scanned core samples was between 6.5 and 16.5 vol%, with an average porosity of 12.2 ± 2.2 vol%.

On the other hand, the average porosity determined for the same set of samples by using the previously described saturation method was 12.4 vol%.

TABLE 11—DUAL SCAN CALCULATED INITIAL POROSITY OF DOLOMITE CORES

Core No.	Air Saturated Avg. CTN, HU	Water Saturated Avg. CTN, HU	Initial Porosity ± Std. Dev., vol%
82	2,075	2,218	14.3 ± 0.9%
79	2,146	2,253	10.7 ± 1.4%
81	2,083	2,180	9.7 ± 0.7%
83	2,057	2,197	14.1 ± 0.8%
Average	2,090	2,212	12.2 ± 2.3%

From the CTN measurements the core samples used in the study can be described as vuggy dolomite with streaks of limestone. These measurements are consistent with previously defined CT numbers for pure dolomite and pure limestone, respectively (Nevans et al. 1999). Also, CT numbers less than 2,200 are indicative of good porosity or fracturing. The CTN measurements of the cores used in the study depart from the theoretical value for pure dolomite due to the calcium-rich composition of the dolomite sample and the presence of vuggy porosity.

CT scan analysis of the fresh (pre-acid) core samples also served to indicate the degree of heterogeneity of the dolomite rock used during the coreflood experiments. By adding all of the porosity histograms (slice-by-slice, frequency histograms of porosity) obtained by scanning the core, the porosity distribution within an entire core (Core #79)

was determined. The standard deviation of the porosity histogram was then used as an indicator of porosity heterogeneity in the core. **Fig. 37** shows a whole-core porosity histogram measured for Core #79. The histogram corresponds to a homogeneous dolomite sample with a mean porosity value of 10.7 vol%. The standard deviation of the porosity distribution was calculated as 1.4 vol%.

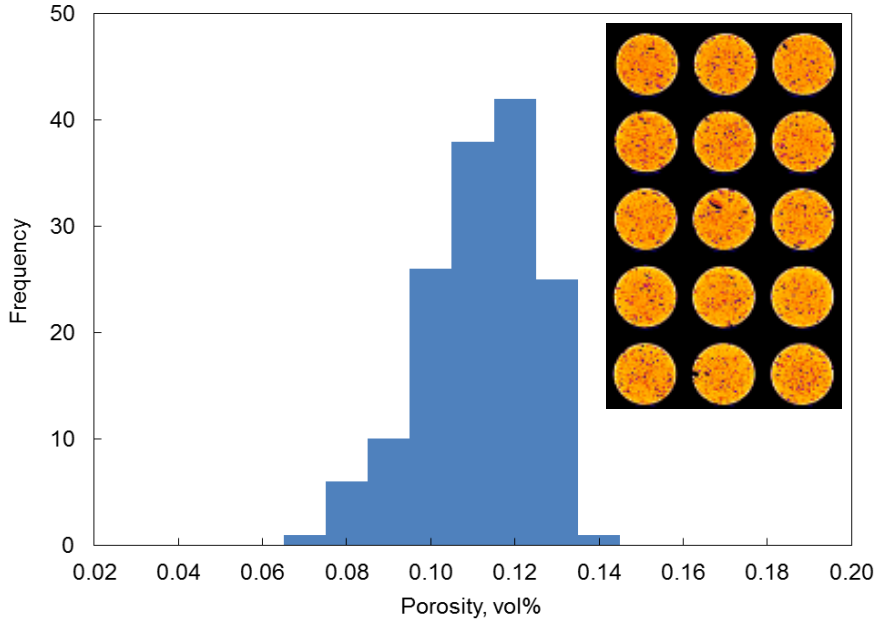

Fig. 37–The effects of porosity heterogeneity on the width of the porosity distribution (Core #79).

For the coreflood study, 7 cores were selected to test the MSA acid system; the cores were selected so that the rocks were mainly homogeneous dolomite. **Table 12** provides a description of all the cores selected to perform the coreflood study.

TABLE 12—PROPERTIES OF DOLOMITE CORES USED WITH 10 WT% MSA AT 250°F AND SUMMARY OF COREFLOOD RESULTS

Core No.	Pore Volume, cm^3	Porosity, vol%	Injection Rate, cm^3/min	Acid Vol. to Breakthrough, PV
91	20.71	11.9	2.0	18.48
115	20.33	11.7	3.0	8.25
82	21.99	12.7	4.0	9.20
79	20.80	12.0	5.0	8.67
81	24.02	13.8	6.0	9.16
90	22.50	12.9	8.0	11.96
83	19.18	11.0	10.0	13.90
Average Porosity = 12 vol%				
Average Permeability = 17 md				

Coreflood Study

Seven coreflood runs were performed using 10 wt% MSA, at injection rates of 2 to 10 cm^3/min. These runs were done to determine the effect of the injection rate on MSA performance, specifically, the acid volume to breakthrough and the resulting wormhole characteristics. This set of experiments was conducted at a temperature of 250°F. Table 12 presents a summary of the results obtained for each of the core samples used. During coreflood injection, the pressure drop across the core was plotted using the LabView® software. Samples of the coreflood effluent were collected and analyzed for calcium concentration, pH, and acid concentration.

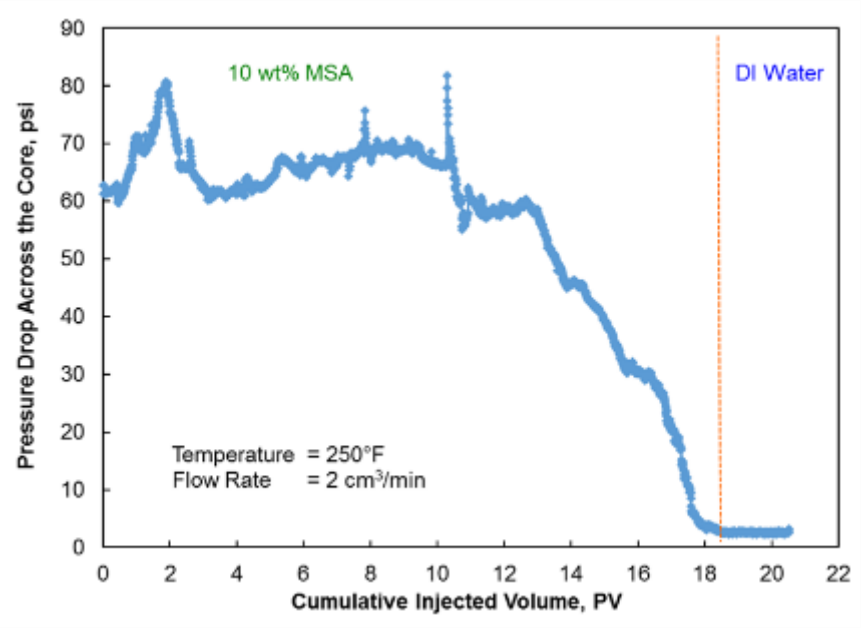

Fig. 38–Pressure drop across Core #91 during the injection of 10 wt% MSA at a rate of 2 cm^3/min.

The analyses performed for Core #91 are provided as an example of the complete coreflood procedure. **Fig. 38** shows the behavior of the pressure drop across the core during the injection of the 10 wt% MSA system at a rate of 2 cm^3/min. The differential pressure, which initially stabilized around 65 psi during the injection of water, started to decrease shortly after the acid injection began. This decrease in pressure indicates the reaction of the acid with the carbonate rock, and the creation of dissolution patterns (wormholes) as the acid front moved along the core length. The differential pressure continued to decrease with time until acid breakthrough occurred.

The volume of acid to breakthrough is defined as the volume of acid needed to propagate the wormhole through the length of the core. When breakthrough was achieved, a low and constant (stable) pressure drop was recorded from the coreflood

apparatus, indicating that the fluid was flowing through the created wormhole structures. For the current case, 18.5 pore volumes (PV) of acid were needed to achieve breakthrough (Fig. 38).

As MSA reacted with the carbonate rock creating dissolution channels along the core, the calcium and magnesium concentrations in the effluent samples started to increase. **Fig. 39** shows the calcium and magnesium concentrations in the core effluent samples, as measured by the ICP. The measured calcium and magnesium concentrations reached maximum values of 11,475 mg/l ± 5% and 6,340 mg/l ± 5%, respectively. These concentrations are in agreement with the theoretical values of calcium and magnesium that are expected from the dissolution of dolomite in a 10 wt% MSA solution.

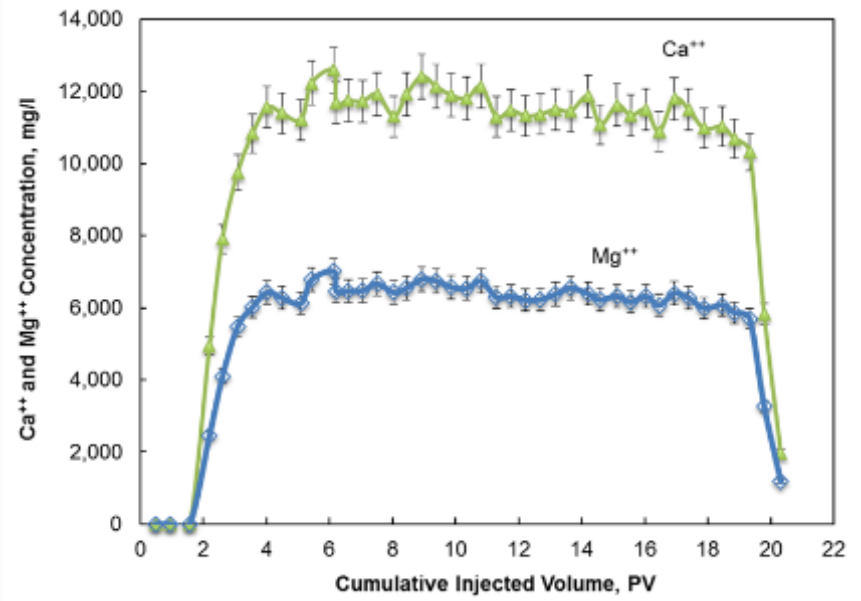

Fig. 39–Calcium and magnesium concentrations in the core effluent samples of Core #91. Error bars represent relative standard deviation (± 5%) from the measurements.

Fig. 40 shows the pH and acid concentration of the coreflood effluent samples for the same experiment. The pH was nearly 7 at the start of the injection (water). Then, it decreased with the injection of acid to a value of 1.3 (after acid breakthrough) and increased again as the injection of water resumed. As expected, an opposite trend was found for the final acid concentration in the effluent samples, which achieved a maximum value of 0.4 wt% MSA after acid breakthrough. This indicated that the acid was almost completely spent after its flow through the carbonate core.

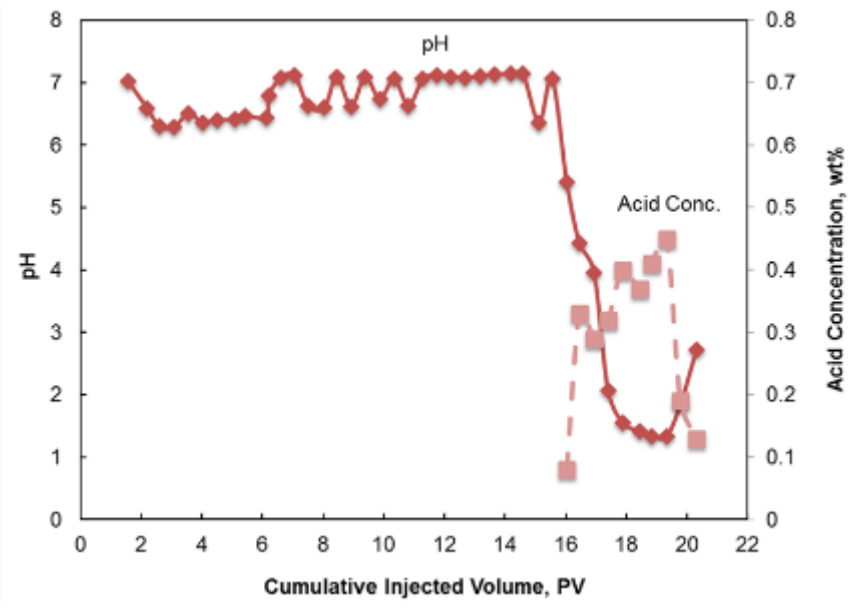

Fig. 40–pH and acid concentration in the core effluent samples of Core #91.

A procedure similar to the one explained above for Core #91 was followed for all the other core samples used in the study (Table 12). **Figs. 41 and 42** present the calcium and magnesium concentrations in the coreflood effluent samples, collected for some of the experiments at different injection rates. As in the case of Core #91, the calcium and

magnesium concentration increased with the injection of acid, reaching a maximum value, then decreased when the injection fluid was switched back to water.

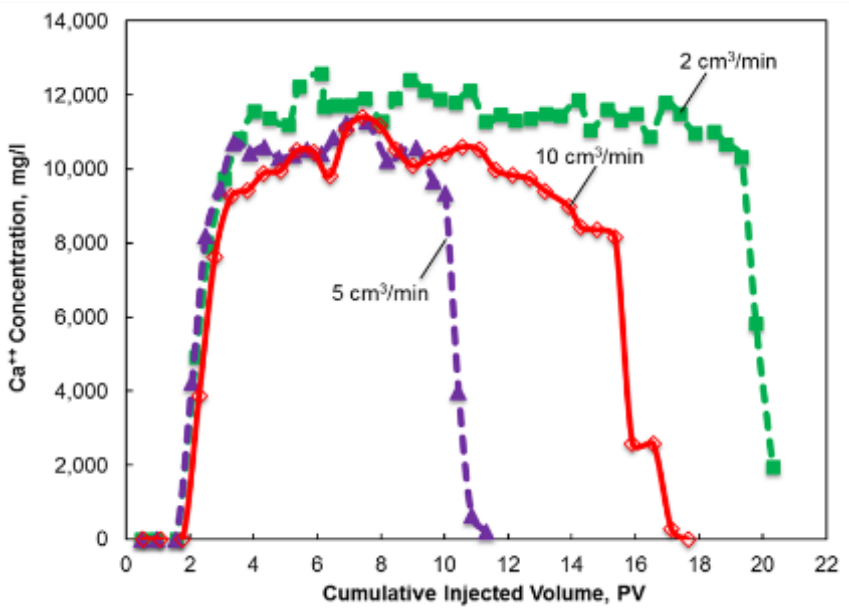

Fig. 41–Calcium concentration in the core effluent samples, collected for the various experiments with MSA at different injection rates.

The calcium and magnesium concentrations plotted in Figs. 41 and 42 indicate the amount of dolomite rock dissolved by the acid at each injection rate, and is a function of the acid/rock contact time and contact area. Both, the contact time and contact area, are minimized when the acid is injected at conditions close to the optimal. As a result, the highest peaks for calcium and magnesium concentration were observed when the acid was injected at conditions far from the optimal, for example 2 cm^3/min.

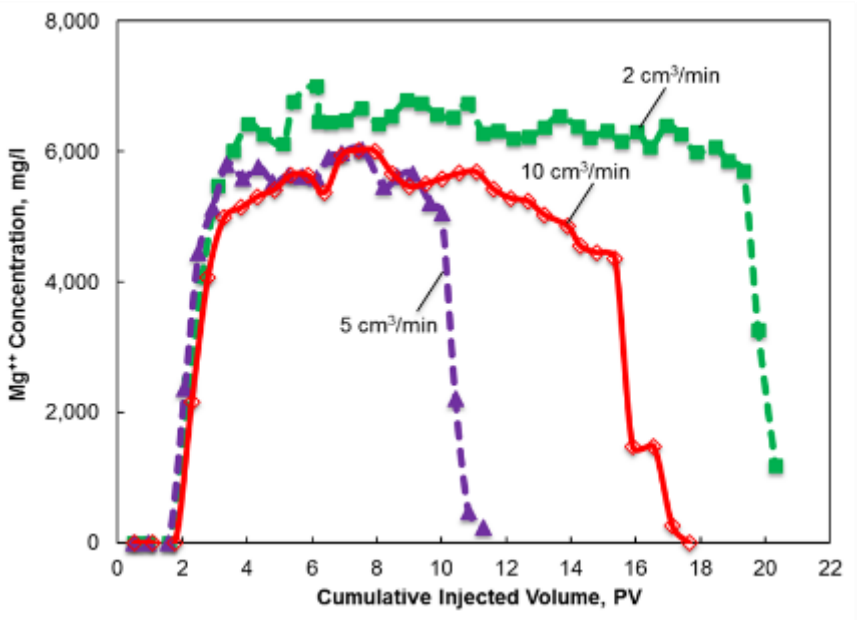

Fig. 42–Magnesium concentration in the core effluent samples collected for the various experiments with MSA at different injection rates.

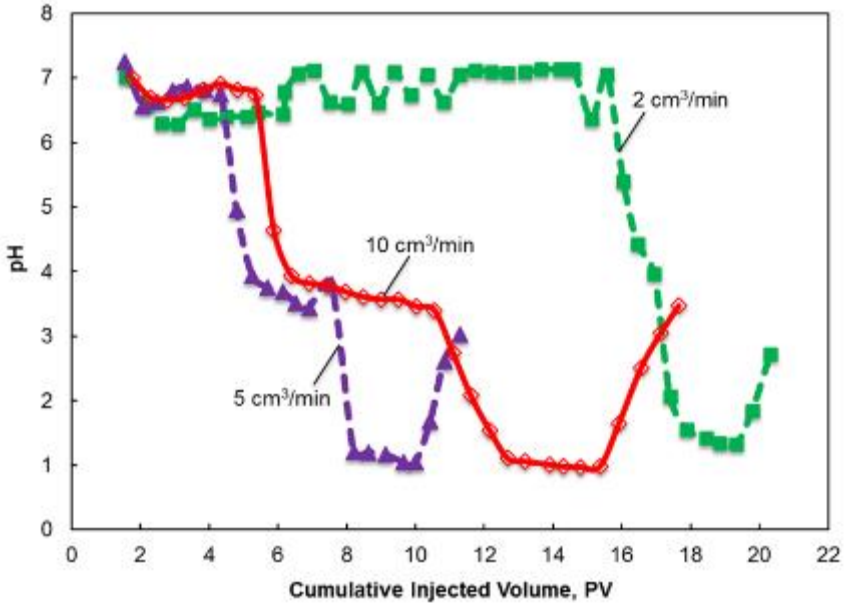

Fig. 43–pH of the core effluent samples, collected for the various experiments with MSA at different injection rates.

Similarly, the change in pH and acid concentration can be compared for all the cases tested. Since these two variables are inversely related (the higher the acid concentration, the lower the pH), they both can be used to confirm the breakthrough determined from the analysis of the pressure drop. For example, the decrease in pH measurements to a minimum value indicates acid breakthrough (**Fig. 43**). This minimum value of pH varied in the range of 0.98 (Core #83, 10 cm^3/min) to 1.33 (Core #91, 2 cm^3/min).

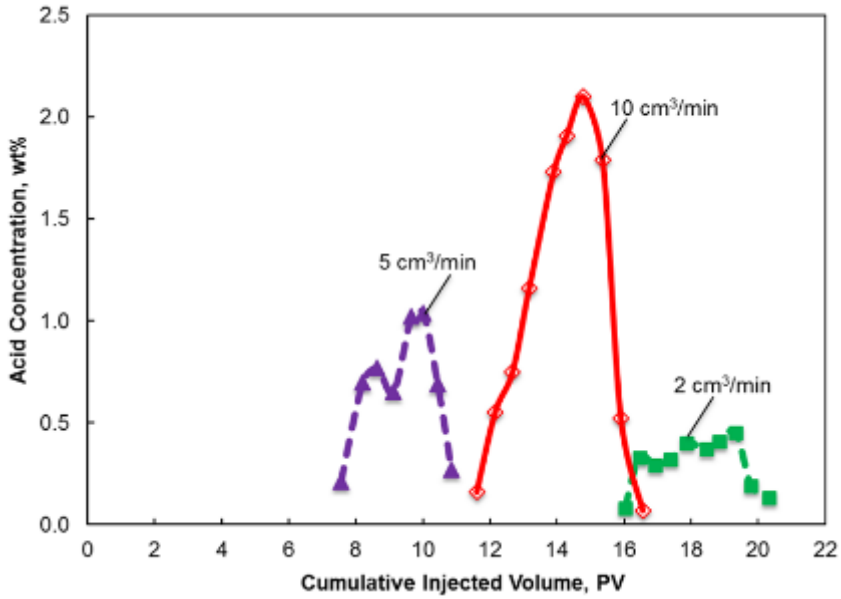

Fig. 44–Acid concentration in the coreflood effluent samples collected for the various experiments with MSA at different injection rates.

On the contrary, the peak (maximum) of the final acid concentration (**Fig. 44**) ranged between 0.45 wt% (Core #91, 2 cm^3/min) and 2.0 wt% (Core #83, 10 cm^3/min). The results presented in Figs. 43 and 44 demonstrate the dependency of pH and acid

concentration on the injection rate. The higher the acid injection rate, the lower the time the acid has for spending upon contact with the carbonate rock, therefore resulting in a higher acid concentration (and lower pH) of the core effluent samples.

Total Amount of Calcium and Magnesium in Effluent Samples

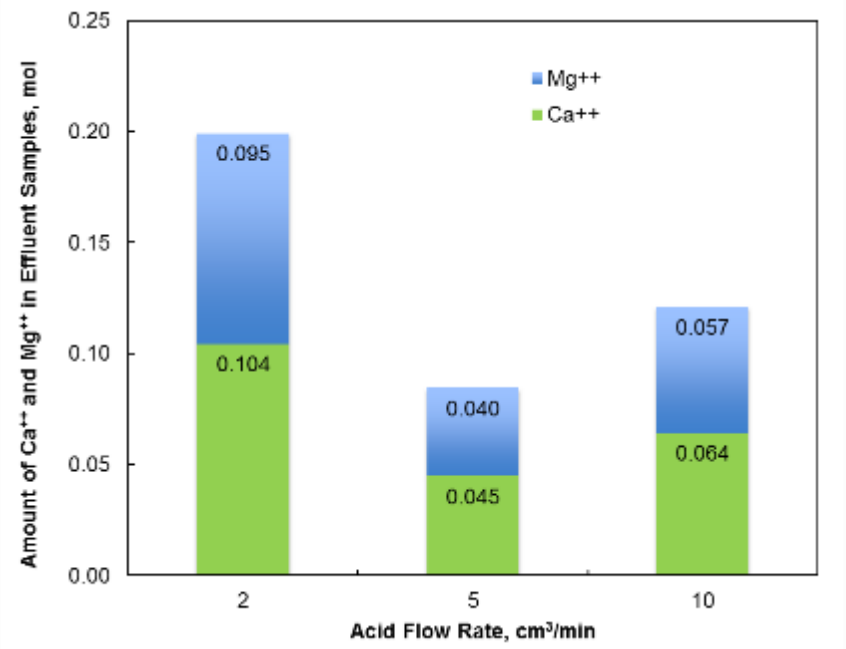

Fig. 45–Amount of calcium and magnesium in the coreflood effluent samples collected for the various experiments with MSA at different injection rates.

The solubility of dolomite cores in MSA is directly indicated by the total amount of calcium and magnesium in the core effluent samples. These amounts can be calculated at different injection rates by integration of the curves corresponding to calcium and magnesium concentration versus volume of acid injected (Figs. 41 and 42). **Fig. 45** shows the calculated total amounts of calcium and magnesium (in moles) collected in the core effluent samples during the injection of MSA in dolomite cores at

injection rates of 2, 5, and 10 cm^3/min. An average calcium to magnesium molar ratio of 1.1 was calculated.

Fig. 46 additionally presents the calculated amount (in grams) of dolomite rock dissolved by the injection of MSA at the same injection rate conditions. From Fig. 46, the total amount of dolomite rock dissolved decreased as the injection rate is increased from 2 to 5 cm^3/min, but increased again at a higher injection rate (10 cm^3/min). This data suggests the existence of an optimal condition where the lowest acid consumption (i.e., least amount of rock dissolved) is required to achieve breakthrough.

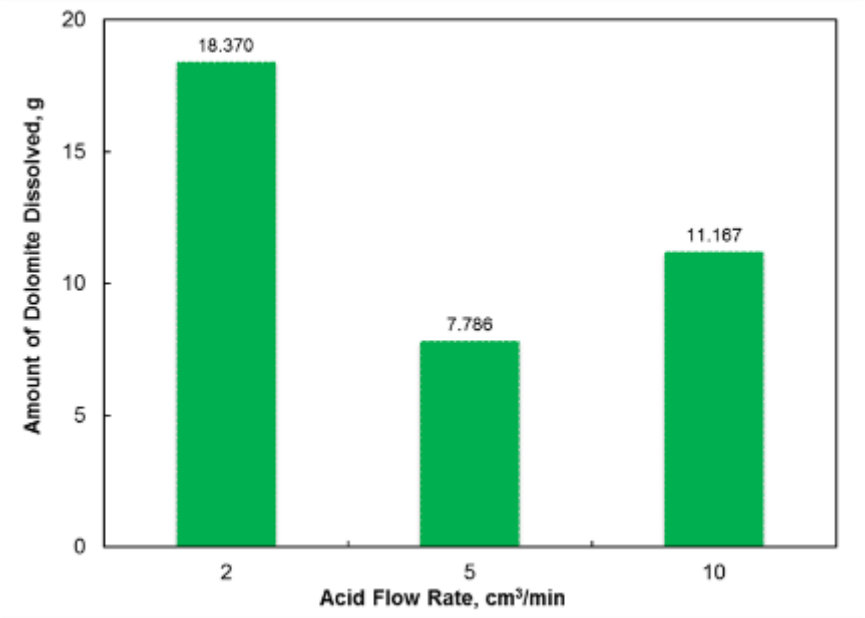

Fig. 46–Calculated amount (mass) of dolomite rock dissolved for the various experiments with MSA at different injection rates.

Volume of Acid to Breakthrough and Optimum Injection Rate

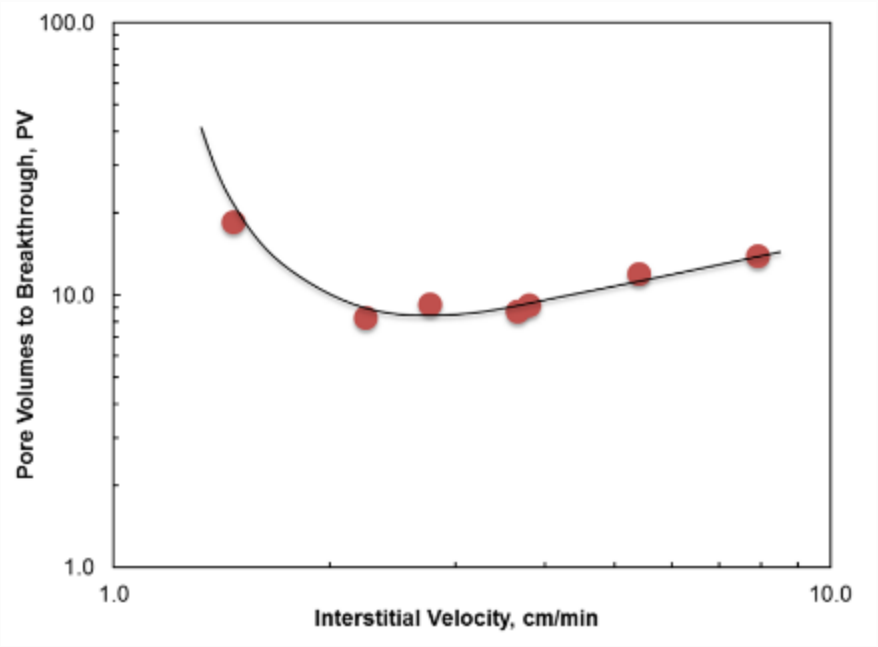

Fig. 47–Optimum injection rate curve for the reaction of 10 wt% MSA with dolomite at 250°F.

The optimum injection rate is defined as the rate at which the volume of acid required to achieve breakthrough is minimum. **Fig. 47** shows the volume of acid to breakthrough as a function of interstitial velocity corresponding to the injection of 10 wt% MSA in dolomite cores at 250°F. The interstitial velocity for each of the core samples treated was calculated by dividing the superficial velocity (volumetric flow rate over the cross area of the core) by the corresponding core porosity (as reported in Table 12). From this figure, as the injection rate increases, the volume of acid to breakthrough decreases and reaches a minimum at a rate between 3 and 6 cm^3/min (2.3 to 3.8 cm/min, interstitial velocity). The volume of acid to achieve breakthrough increases again at

injection rates higher than the optimum. However, the curve is steeper on the left side of the optimum injection rate and relatively flat for rates higher than the optimum. This fact indicates that the effect of the injection rate is more pronounced at low injection rates, corresponding to a mass-transfer-limited regime. On the other hand, at high injection rates the pore volumes to breakthrough are less affected by changes in the injection rate.

CT-Scan Study of Stimulated Core Samples

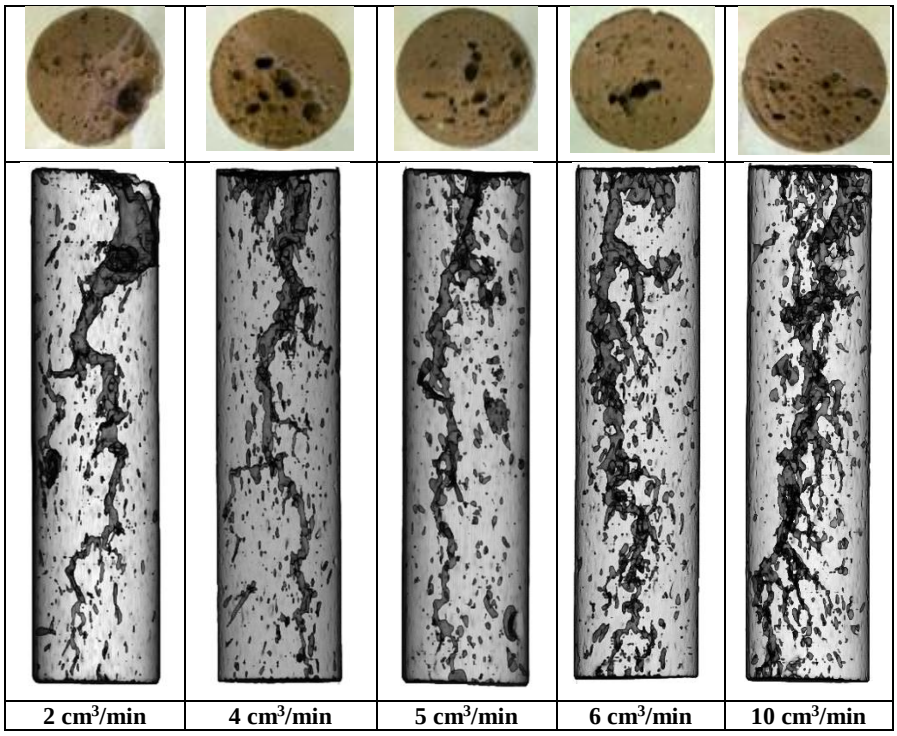

Fig. 48–Low injection (left) leads to face dissolution and conical wormholes. Dominant wormholes are a characteristic of the intermediate rate case (center). High injection rates result in ramified dissolution structures (right).

CT scan images of the cores treated with 10 wt% MSA at 250°F can be used to characterize the dissolution structures that were created at the different flow rates. **Fig. 48** presents CT scan images, along with some photographs of the inlet side of the core

samples after acid injection, for a low-injection rate (2 cm^3/min), an intermediate-injection rate (4 to 6 cm^3/min), and a high-injection rate (10 cm^3/min), showing the wormholing ability of MSA in dolomite cores within the range of injection rates tested.

Due to a low reactivity of MSA with dolomite, even at high temperature conditions, several of the original pores in the core are prospective candidates for wormhole initiation. Consequently, especially at high injection rates, narrowly spaced multiple wormholes are expected to form producing inefficient, highly branched dissolution structures that do not correspond to optimal etch patterns comprising single or few dominant wormholes. The photographs of the inlet flow faces of the stimulated cores presented in Fig. 48 serve to illustrate this point. The inlet faces of the dolomite cores showed a spongy structure instead of displaying well-defined, single dominant wormholes, particularly at the highest flow rates.

In general terms, the CT scan images of the treated dolomite cores (Fig. 48) showed an acid-robbing dissolution structure. For example, at low-injection rates dissolution of the inlet face of the core (face dissolution) and conical wormholes were observed in the scan images, which caused the core stimulation to be inefficient (sub-optimal). At rates close to the optimum injection rate, dominant wormhole were created penetrating the total length of the core with no face dissolution. The size of the generated wormhole decreased as the acid penetrated deeply into the core, until acid breakthrough was achieved. This dissolution pattern resulted in a more efficient stimulation of the core. At high-injection-rates, a ramified dissolution structure was generated as a result of

live acid penetration into new pore space before being consumed. Consequently, the acid efficiency decreased with respect to the intermediate-rate case.

The existence of an optimum injection condition can be explained as a result of the effect of acid flow rate on the created dissolution pattern (Fig. 48). At a low injection rate (2 cm^3/min), a large volume of MSA is consumed on the inlet face of the core (face dissolution). Also at this rate, the reactant penetrates into the porous matrix and enlarges flow channels. However, a significant amount of MSA is consumed on the walls of these flow channels, causing the formation of a conical-shaped dissolution channel. From the CT scan images at 2 cm^3/min, the average diameter of the conical wormhole was about 0.25 in (6.4 mm). This conical channel requires the injection of several pore volumes of acid for the channel to break through the porous medium. The combined effect of face dissolution and conical channels results in a high degree of acid reaction with the rock, which in turn generates a high amount of calcium ions in the effluent samples.

On the other hand, at an intermediate injection rate (3 to 6 cm^3/min) unconsumed MSA reaches the tip of the growing flow channels. Successive consumption at the tip extends the dissolution channels and leads to the development of a dominant wormhole of reduced size. From the CT scan images at 5 cm^3/min, the average diameter of the dominant wormhole was about 0.11 in (2.8 mm). This dominant wormhole requires a minimum pore volume of acid to break through the rock matrix. For that reason, the calcium concentration of the effluent samples at this intermediate rate is lower than the corresponding concentration for the low injection rate case.

Lastly, at a high injection rate (10 cm^3/min) a dominant channel rapidly generates and propagates. With continued acid injection, very fine branches around the main wormhole are created, having an effect similar to an increase of the main wormhole diameter. From the CT scan images at 10 cm^3/min, the maximum diameter of the combined dominant wormhole and ramifications was about 0.23 in (5.8 mm). Since dissolution occurs over a high surface area, a higher degree of acid reactivity results in a higher amount of calcium ions in the effluent samples than the amount measured for the intermediate injection rate case.

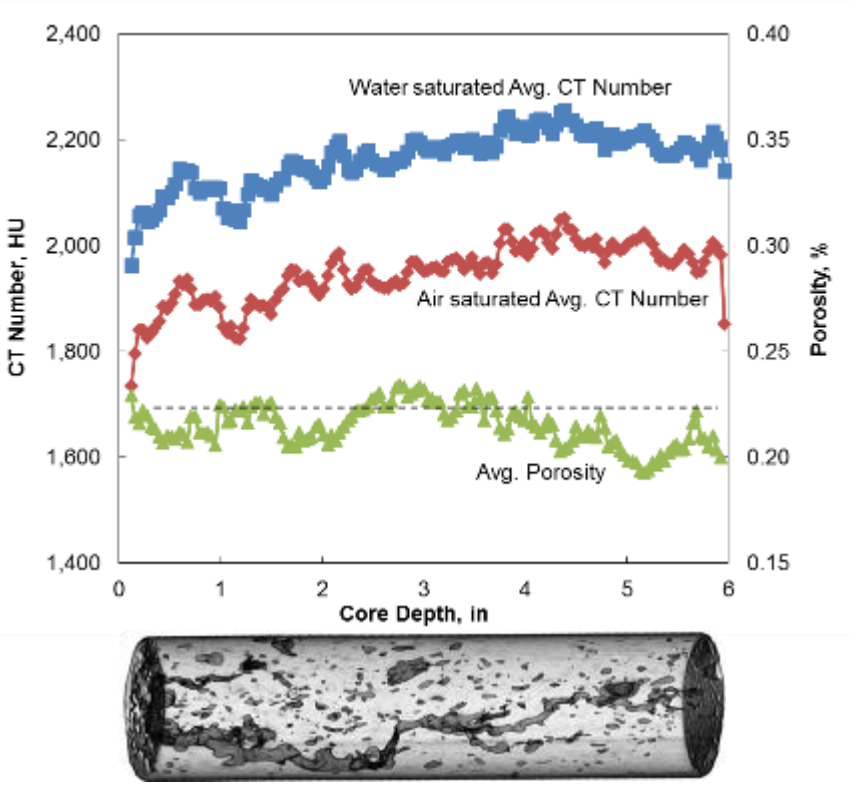

Fig. 49–CT scan of acidized core sample (Core #79).

The study of the CT scan images confirms that MSA can be used as an effective stimulation fluid, as it creates and propagates deep, dominant wormholes when injected into high-temperature dolomite formations. The generation of these dominant wormholes provides a significant increase in core porosity and permeability. As an example, **Fig. 49** shows the final average porosity (after stimulation) determined for Core #79, following the same dual-scan method previously described. A final average porosity of 22 vol% was calculated for Core #79, which is about double the initial porosity value.

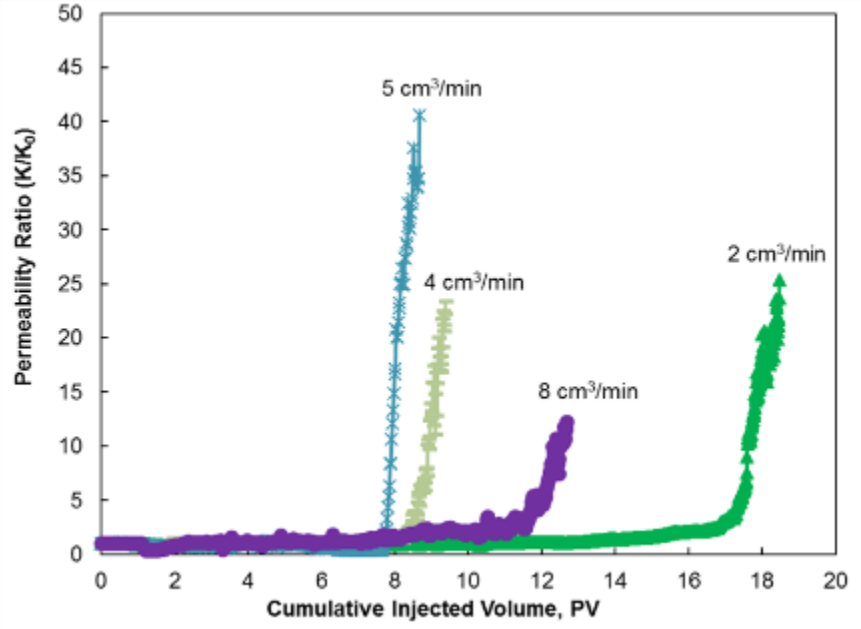

Fig. 50–Permeability enhancement by injection of 10 wt% MSA in dolomite cores.

Correspondingly, the generation of additional porosity results in improved core permeability. **Fig. 50** shows the permeability enhancement obtained in dolomite cores tested with MSA at different injection rates, after acid breakthrough occurred. It can be

observed from results in Fig. 50 that the amount of acid required to increase the average permeability by a certain degree depends on the acid injection rate. For example, at a low injection rate (i.e., 2 cm^3/min) the average permeability increases slowly with the pore volumes of acid injected. As the acid injection rate is increased, the rate of increase in average permeability increases up to a certain acid injection rate (4 to 6 cm^3/min). At this acid-injection rate (the optimum injection rate) permeability increment is steepest as compared with other acid-injection rates. For acid-injection rates higher than the optimum acid-injection rate (i.e., 10 cm^3/min), the rate of permeability increment decreases with the increase in the injection rate.

Comparison with Limestone Cores

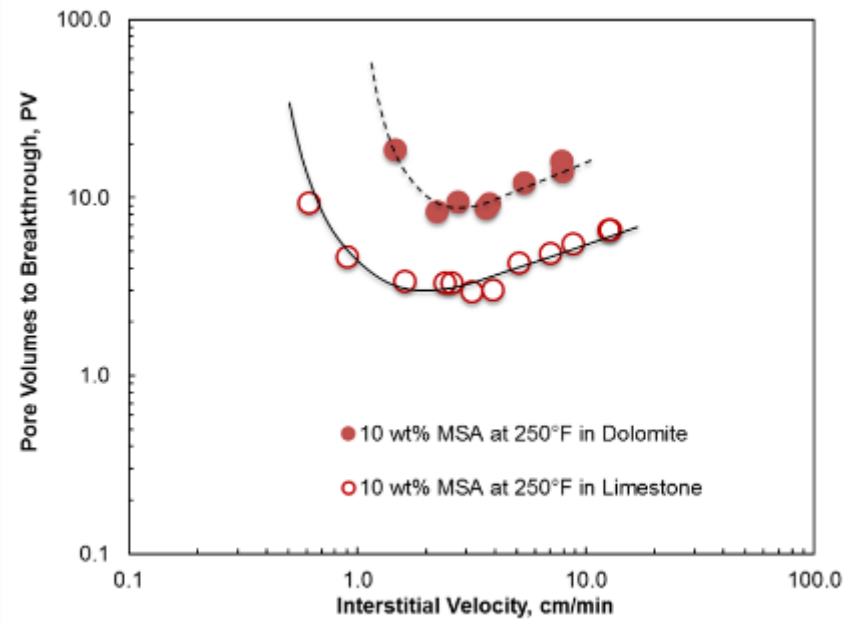

Fig. 51–Effect of lithology on MSA acid efficiency. The dolomite cores required relatively large volumes of MSA as compared with the limestone cores.

The dolomite cores required relatively large volumes of MSA as compared with the limestones (**Fig. 51**). This is a consequence of a slower MSA-dolomite reaction rate that results in a more uniform mode of acid attack. In other words, with a lower reaction rate, more acid is needed to propagate a wormhole a given distance in dolomite. In addition to this, a larger mineral (dolomite) surface area is exposed to live acid due to reaction limitations. Therefore, as live acid can penetrate into new pore space before it is consumed, higher rates will result in increased branching in dolomite.

Dolomite coreflood results indicate that when the reaction rates are slow, greater volumes may be required to stimulate (Fig. 47). The coreflood results also show acid breakthrough only after large volumes of acid were injected compared with the limestone results (Fig. 51). Breakthrough occurred in the limestone cores after 2.9 to 9.2 PV of fluid had been injected, depending on the rate. Dolomite injected under similar conditions required up to 18.5 PV. On the other hand, corresponding to a decrease in the reaction rate, an associated decrease in the optimum acid injection rate was also observed.

A comparison of the dissolution patterns created in each core lithology at low, intermediate, and high injection rates is provided in **Fig. 52**. It can be observed that despite of the lower acid reactivity of dolomite, the dissolution of this material by the injection of 10 wt% MSA produced patterns that are comparable to the patterns obtained with limestone cores. Similar to limestone, the created dissolution structure in dolomite cores were wormholes and not uniform dissolution patterns, as typically observed during coreflood injections of HCl in dolomite at room temperature (Hoefner and Fogler 1988).

The main differences were a higher degree of branching in dolomite than in limestone, and a bigger size of the wormholes in dolomite (i.e., 0.18 in versus 0.15 in for maximum wormhole diameter for dolomite and limestone at optimum rate conditions, respectively), likely a result of the higher volume of acid that was injected in the dolomite case.

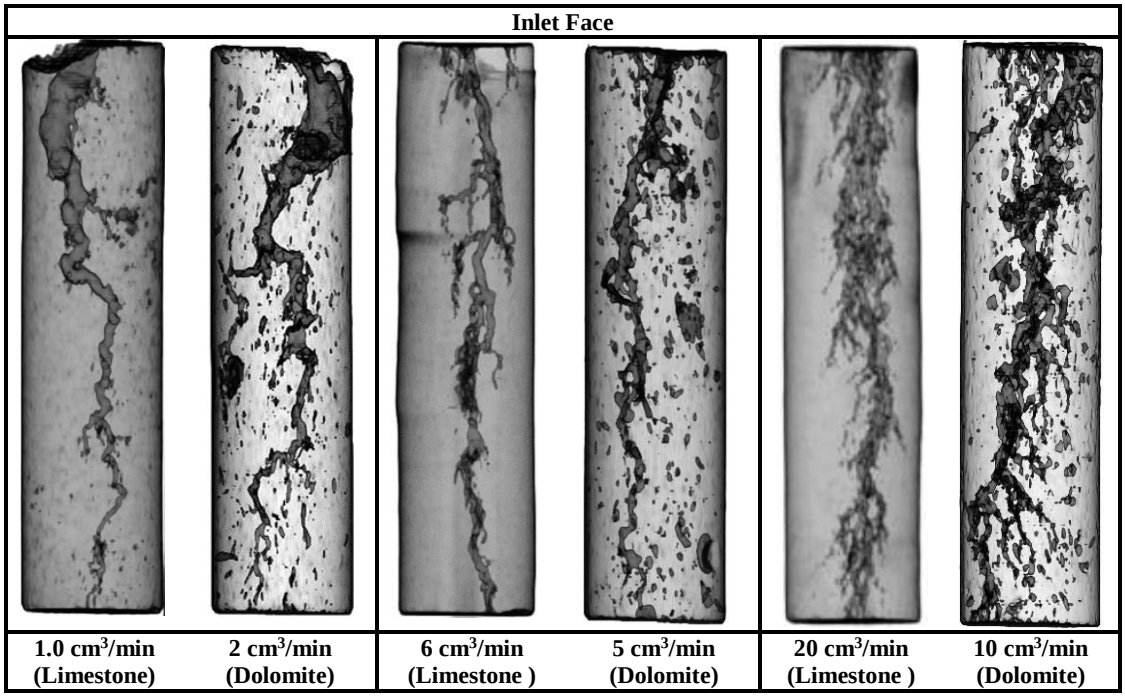

Fig. 52–Comparison of dissolution structures created by MSA (dolomite versus limestone).

The total ion (calcium and magnesium) concentration, pH, and final acid concentration were compared for the effluent samples collected during the coreflood experiments performed using dolomite and limestone cores (10 wt% MSA at 250°F) at an injection rate close to the optimum (5 cm^3/min). In **Fig. 53**, the total measured calcium and magnesium concentration reached a maximum value of 17,313 mg/l ± 5%,

for the case of dolomite cores, and 21,595 mg/l ± 4%, for the case of limestone. These values are in agreement with the theoretical dissolution expected for this acid concentration.

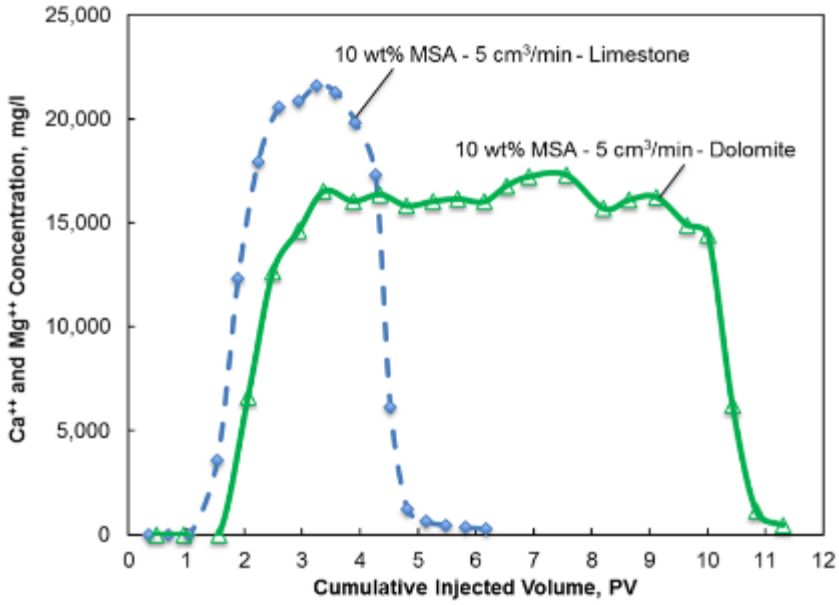

Fig. 53–Calcium and magnesium concentration in the coreflood effluent samples collected for experiments with 10 wt% MSA using dolomite and limestone cores at 5 cm^3/min.

The comparison of effluent-pH profiles in **Fig. 54** shows that in the case of dolomite there is a constant pH during most of the acid injection and a more gradual decrease to a pH value around 1 before acid breakthrough. By contrast, in the case of limestone, the pH value kept constant close to a value of 6 all along the acid injection and then suddenly dropped to 1 as acid breakthrough occurred. This difference in pH behavior is another evidence of the lower acid reactivity of dolomite.

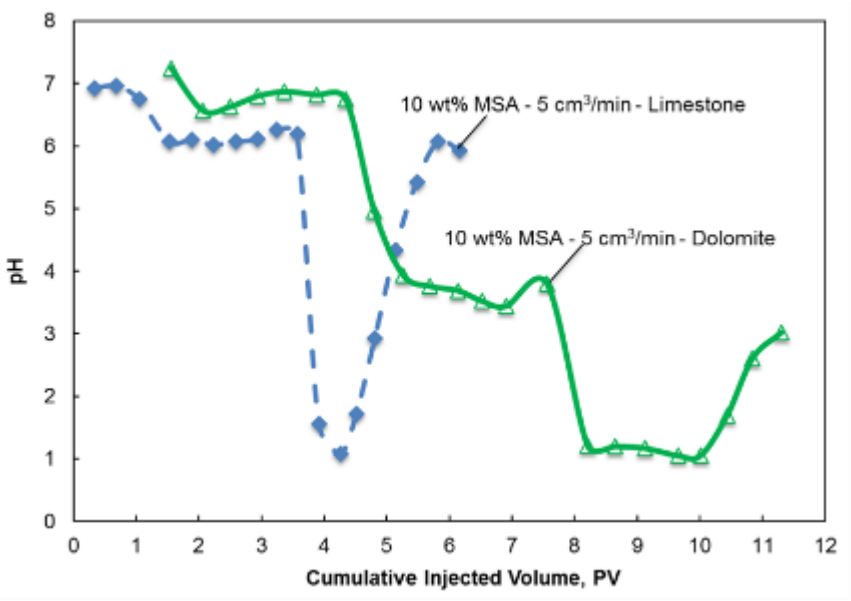

Fig. 54–pH of the coreflood effluent samples collected for experiments with 10 wt% MSA using dolomite and limestone cores at 5 cm^3/min.

Finally, **Fig. 55** shows a comparison of the final acid concentration in the effluent samples collected during the same experiments. Maximum values of 1.04 and 1.13 wt% MSA were measured for the dolomite and limestone cases, respectively. These peaks in concentration serve as a confirmation of the breakthrough condition for each of the lithologies tested.

Effects of Concentration

One additional experiment at a higher acid concentration was performed to determine the effect of this parameter on the volume of acid required to breakthrough in dolomite. In this additional test, a 20 wt% MSA acid solution was used and was injected into the dolomite core at a temperature of 250°F.

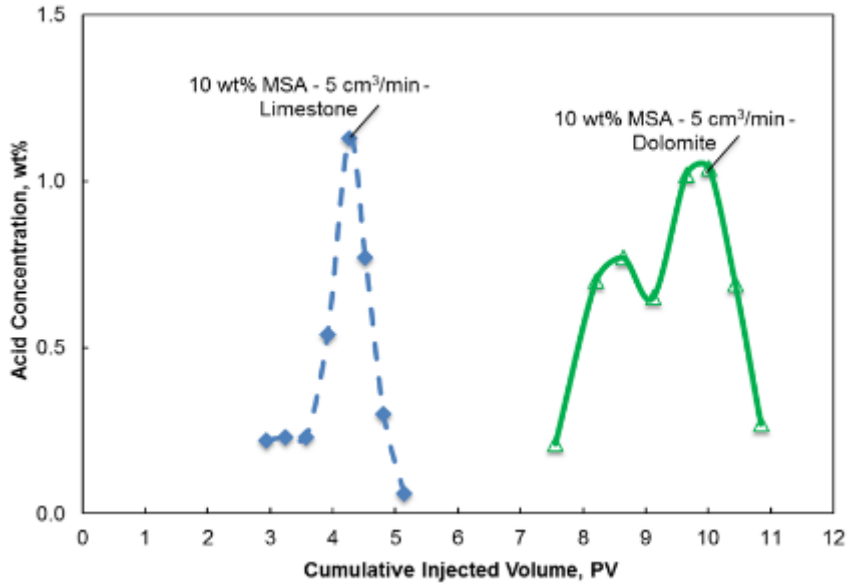

Fig. 55–Acid concentration in the coreflood effluent samples collected for experiments with 10 wt% MSA using dolomite and limestone cores at 5 cm^3/min.

In spite of the high acid concentration, a relatively large acid volume (6 PV) was required before breakthrough was achieved. Analysis of the CT scan images of the treated core structure (**Fig. 56**) shows a lower degree of branching in the dominant wormhole; however, narrowly spaced multiple wormholes are initiated from the original pores, producing an inefficient dissolution structure. Regardless of the comparatively rapid injection (5 cm^3/min), the scan images also show acid spending at the inlet surface of the core (face dissolution).

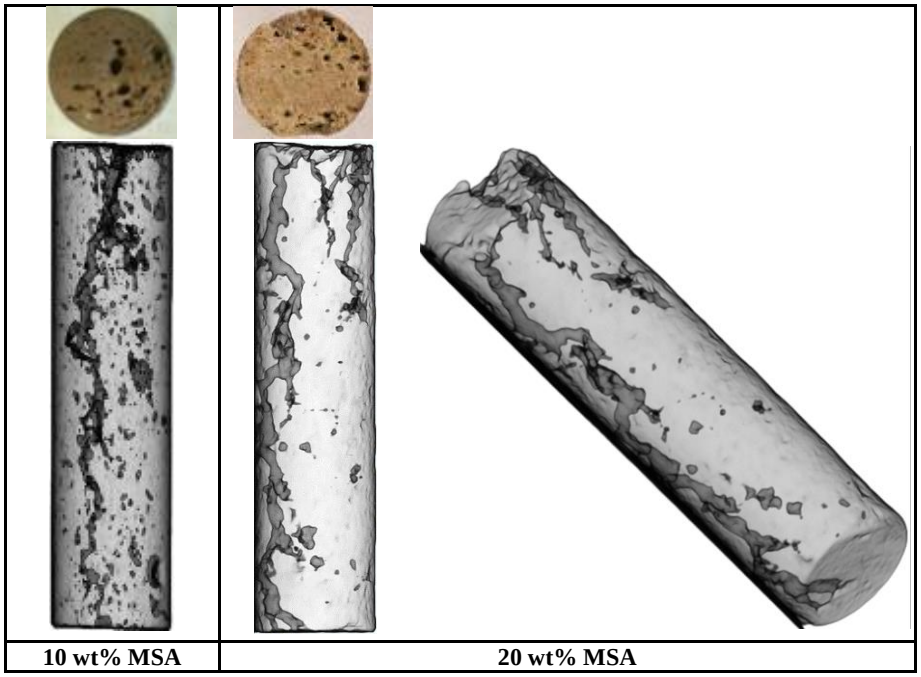

Fig. 56–Effect of acid concentration on the wormhole structures formed near the optimum injection rates at 250°F. A lower degree of branching in the dominant wormhole is observed at the higher concentration. The scan images also show acid spending at the inlet surface of the core when 20 wt% MSA is used.

TABLE 13—AMOUNT (MASS) OF ACID INJECTED TO PENETRATE THE DOLOMITE CORES AT DIFFERENT ACID CONCENTRATIONS

Acid Concentration, wt%	Acid Injected, V/VP	Mass of Acid, g
10	8.67	18.7
20	6.03	27.6

The efficiency of different MSA acid solutions is compared in **Table 13** based on the acid quantity injected at 5 cm3/min. From the results using dolomite, in terms of acid

consumption, a low MSA concentration was better. However, the volumes of dilute acid may have been excessive. Therefore, if injection time is crucial to the cost of treatment, high concentrations of MSA may be preferred.

Effects of Temperature

Coreflood experiments performed using dolomite cores demonstrate an effect of temperature on MSA wormholing efficiency. Four additional coreflood tests were run with 10 wt% MSA at 320°F using Silurian dolomite cores. The properties of the core samples used and the results obtained from coreflood testing are given in **Table 14**.

TABLE 14—PROPERTIES OF DOLOMITE CORES USED WITH 10 WT% MSA AT 320°F AND SUMMARY OF COREFLOOD RESULTS

Core No.	Pore Volume, cm^3	Porosity, vol%	Injection Rate, cm^3/min	Acid Vol. to Breakthrough, PV
107	19.21	11.1	3.0	10.07
110	21.90	12.6	4.0	9.83
109	23.39	13.5	6.0	10.31
112	19.28	11.1	10.0	20.18
Average Porosity = 12 vol%				
Average Permeability = 37 md				

Fig. 57 shows a comparison of the acid efficiency curves for dolomite cores treated with MSA at 250°F and 320°F. These results showed an increase in the acid volume required to achieve breakthrough at a higher temperature. The decrease in acid efficiency for wormhole formation is a result of the reaction of MSA with dolomite

becoming more mass-transfer limited as the temperature is increased. It has been previously determined that, similarly to limestone, the dissolution of dolomite is mass transfer limited at temperatures greater than 200°F (Lund et al. 1973). Because of a higher acid reactivity at higher temperatures, the acid is less effectively transported to the tip of the wormhole, being significantly consumed on the wormhole walls and in lateral branches. Consequently, the average diameter of the dominant wormhole tends to increase with temperature.

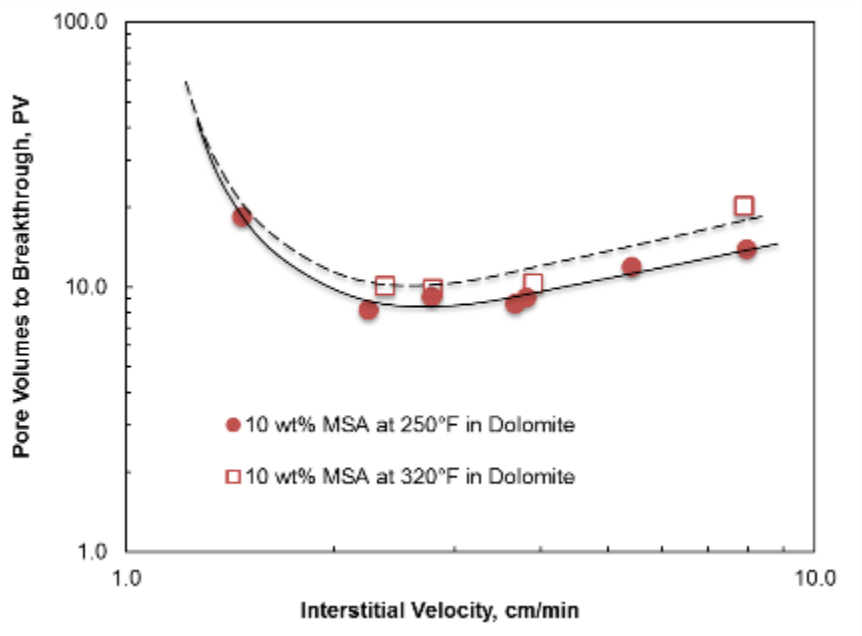

Fig. 57–Effect of temperature on the number of pore volumes to breakthrough for dolomite cores acidized with 10 wt% MSA.

From the coreflood experiments, it was confirmed that MSA can be used as an effective stimulation fluid at 320°F, showing the wormholing ability of MSA in the range of injection rates tested. The dissolution structures that were created by the

injection of 10 wt% MSA in dolomite cores at 320°F can be characterized by analyzing the 3D scan images of the treated cores (**Fig.58**). A similar trend to the one described in Fig. 16 for the case of 250°F was observed, regarding the dependency of dissolution structure on the injection rate; however, at corresponding flow rates, the CT scan images displayed a lower degree of wormhole branching for the higher temperature case (320°F).

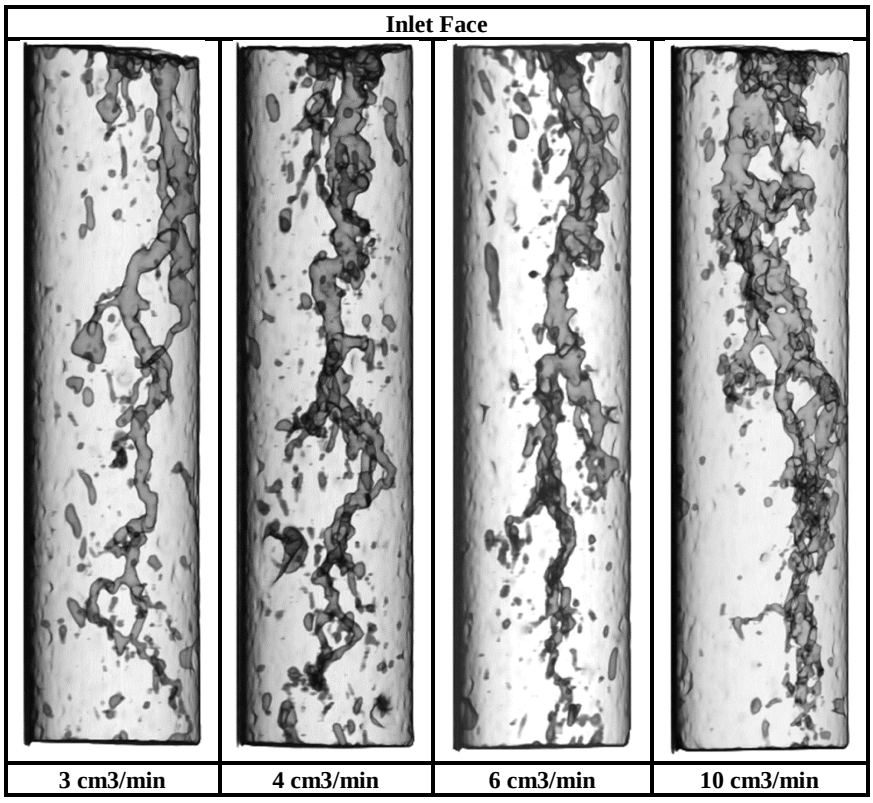

Fig. 58–Dissolution patterns identified from 3D scan images of dolomite cores treated with 10 wt% MSA at 320°F.

Conclusions

A 10 wt% MSA aqueous acid solution was used to stimulate dolomite cores using a coreflood setup. The effects of acid injection rate and temperature on the propagation of MSA in dolomite cores were examined in detail. Based on the results obtained, the following conclusions can be made:

1. MSA was found to be effective in creating and propagating wormholes in dolomite cores at temperatures up to 320°F, providing a significant increase in porosity and permeability.
2. For the acid injection rates covered in the current study, an optimum injection rate of 5 cm^3/min was determined when 10 wt% MSA was used to stimulate dolomite cores at 250°F.
3. Having a slower reactivity than limestone, a decrease in optimum injection rate and an increase in MSA volume to breakthrough were expected and observed when using dolomite cores.
4. The volumetric acid efficiency of the wormhole formation in dolomite cores increased with increasing MSA concentration.
5. The efficiency of wormhole formation with 10 wt% MSA in dolomite cores decreased with increasing temperature.

CHAPTER VI

NUMERICAL SIMULATION OF ACIDIZING IN CARBONATE RESERVOIRS

Introduction

Several mathematical models have been developed to characterize the wormholing phenomena associated with the acidizing of carbonate formations. A detailed description of some of the different approaches considered is presented by Fredd and Miller (2000) and can be summarized as transition pore theories (Wang et.al. 1993; Huang et.al. 1997), capillary tube models (Hung et.al. 1989; Buijse 1997; Gdanski 1999), Peclet number theories (Daccord et.al. 1989; Frick et.al. 1994), Damkohler number theories (Fredd and Fogler 1998b; Hoefner and Fogler 1988; Fredd 2000b), and network models (Hoefner and Fogler 1988; Fredd and Fogler 1998b). However, due to their simplified approaches, these models can be used to explain only certain aspects of the flow and reaction of acid in porous media.

A more comprehensive approach, called averaged or continuum, has been described in the literature by Liu et al. (1997), Chen et al. (1997), Pomès et al. (2001), and Golfier et al (2002). Liu et al. and Chen et al. did not consider diffusion effects, therefore their models are valid only in the kinetic regimes. On the other hand, the models by Pomès et al. and Golfier et al. ignore the reaction kinetics, so they are valid only in the mass-transfer controlled regime.

More recently, Panga (2005) formulated a new averaged model that can capture both effects (mass-transfer and reaction kinetics) and so it could be used to evaluate a broader range of rock-fluid systems (i.e., MSA and limestone/dolomite rocks).

The objective of this section is to develop the basis for the implementation of an averaged model using a commercial computational fluid dynamics (CFD) software, Fluent, which uses a finite-volume discretization method. The results from the simulator serve to supplement and validate the laboratory tests performed during the study of the acidification of carbonate cores with acids systems such as HCl or MSA. Since the reaction kinetics of MSA with carbonates has not been yet studied (i.e., using a rotating disk apparatus), the simulations in this study used the kinetics parameters corresponding to the reaction of limestone with HCl. This was also done to validate the results of the model against previous works by other authors. Once the kinetics data corresponding to MSA become available, they could be easily incorporated into the model.

The model included in the present work is based on the work by Panga (2005) but considering Fluent's own formulation for the momentum conservation equation. An acid efficiency (pore volume of acid to breakthrough vs. injection rate) curve was built using the results of the 3D simulations and the predictions from the model were compared against available experimental data.

Model Description

In this section a brief description of the averaged model implemented in the commercial software Fluent is presented. The implementation of the flow and reaction

equations not available in Fluent, was done by means of user-defined-functions (UDF) written in C programming language.

Darcy-Scale Model

The Darcy scale model equations for a laminar, single-phase, multicomponent and isothermal flow in porous media are given by **Eq. 5 to 10**, corresponding to mass conservation (Eq. 5), momentum conservation (Eq. 6), Darcy viscous loss of a porous media (Eq. 7), transport of acid species (Eq. 8), acid consumption by chemical reaction (Eq. 9), and porosity evolution (Eq. 10).

$$\frac{\partial}{\partial t}(\phi\rho) + \nabla \cdot (\phi\rho\vec{v}) = 0 \quad (5)$$

$$\frac{\partial}{\partial t}(\phi\rho\vec{v}) + \nabla \cdot (\phi\rho\vec{v}\vec{v}) = -\varphi\nabla \mathrm{P} + \nabla \cdot (\phi\vec{\tau}) + \vec{S} \quad (6)$$

$$\vec{S} = -\left(\frac{\phi^2\mu}{\vec{K}}\vec{v}\right) \quad (7)$$

$$\frac{\partial}{\partial t}(\phi\rho y_i) + \nabla \cdot (\phi\rho\vec{v}y_i) = \nabla \cdot \left(\phi\rho\vec{\Gamma}\nabla y_i\right) + \phi R \quad (8)$$

$$R = -(k_{eff})C = -\left(\frac{k_s k_c}{k_s + k_c}a_v\right)\rho y_i \quad (9)$$

$$\frac{\partial \phi}{\partial t} = \left(\frac{k_s k_c}{k_s + k_c} a_v\right)\left(\frac{\alpha}{\rho_s}\right)\left(\frac{\rho y_i}{M}\right) \cdots\cdots\cdots\cdots\cdots \quad (10)$$

Where $\vec{v}$ is the Darcy velocity vector, μ is the viscosity, $\vec{K}$ is the permeability tensor, P is the pressure, $\vec{\tau}$ is the stress tensor, ϕ is the porosity, ρ the fluid density, M is the molecular mass of the acid, a_v is the interfacial area available for reaction per unit volume of the medium, ρ_s is the density of the solid phase, α is the dissolving power of the acid, C is the mass concentration of acid in the fluid phase, y_i is the mass fraction of acid in the fluid phase, $\vec{\Gamma}$ is the dispersion tensor, k_c is local mass-transfer coefficient, and k_s is the surface reaction rate constant.

Eq. 5 approximates the continuity equation for the fluid phase. The momentum equation, given by Eq. 6, describes the Navier-Stokes flow with a sink of momentum (Eq. 7) that is used to model the Darcy viscous loss of a porous media. The two terms in the right hand side of Eq. 8 represent the (anisotropic) acid dispersion and the consumption of acid by a first-order irreversible reaction (Eq. 9), respectively. Finally, Eq. 10 describes the increment in local porosity as a result of the dissolution of the porous medium by acid reaction.

Pore-Scale Model

Structure – Property Relations

Pore-scale properties such as permeability, pore radius, and interfacial surface area change during each time step of the simulation due to the increase in porosity that results from acid reaction (Eq. 9). The present study uses the permeability-porosity, pore

radius-porosity, and interfacial area-porosity relations suggested by Maheshwari and Balakotaiah (2013), which are given by **Eq. 11 to 13**, respectively.

$$\frac{K}{K_o} = \left(\frac{\phi}{\phi_o}\right)^{\gamma} \left[\frac{\phi(1-\phi_o)}{\phi_o(1-\phi)}\right]^{2\beta} \text{..... (11)}$$

$$\frac{r}{r_o} = \left[\frac{\phi(1-\phi_o)}{\phi_o(1-\phi)}\right]^{\beta} \text{..... (12)}$$

$$\frac{a_v}{a_o} = \left(\frac{\phi}{\phi_o}\right) \left[\frac{\phi(1-\phi_o)}{\phi_o(1-\phi)}\right]^{-\beta} \text{..... (13)}$$

Where K is the local permeability magnitude, K_o is the initial average value of permeability, ϕ_o is the initial average rock porosity, r_o is the initial mean pore radius, and a_o is the initial interfacial surface area per unit volume. The parameters γ and β in the previous equations correspond to the pore-connectivity and pore broadening parameters, respectively, as defined by Maheshwari and Balakotaiah (2013).

Mass Transfer and Dispersion Coefficients

As shown in Eq. 9, acid-rock reaction is a function of mass transfer rate of the acid inside the pores, which in turn depends on flow regime and pore structure. Literature correlations (Maheshwari and Balakotaiah 2013) are used to calculate the local mass-transfer coefficient and the effective dispersion coefficients, as shown in **Eq. 14 to 16** below.

$$k_c = \left(\frac{D_m}{2r}\right)\left(Sh_\infty + 0.7Re_p^{1/2}Sc^{1/3}\right) \cdots\cdots\cdots\cdots \quad (14)$$

$$\frac{D_{eX}}{D_m} = \alpha_{os} + \lambda_X Pe_p \cdots\cdots\cdots\cdots \quad (15)$$

$$\frac{D_{eT}}{D_m} = \alpha_{os} + \lambda_T Pe_p \cdots\cdots\cdots\cdots \quad (16)$$

Where Sh_∞ is the asymptotic Sherwood number, Re_p is the pore-scale Reynolds number (defined in **Eq. 17**), and Sc is the Schmidt number (**Eq. 18**). The calculation of the longitudinal and transverse dispersion coefficients (D_{eX} and D_{eT} in Eq. 15 and 16, respectively) requires the definition of the Peclet number in the pore (shown in **Eq. 19**) and the use of various constants (α_{os}, λ_X, λ_T) that depend on pore connectivity and pore structure.

$$Re_p = \frac{2\|U\|r}{\nu} \cdots\cdots\cdots\cdots \quad (17)$$

$$Sc = \frac{\nu}{D_m} \cdots\cdots\cdots\cdots \quad (18)$$

$$Pe_p = \frac{2\|U\|r}{\phi D_m} \cdots\cdots\cdots\cdots \quad (19)$$

Boundary and Initial Conditions

The boundary and initial conditions used to solve the above system of equations for constant injection rate are:

- Boundary conditions: constant injection velocity at inlet, constant acid concentration of 1.55 wt% at inlet, zero average pressure at outlet, no-flux B.C. in the transverse direction (walls).
- Initial conditions: domain filled with pure water, uniform velocity field (equal to zero), randomly assigned porosity field with a fluctuation distributed uniformly around an average value.

Initial Porosity Distribution

The formation and propagation of wormholes is greatly affected by the initial spatial distribution of porosity and permeability. In the present study a heterogeneous porosity field is created by: (1) assigning to certain coordinate points in the domain randomly distributed porosity values that were generated from the definition of an initial average porosity and a porosity (heterogeneity) range, and (2) interpolating the porosity values at each cell grid of the numerical domain from the porosity values at the coordinate points.

The random and spatially correlated porosity field is generated using **Eq. 20** below:

$$\phi_0\,(x,y) = \overline{\phi_{\,0}} + CV\overline{\phi_{\,0}}\,N(x,y) \cdots\cdots\cdots\cdots\cdots \quad (20)$$

Where, N(x,y) is the spatially correlated number, an output from the geostatistical software GSLIB (Deutsch and Journel 1998); $\overline{\phi_0}$ = 0.20 is the initial average porosity; and, CV = 0.5 is the magnitude of porosity heterogeneity.

Following the procedure above, a total of 232,713 porosity-profile points were generated; then, an interpolation method (least squares) was used to generate the heterogeneous porosity field shown in **Fig. 59**.

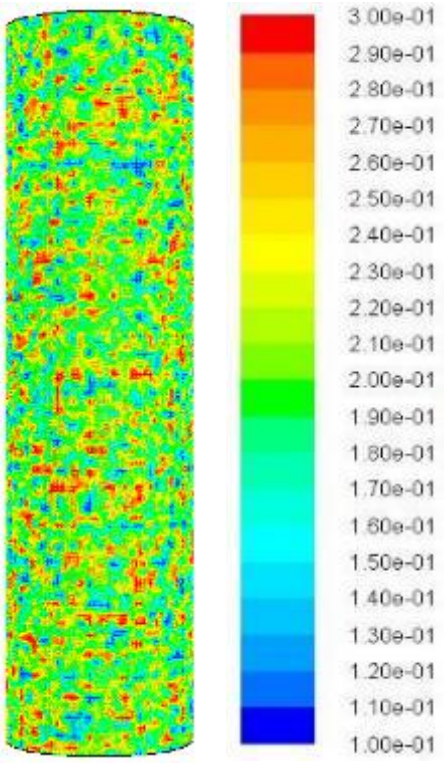

Fig. 59–Initial distribution of porosity used during the numerical simulations.

Input Data for the Simulations

To be able to build a numerical acid efficiency curve, different simulations were performed at different injection conditions. The numerical domain employed resembles

the geometry of a typical coreflood core (3D cylinder of 0.152 m length by 0.038 m diameter). To cover the domain geometry, a total of 385,056 hexahedral grid cells were used.

Table 15 present the value of the different parameters required during the numerical simulations. As mentioned before, for comparison purposes values corresponding to HCl and limestone rock are used, similar to the ones included in Fredd and Fogler (1998b).

TABLE 15—INPUT DATA USED FOR NUMERICAL SIMULATIONS

Parameter	Value
Core length (L)	0.152 m
Initial mean pore size (r_o)	1 μm
Initial interface area per unit volume (a_o)	5000 m^2/m^3
Initial average permeability	1 md
Surface dissolution reaction-rate constant (k_s)	0.002 m/s
Acid diffusivity (D_m)	3.6×10^{-9} m^2/s
Acid viscosity (μ)	0.001 kg/m·s
Acid molecular mass (M)	36.46 kg/kmol
Acid dissolving power (α)	50.11 kg/kmol
Rock density (ρ_s)	2,710 kg/m^3
Asymptotic Sherwood number (Sh_∞)	3.66
Average porosity (φ)	0.20
Pore-broadening parameter (β)	1.5
Pore-connectivity parameter (γ)	1.0
Constant in dispersion correlations (α_{os})	0.5
Constant in axial dispersion correlation (λ_x)	0.5
Constant in transverse dispersion correlation (λ_T)	0.1

Numerical Solution

The governing equations are discretized with a finite volume discretization method and solved sequentially using a pressure-based segregated solver in Fluent. Following an iterative approach, the velocity field is obtained from the momentum equations, and the pressure field is extracted by solving a pressure or pressure correction equation which is obtained by manipulating continuity and momentum equations. After this, the acid transport equation (convection, diffusion, and reaction) is solved to get the acid mass fraction distribution in the domain. Finally, the pore properties (porosity, permeability, pore radius, and interfacial area) are updated using the porosity evolution equation (Eq. 9) and the structure–property relations (Eq. 10 to 12).

Effect of Injection Rate on Dissolution Patterns

Fig. 60 presents iso-surfaces of porosity (60 vol% porosity), varying along the length of the cores, obtained from numerical simulation of the carbonate acidizing process. Different patterns of dissolution were obtained by increasing the prescribed injection rate at the inlet boundary (or decreasing the Damkhöler number), going from a dominant, narrow wormhole at the lowest injection rate (highest Damkhöler number) to a ramified wormhole patterns at the intermediate rates, to the start of a uniform dissolution pattern at the highest flow rate (lowest Damkhöler number). The Damkhöler number calculation was performed using the definitions given by Fredd and Fogler (1999), substituting in the corresponding equations the parameters shown in Table 15.

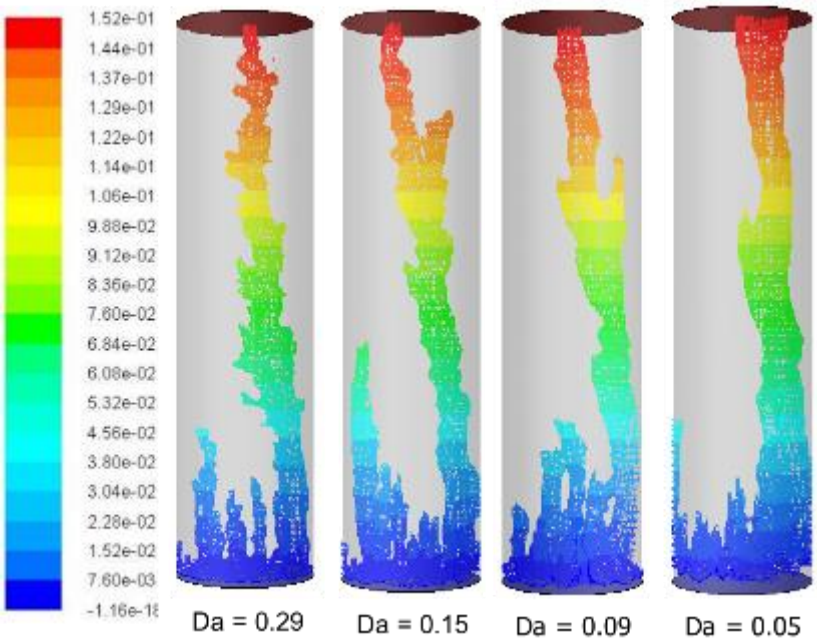

Fig. 60–Iso-surfaces of porosity (60 vol% porosity), varying along the length of the cores, obtained from numerical simulation of the carbonate acidizing process.

Definition of the Acid Breakthrough Condition

Following the same criteria employed by other authors (De Oliveira et al. 2012; Kalia and Balakotaiah, 2009), in the present study the numerical acid breakthrough condition is considered achieved when the pressure drop across the porous media decreases to 1% of the initial pressure drop value. As an example, **Fig. 61** shows the behavior of the pressure drop across the core during the injection of acid at a Damkhöler number of 0.29. For this particular case, 1.11 PV of acid were required to achieve the breakthrough condition. **Table 16** presents the PVBT results of some of the simulations performed indicating the type of dissolution pattern observed in each case.

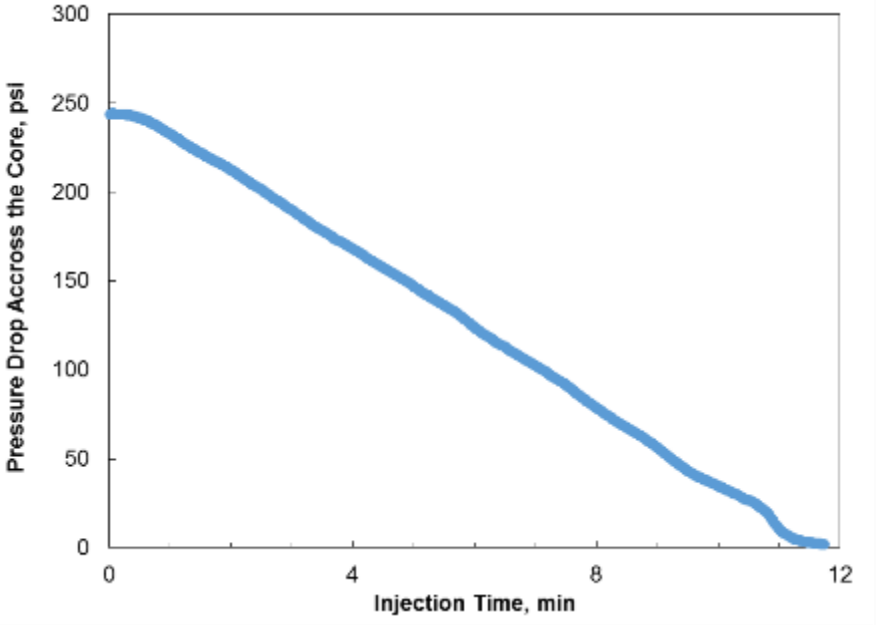

Fig. 61–Typical pressure drop across the core behavior during numerical simulation (Da = 0.29).

TABLE 16—DISSOLUTION PATTERNS OBTAINED AT DIFFERENT INJECTION CONDITIONS FROM NUMERICAL SIMULATIONS

Dissolution Pattern	Damkhöler Number	Pore volumes to Breakthrough
Dominant Wormhole	0.29	1.11
Ramified Wormhole	0.09	1.51
Uniform Dissolution	0.05	1.97

Acid Efficiency Curve

The pore volume of acid required to breakthrough obtained from numerical simulations can be plotted versus the inverse of the Damkhöler number to analyze the effect of injection rate on acid efficiency. From the results shown in **Fig. 62**, an optimal

injection condition can be identified at which the minimum PVBT is required. It can be also noticed that the PVBT results shown in this figure have been normalized by dividing the breakthrough volume at each rate by the minimum pore volume to breakthrough determined at the optimal rate.

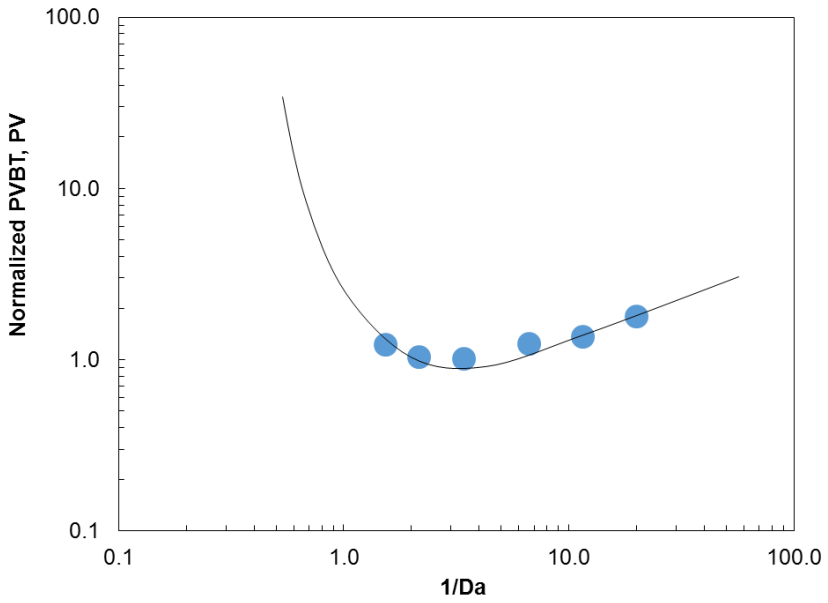

Fig. 62–Numerical normalized acid efficiency curve.

The normalization of the acid efficiency curve is done in order to compare the numerical results against also normalized (dimensionless) experimental data. Besides, the normalization of the PVBT curve will account for mesh refinements effects (i.e., wormhole size smaller than grid cell size) that will normally result in numerical value of acid volume to breakthrough higher than the corresponding experimental values.

Fig. 63 shows the comparison of the numerical results versus experimental data (Fredd and Fogler 1998b). Both data shows the existence of an optimum injection condition at a Damkhöler number of 0.29.

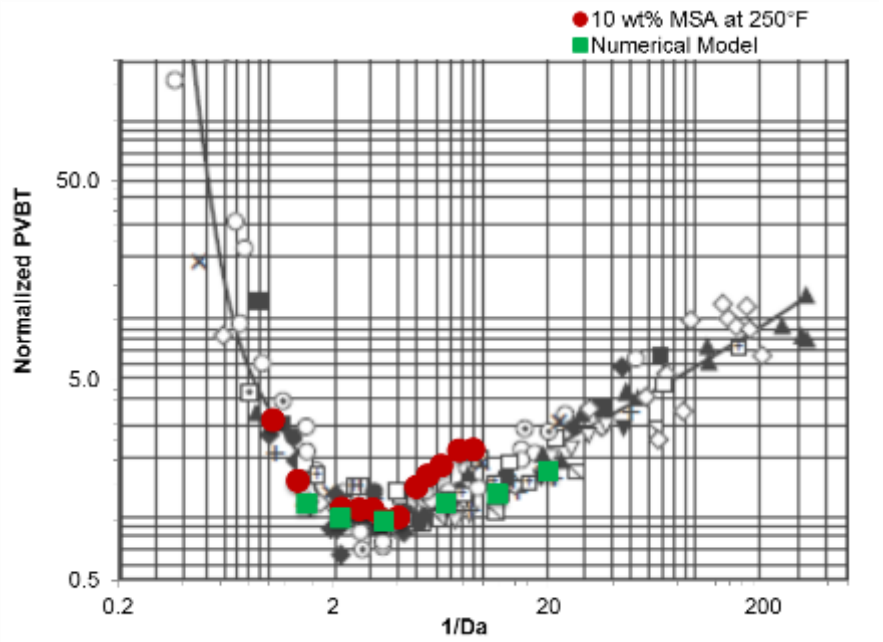

Fig. 63–Comparison of numerical results versus experimental data (Fredd and Fogler 1998b).

Conclusions

An averaged model of the transport and reaction of acid in a porous media was implemented on a CFD commercial package to study the reactive dissolution of carbonate rocks by the injection of acid. A comparison of the numerical results against results from coreflood experiments shows agreement regarding the different types of dissolution patterns generated by the injection of acid at various flow rates and the existence of optimum injection conditions. There is also a good match between the

normalized numerical and experimental acid efficiency curves. This tool can be used to evaluate the effect of various parameters (temperature, acid concentration, rock lithology, rock permeability) on the performance of acid systems such as methanesulfonic acid.

CHAPTER VII

GENERAL CONCLUSIONS AND RECOMMENDATIONS

Aqueous MSA acid solutions were used to stimulate limestone and dolomite cores using a coreflood setup. The effects of acid flow rate, temperature, acid concentration, rock permeability, and rock lithology on the propagation of MSA in carbonate cores were examined in detail. Based on the results obtained, the following conclusions can be drawn:

1. Even though HCl is the most common acid used in carbonate matrix acidizing, the current study proved MSA to be a technically viable alternative for the stimulation of high-temperature carbonate (limestone and dolomite) formations. Some of the advantages MSA has over conventional stimulation systems are: high acidity, high solubility of its salts, high thermal stability, readily biodegradable composition, and favorable corrosion profile on metals such as high chromium alloys.
2. The coreflood experiments performed with both limestone and dolomite cores resulted in deeper acid penetration (improved acid efficiency) when high MSA concentrations were used. Also, the employed acid concentration showed not to be limited by precipitation reactions (methanesulfonate salt precipitation). Consequently, strong solutions of MSA are recommended over diluted MSA solutions.

3. Because of the increased reactivity of MSA in limestone and dolomite with increasing reaction temperature, higher temperature reservoirs will require higher injection rates to stay at optimum. Moreover, since at rates higher than optimum the volume of acid required to penetrate a given distance does not generally change rapidly, the acid stimulation of deep (high-temperature) carbonate formations using MSA should be performed at the highest possible rate (or at a rate above the optimum).
4. Among all the factors studied, carbonate rock mineralogy appears to have the biggest influence on the MSA acid efficiency. However, as a result of the effect of temperature on the dolomite reaction rate the coreflood results for dolomite at 250°F tend to be similar to the ones obtained with Indiana limestone.
5. In order to have a more complete understanding of the potential use of MSA in carbonate acidizing, the current coreflood study should be complemented with a detailed examination of the different parameters affecting the kinetics of the reaction between MSA and limestone / dolomite. This type of study generally requires the use of a rotating disk apparatus to simulate dynamic reaction conditions.
6. Being both strong acids, MSA has a common limitation with HCl regarding a very high reaction rate with carbonate rocks, which may limit acid penetration especially at high-temperature conditions. A study of

chemical mechanisms to reduce MSA reactivity with carbonate materials is recommended (i.e., the use of special surfactants as acid retarders).

7. It has been experimentally proven that combining MSA with other acids can enhance product performance. For example, the synergy of MSA with phosphoric acid and complexing agents such as MGDA (methylglycin diacetic acid) in rust removal applications has been successfully tested. Therefore, in order to make cost-effective stimulation treatments with MSA, it is proposed to study the acidizing of carbonate rocks by a mixture of MSA and HCl.
8. The use of MSA in the oilfield is not limited to the matrix acidizing of carbonate formations, the topic of the present study, but it also includes application of MSA in scale removal (i.e., calcium carbonate, gypsum, and iron sulfide) in oil/gas and geothermal water wells. A more detailed study of this applications is recommended.

REFERENCES

Ahr, W.M. 2008. *Geology of Carbonate Reservoirs: The Identification, Description and Characterization of Hydrocarbon Reservoirs in Carbonate Rocks*. Hoboken, NJ: John Wiley & Sons, 296 pp.

Al-Katheeri, M.I., Nasr-El-Din, H.A., Taylor, K.C. et al. 2002. Determination and Fate of Formic Acid in High Temperature Acid Stimulation Fluids. Presented at the International Symposium and Exhibition on Formation Damage Control, held in Lafayette, Louisiana, 20-21 February. SPE-73749-MS. http://dx.doi.org/10.2118/73749-MS.

Alkhaldi, M.H., Nasr-El-Din, H.A., Sarma, H.K. 2009. Application of Citric Acid in Acid Stimulation Treatments. Presented at the Canadian International Petroleum Conference, held in Calgary, Alberta, 16 - 18 June. PETSOC-2009-015. http://dx.doi.org/10.2118/2009-015.

Anderson, M.S. 1991. Reactivity of San Andres Dolomite. *SPE Prod Eng* **6** (2): 227-232. SPE-20115-PA http://dx.doi.org/10.2118/20115-PA.

Bartko, K.M., Nasr-El-Din, H.A., Rahim, Z. et al. 2003. Acid Fracturing of a Gas Carbonate Reservoir: The Impact of Acid Type and Lithology on Fracture Half Length and Width. Presented at the SPE Annual Technical Conference and Exhibition, held in Denver, Colorado, 5-8 Oct. 2003. SPE-84130-MS. http://dx.doi.org/10.2118/84130-MS.

Bazin, B. 2001. From Matrix Acidizing to Acid Fracturing: A Laboratory Evaluation of Acid/Rock Interactions. *SPE Prod & Oper* **16** (1): 22-29. SPE-66566-PA. http://dx.doi.org/10.2118/66566-PA.

Bazin, B., Bieber, M.T., Roque, C. et al. 1996. Improvement in the Characterization of the Acid Wormholing by “In Situ” X-Ray CT Visualizations. Presented at the SPE International Symposium on Formation Damage Control, held in Lafayette, Louisiana, Feb. 14 - 15, 1996. SPE-31073-MS. http://dx.doi.org/10.2118/31073-MS.

Bazin, B., Roque, C., Chauveteau, G. et al. 1997. Acid Filtration in Dynamic Conditions to Mimic Fluid Loss in Acid Fracturing. Presented at the SPE European Formation Damage Conference, held in The Hague, The Netherlands, 2-3 June 1997. SPE-38168-MS. http://dx.doi.org/10.2118/38168-MS.

Bertkau, W. and Steidl, N. 2012. Alkanesulfonic Acid Microcapsules and Use Thereof in Deep Wells, US 2012/0222863 A1, Sep. 6, 2012. United States.

Buijse, M.A. 1997. Understanding Wormholing Mechanisms Can Improve Acid Treatments in Carbonate Formations. Presented at the SPE European Formation Damage Conference, held in The Hague, Netherlands, 2-3 June 1997. SPE-38166. http://dx.doi.org/10.2118/38166-ms.

Buijse, M., Boer, P.D., Breukel, B. et al. 2004. Organic Acids in Carbonate Acidizing. *SPE Prod & Oper* **19** (3): 128-134. SPE-82211-PA. http://dx.doi.org/10.2118/82211-PA.

Buijse, M.A. and Glasbergen, G. 2005. A Semiempirical Model to Calculate Wormhole Growth in Carbonate Acidizing. Presented at the SPE Annual Technical Conference and Exhibition, held in Dallas, Texas, 9-12 October. SPE-96892-MS. http://dx.doi.org/10.2118/96892-MS.

Chang, F.F., Nasr-El-Din, H.A., Lindvig, T. et al. 2008. Matrix Acidizing of Carbonate Reservoirs Using Organic Acids and Mixture of HCl and Organic Acids. Presented at the SPE Annual Technical Conference and Exhibition, held in Denver, Colorado, 21-24 September. SPE-116601-MS. http://dx.doi.org/10.2118/116601-MS.

Chatelain, J.C., Silberberg, I.H., Schechter, R.S. 1976. Thermodynamic Limitations in Organic-Acid/Carbonate Systems. *SPE J.* **16** (4): 189-195. SPE-5647-PA. http://dx.doi.org/10.2118/5647-PA.

Chen Y, Fambrough J, Bartko K, Li Y, Montgomery C, Ortoleva P. 1997. Reaction-Transport simulation of matrix acidizing and optimal acidizing strategies. SPE 37282. SPE International Symposium on Oilfield Chemistry, pp. 679-682.. Houston, Texas. http://dx.doi.org/10.2118/37282-MS.

Coles, M., Muegge, E., Auzerais, F. et al. 1995. The Use of Attenuation Standards for Ct Scanning. *SCA1995-13*.

Covington, A. and Thompson, R. 1974. Ionization of Moderately Strong Acids in Aqueous Solution. Part III. Methane, Ethane, and Propanesulfonic Acids at 25°C. *Journal of Solution Chemistry* **3** (8): 603-617. http://dx.doi.org/10.1007/BF00650404.

Crowe, C.W. 1985. Evaluation of Agents for Preventing Precipitation of Ferric Hydroxide from Spent Treating Acid. *J Pet Technol* **37** (4): 691-695. 00012497. http://dx.doi.org/10.2118/12497-PA.

Daccord, G. and Lenormand, R. 1987. Fractal Patterns from Chemical Dissolution. *Nature* **325** (6099): 41-43. http://dx.doi.org/10.1038/325041a0.

Daccord, G., Lenormand, R., and Liétard, O. 1993. Chemical Dissolution of a Porous Medium by a Reactive Fluid—I. Model for the "Wormholing" Phenomenon. *Chemical Engineering Science* **48** (1): 169-178. http://dx.doi.org/10.1016/0009-2509(93)80293-Y.

Daccord, G., Liétard, O., and Lenormand, R. 1993. Chemical Dissolution of a Porous Medium by a Reactive Fluid—II. Convection Vs Reaction, Behavior Diagram. *Chemical Engineering Science* **48** (1): 179-186. http://dx.doi.org/10.1016/0009-2509(93)80294-Z.

Daccord, G., Touboul, E., Lenormand, R. 1989. Carbonate Acidizing: Toward a Quantitative Model of the Wormholing Phenomenon. *SPE Prod Eng* **4** (1): 63-68. SPE-16887-PA. http://dx.doi.org/10.2118/16887-PA.

Davis, L.A., Moss, R.M., and Pepin, G.P. 1992. Direct Measurement of the Constituent Porosities in a Dual-Porosity Matrix. *The Log Analyst* **33** (02).

De Oliveira, T.J.L., De Melo, A.R., Oliveira, J.A.A., et al. 2012. Numerical Simulation of the Acidizing Process and PVBT Extraction Methodology Including Porosity/Permeability and Mineralogy Heterogeneity. Presented at the SPE International Symposium and Exhibition on Formation Damage Control, Lafayette, Louisiana, USA, 15-17 February 2012. SPE-151823-MS. http://dx.doi.org/10.2118/151823-ms.

Deutsch, C.V., Journel, A.G. 1998. GSLIB Geostatistical Software Library and User's Guide. Oxford University Press, New York.

Finšgar, M. and Milošev, I. 2010. Corrosion Behaviour of Stainless Steels in Aqueous Solutions of Methanesulfonic Acid. *Corrosion Science* **52** (7): 2430-2438. http://dx.doi.org/http://dx.doi.org/10.1016/j.corsci.2010.04.001.

Finšgar, M. and Jackson, J. 2014. Methanesulfonic acid (MSA) as an Acid used in the Well Stimulation Procedure, Corrosion Behaviour. Presented at the European Corrosion Congress, held in Pisa, Italy, 8-12 September.

Fredd, C.N. 2000a. Advances in Understanding and Predicting Wormhole Formation. In *Reservoir Stimulation*, ed. Economides, M.J. and Nolte, K.G., Chap. 16A, 1-18, third edition. Chichester, England: Wiley.

Fredd, C.N. 2000b. Dynamic Model of Wormhole Formation Demonstrates Conditions for Effective Skin Reduction During Carbonate Matrix Acidizing. Presented at the SPE Permian Basin Oil and Gas Recovery Conference, held in Midland, Texas, 21-23 March 2000. SPE-59537-MS. http://dx.doi.org/10.2118/59537-ms.

Fredd, C.N. 1997. The Influence of Transport and Reaction of Wormhole Formation in Carbonate Porous Media: A Study of Alternative Stimulation Fluids. PhD dissertation, University of Michigan, Ann Arbor, Michigan (1997).

Fredd, C.N. and Fogler, H.S. 1998a. Alternative Stimulation Fluids and Their Impact on Carbonate Acidizing. *SPE J.* **3** (1): 34-41. SPE-31074-PA. http://dx.doi.org/10.2118/31074-PA.

Fredd, C.N. and Fogler, H.S. 1998b. The Influence of Transport and Reaction on Wormhole Formation in Porous Media. *AIChE J.* **44** (9): 1933-1949. http://dx.doi.org/10.1002/aic.690440902.

Fredd, C.N. and Fogler, H.S. 1999. Optimum Conditions for Wormhole Formation in Carbonate Porous Media: Influence of Transport and Reaction. *SPE J.* **4** (3): 196-205. SPE-56995-PA. http://dx.doi.org/10.2118/56995-PA.

Fredd, C.N. and Miller, M.J. 2000. Validation of Carbonate Matrix Stimulation Models. Presented at the SPE International Symposium on Formation Damage Control, held in Lafayette, Louisiana, 23-24 February 2000. SPE-58713. http://dx.doi.org/10.2118/58713-ms.

Fredd, C.N., Tjia, R., and Fogler, H.S. 1997. The Existence of an Optimum Damkohler Number for Matrix Stimulation of Carbonate Formations. Presented at the SPE European Formation Damage Conference held in The Hague, The Netherlands, 2-3 June 1997. SPE-38167-MS. http://dx.doi.org/10.2118/38167-MS.

Frick, Thomas P., Michael Kurmayr, and Michael J. Economides.1994. An Improved Modeling Of Fractal Patterns In Matrix Acidizing And Their Impact On Well Performance. *SPE Prod & Fac* **9** (01) (1994): 61-68. SPE-23789-PA. http://dx.doi.org/10.2118/23789-PA.

Fu, D. 2010. Self-Diverting Pre-Flush Acid for Sandstone, US 7,666,821 B2, Feb. 23, 2010. United States: Schlumberger Technology Corporation.

Fuller, M.J. 2010. Method for Treating a Subterranean Formation, US 7,753,123 B2, July 13. United States: Schlumberger Technology Corporation.

Furui, K., Burton, R.C., Burkhead, D.W. et al. 2012a. A Comprehensive Model of High-Rate Matrix-Acid Stimulation for Long Horizontal Wells in Carbonate Reservoirs: Part I--Scaling up Core-Level Acid Wormholing to Field Treatments. *SPE J.* **17** (1): 271-279. SPE-134265-PA. http://dx.doi.org/10.2118/134265-PA.

Furui, K., Burton, R.C., Burkhead, D.W. et al. 2012b. A Comprehensive Model of High-Rate Matrix-Acid Stimulation for Long Horizontal Wells in Carbonate Reservoirs: Part II - Wellbore/Reservoir Coupled-Flow Modeling and Field Application. *SPE J.* **17** (1): 280-291. SPE-155497-PA. http://dx.doi.org/10.2118/155497-PA.

Gautelier, M., Oelkers, E.H., and Schott, J. 1999. An Experimental Study of Dolomite Dissolution Rates as a Function of pH from −0.5 to 5 and Temperature from 25 to 80°C. *Chemical Geology* **157** (1–2): 13-26. http://dx.doi.org/10.1016/S0009-2541(98)00193-4.

Gdanski, R. 1999. A Fundamentally New Model of Acid Wormholing in Carbonates. Presented at the SPE European Formation Damage Conference, held in The Hague, The Netherlands, 31 May - 1 June 1999. SPE-54719-MS. http://dx.doi.org/10.2118/54719-ms.

Gernon, M.D., Wu, M., Buszta, T. et al. 1999. Environmental Benefits of Methanesulfonic Acid. Comparative Properties and Advantages. *Green Chemistry* **1** (3): 127-140. http://dx.doi.org/10.1039/A900157C.

Glasbergen, G., van Batenburg, D.W., Van Domelen, M.S. et al. 2005. Field Validation of Acidizing Wormhole Models. Presented at the held in 2005/1/1/. http://dx.doi.org/10.2118/94695-MS.

Golfier F, Zarcone C, Bazin B, Lenormand R, Lasseux D, Quintard M. 2002. On the ability of a Darcy-scale model to capture wormhole formation during the dissolution of a porous medium. *J Fluid Mech.* **457** (2002): 213-254. http://dx.doi.org/10.1017/S0022112002007735.

Gong, M. and El-Rabaa, A.M. 1999. Quantitative Model of Wormholing Process in Carbonate Acidizing. Presented at the SPE Mid-Continent Operations Symposium, held in Oklahoma City, OK, 28-31 March 1999. SPE-52165-MS. http://dx.doi.org/10.2118/52165-MS.

Guthrie, J.P. 1978. Hydrolysis of Esters of Oxy Acids: PKa Values for Strong Acids; Brønsted Relationship for Attack of Water at Methyl; Free Energies of Hydrolysis of Esters of Oxy Acids; and a Linear Relationship between Free Energy of Hydrolysis and PKa Holding over a Range of 20 PK Units. *Canadian Journal of Chemistry* **56** (17): 2342-2354. http://dx.doi.org/10.1139/v78-385.

Ham, W.E. and Pray, L.C. 1962. Modern Concepts and Classifications of Carbonate Rocks. In *Classification of Carbonate Rocks*, Memoir No. 1, 2-19. Tulsa, OK: AAPG.

Harp, L.J., Carver, J., and Matson, B.G. 1968. Controlled Stimulation of Deep, Hot Wells with Binary and Trinary HCl-Organic Acid Blends. Presented at the API Prod. Div. Mid-Cont. Dist. Spring Mtg.; (United States), 851(CONF-680483-), held in April 1968. API-68-006.

Hauthal, H.G. 2007. Second European Detergents Conference Report. *Tenside Surfactants Detergents* **44** (1): 45-61. http://dx.doi.org/10.3139/113.100327.

Heidenfelder, T., Guzmann, M., Witteler, H. et al. 2009. Methods of Increasing Permeability in Carbonatic Rock Formations with Alkanesulfonic Acids, US 7,638,469 B2, December 29. United States.

Herman, J.S. and White, W.B. 1985. Dissolution Kinetics of Dolomite: Effects of Lithology and Fluid Flow Velocity. *Geochimica et Cosmochimica Acta* **49** (10): 2017-2026. http://dx.doi.org/10.1016/0016-7037(85)90060-2.

Hill, A.D., Ehlig-Economides, C., Zhu, D. et al. 2012. Carbonate Acidizing Design. In *Petroleum Production Systems*, Chap. 16, 438-467, second edition. Upper Saddle River, NJ : Prentice Hall.

Hill, A.D. and Schechter, R.S. 2000. Fundamentals of Acid Stimulation. In *Reservoir Stimulation*, ed. Economides, M.J. and Nolte, K.G., Chap. 16, 1-28, third edition. Chichester, England: Wiley.

Hoefner, M. and Fogler, H.S. 1988. Pore Evolution and Channel Formation during Flow and Reaction in Porous Media. *AIChE J* 34 (1): 45-54. http://dx.doi.org/10.1002/aic.690340107.

Hoefner, M.L. and Fogler, H.S. 1989. Fluid-Velocity and Reaction-Rate Effects During Carbonate Acidizing: Application of Network Model. *SPE Prod Eng* **4** (1): 56-62. SPE-15573-PA. http://dx.doi.org/10.2118/15573-PA.

Huang, T., A.D. Hill, and Schechter, R.S. 1997. Reaction Rate and Fluid Loss: The Keys to Wormhole Initiation and Propagation in Carbonate Acidizing. Paper SPE 37312 presented at the International Symposium on Oilfield Chemistry, Houston, TX, 18-21 February. http://dx.doi.org/10.2118/37312-MS

Huang, T., Ostensen, L., Hill, A.D. 2000. Carbonate Matrix Acidizing with Acetic Acid. Paper SPE 58715 presented at the SPE International Symposium on Formation Damage Control, held in Lafayette, Louisiana, 23-24 February. http://dx.doi.org/10.2118/58715-MS.

Hung, K.M., Hill, A.D., Sepehrnoori, K. 1989. A Mechanistic Model of Wormhole Growth in Carbonate Matrix Acidizing and Acid Fracturing. *J Pet Technol* **41** (1): 59-66. SPE-16886-PA. http://dx.doi.org/10.2118/16886-PA.

Kalia, N. and Balakotaiah, V. 2007. Modeling and Analysis of Wormhole Formation in Reactive Dissolution of Carbonate Rocks. *Chemical Engineering Science* **62** (4): 919-928. http://dx.doi.org/10.1016/j.ces.2006.10.021.

Kalia, N. and Balakotaiah, V. 2009. Effect of Medium Heterogeneities on Reactive Dissolution of Carbonates. *Chemical Engineering Science* **64** (2009): 376-390. http://dx.doi.org/10.1016/j.ces.2008.10.026.

Kasza, P., Dziadkiewicz, M., and Czupski, M. 2006. From Laboratory Research to Successful Practice: A Case Study of Carbonate Formation Emulsified Acid Treatments. Presented at the International Symposium and Exhibition on Formation Damage Control, held in Lafayette, Louisiana, 15-17 Feb. 2006. SPE-98261-MS. http://dx.doi.org/10.2118/98261-ms.

King, J.F. 1991. Acidity. In *The Chemistry of Sulphonic Acids, Esters, and Their Derivatives*, ed. Patai, S. and Rappoport, Z., Chap. 6, 249-260. Chichester, England: The Chemistry of Functional Groups, John Wiley & Sons.

Laws, M.S., Al-Riyami, A.M., Soek, H. et al. 2005. Optimisation of Stimulation Techniques for Hp, Deep Wells in the Harweel Cluster, Oman. Presented at the SPE Middle East Oil and Gas Show and Conference, held in Kingdom of Bahrain, March 12 -15, 2005. SPE-93494-MS. http://dx.doi.org/10.2118/93494-MS.

Liu, X., Ormond, A., Bartko, K., Ying, L., & Ortoleva, P. 1997. A geochemical reaction-transport simulator for matrix acidizing analysis and design. *Journal of Petroleum Science and Engineering*, **17** (1), 181-196. http://dx.doi.org/10.1016/S0920-4105(96)00064-2.

Lucia, F.J. and Major, R.P. 1994. Porosity Evolution through Hypersaline Reflux Dolomitization. In *Dolomites, A Volume in Honor of Dolomieu*, ed, Purser B. H., Tucker M. E., and Zenger D. H., International Associational Sedimentologists Special Publication No. 21, 325-341. Oxford, UK: Blackwell Publishing Ltd. doi: 10.1002/9781444304077.ch18.

Lund, K., Fogler, H.S., and McCune, C.C. 1973. Acidization—I. The Dissolution of Dolomite in Hydrochloric Acid. *Chemical Engineering Science* **28** (3): 691-IN691. http://dx.doi.org/10.1016/0009-2509(77)80003-1.

Maheshwari, P. and Balakotaiah, V. 2013. Comparison of Carbonate HCl Acidizing Experiments with 3D Simulations. *SPE Prod & Oper* **28** (4): 402-413. SPE-164517-PA. http://dx.doi.org/10.2118/164517-PA.

Nasr-El-Din, H.A., Al-Dirweesh, S., and Samuel, M.M. 2008. Development and Field Application of a New, Highly Stable Emulsified Acid. Presented at the SPE Annual Technical Conference and Exhibition, held in Denver, Colorado, 21-24 Sept. 2008. SPE-115926-MS. http://dx.doi.org/10.2118/115926-MS.

Nasr-El-Din, H.A., Al-Humaidan, A.Y., Fadhel, B.A. et al. 2002. Investigation of Sulfide Scavengers in Well-Acidizing Fluids. *SPE Prod & Oper* **17** (4): 229-235. SPE-80289-PA. http://dx.doi.org/10.2118/80289-PA.

Nasr-El-Din, H.A., Al-Mutairi, S.H., Al-Jari, M. et al. 2002. Stimulation of a Deep Sour Gas Reservoir Using Gelled Acid. Presented at the SPE Gas Technology Symposium, held in Calgary, Alberta, Canada, 30 April - 2 May 2002. SPE-75501-MS. http://dx.doi.org/10.2118/75501-MS.

Nasr-El-Din, H.A., Driweesh, S.M., Muntasheri, G.A. 2003. Field Application of HCl-Formic Acid System to Acid Fracture Deep Gas Wells Completed with Super Cr-13 Tubing in Saudi Arabia. Presented at the SPE International Improved Oil Recovery Conference in Asia Pacific, held in Kuala Lumpur, Malaysia, 20-21 October. SPE-84925-MS. http://dx.doi.org/10.2118/84925-MS.

Nasr-El-Din, H.A., Lynn, J.D., Taylor, K.C. 2001. Lab Testing and Field Application of a Large-Scale Acetic Acid-Based Treatment in a Newly Developed Carbonate Reservoir. Presented at the SPE International Symposium on Oilfield Chemistry, held in Houston, Texas, 13-16 February. SPE-65036-MS. http://dx.doi.org/10.2118/65036-MS.

Nasr-El-Din, H., Sayed, M., Aften, C. et al. 2013. A New Organic Acid to Stimulate Deep Wells in Carbonate Reservoirs. Presented at the 2013 SPE International Symposium on Oilfield Chemistry, held in The Woodlands, TX, USA, 8 - 10 April. SPE-164110-MS. http://dx.doi.org/10.2118/164110-MS.

Nasr-El-Din, H.A., Solares, J.R., Al-Mutairi, S.H. et al. 2001. Field Application of Emulsified Acid-Based System to Stimulate Deep, Sour Gas Reservoirs in Saudi Arabia. Presented at the SPE Annual Technical Conference and Exhibition, held in New Orleans, Louisiana, 30 Sept.-3 Oct. 2001. SPE-71693-MS. http://dx.doi.org/10.2118/71693-ms.

Navarrete, R.C., Holms, B.A., McConnell, S.B. et al. 2000. Laboratory, Theoretical, and Field Studies of Emulsified Acid Treatments in High-Temperature Carbonate Formations. *SPEPF* **15** (2): 96-106. SPE-63012-PA http://dx.doi.org/10.2118/63012-PA.

Nevans, J.W., Blasingame, T., Doublet, L. et al. 1999. Application of Integrated Reservoir Management and Reservoir Characterization to Optimize Infill Drillings. Annual Technical Progress Report, June 13, 1996 to June 12, 1998.

Ortega, A., Nasr-El-Din, H.A., and Rimassa, S. 2014. Acidizing High Temperature Carbonate Reservoirs Using Methanesulfonic Acid: A Coreflood Study. Presented at the AADE Fluids Technical Conference and Exhibition, held in Houston, Texas, 15-16 April 2014. AADE-14-FTCE-3.

Panga, M.K.R., Balakotaiah, V., and Ziauddin, M. 2002. Modeling, Simulation and Comparison of Models for Wormhole Formation During Matrix Stimulation of Carbonates. Presented at the SPE Annual Technical Conference and Exhibition, held in San Antonio, Texas, 29 Sept. - 2 Oct. 2002. SPE-77369. http://dx.doi.org/10.2118/77369-ms.

Panga, M. K., Ziauddin, M., & Balakotaiah, V. 2005. Two-scale continuum model for simulation of wormholes in carbonate acidization. *AIChE J.*, **51** (12), 3231-http://dx.doi.org/10.1002/aic.10574.

Pichler, T., Frick, T.P., Economides, M.J. et al. 1992. Stochastic Modeling of Wormhole Growth in Carbonate Acidizing with Biased Randomness. Presented at the European Petroleum Conference, held in Cannes, France, 16-18 November. SPE-25004-MS. http://dx.doi.org/10.2118/25004-MS.

Pomès, V., Bazin, B., Golfier, F., Zarcone, C., Leonormand, R. and Quintard, M. 2001. On the Use of Upscaling Methods to Describe Acid Injection in Carbonates. Presented at the 2001 Annual Technical Conference and Exhibition held in New Orleans, Louisiana, 30 Sept. - 3 Oct. 2001. SPE-71551. http://dx.doi.org/10.2118/71511-ms.

Reeder, R.J. 1983. *Carbonates: Mineralogy and Chemistry*. Reviews in Mineralogy, Vol. 11. Washington: Mineralogical Society of America, 394 pp.

Robert, J.A. and Crowe, C.W. 2000. Carbonate Acidizing Design. In *Reservoir Stimulation*, ed. Economides, M.J. and Nolte, K.G., Chap. 17, 1-15, third edition. Chichester, England: Wiley.

Schechter, R.S. 1992. Design Considerations in Matrix Acidizing of Sandstones. In *Oil Well Stimulation*, Chap. 16, 469-500. Englewood Cliffs, NJ: Prentice Hall.

Tate, J.F. 1982. Aqueous Acid Solution Containing an Acrylamido Alkanesulfonic Acid Polymer, 4,332,688, Jun. 1. United States.

Taylor, K.C., Al-Ghamdi, A.H., and Nasr-El-Din, H.A. 2004a. Effect of Additives on the Acid Dissolution Rates of Calcium and Magnesium Carbonates. *SPE Prod & Oper* **19** (3): 122-127. SPE-80256-PA. http://dx.doi.org/10.2118/80256-PA.

Taylor, K.C., Al-Ghamdi, A.H., and Nasr-El-Din, H.A. 2004b. Measurement of Acid Reaction Rates of a Deep Dolomitic Gas Reservoir. *Journal of Canadian Petroleum Technology* **43** (10). PETSOC-04-10-05. http://dx.doi.org/10.2118/04-10-05.

Taylor, K.C., Nasr-El-Din, H.A., Al-Alawi, M.J. 1999. Systematic Study of Iron Control Chemicals Used During Well Stimulation. *SPE J.* **4** (1): 19-24. 00054602. http://dx.doi.org/10.2118/54602-PA.

Telfah, A.D. 2008. Transport of Protonic Charge Carriers in Methyl-Sulfonic-Acid/Water Mixtures: A Model for Lowly Hydrated Sulfonic Acid Based Ionomers. PhD dissertation, University of Stuttgart, Stuttgart, Germany.

Tully, P.S. 2000. Sulfonic Acids. In *Kirk-Othmer Encyclopedia of Chemical Technology*, first edition. John Wiley & Sons.

Van Domelen, M.S. and Jennings, J., A.R. 1995. Alternate Acid Blends for HPHT Applications. Presented at the Offshore Europe, held in Aberdeen, United Kingdom, 5-8 September. SPE-30419-MS. http://dx.doi.org/10.2118/30419-MS.

Wang, Y., Hill, A.D., Schechter, R.S. 1993. The Optimum Injection Rate for Matrix Acidizing of Carbonate Formations. Presented at the SPE Annual Technical Conference and Exhibition, held in Houston, Texas, 3-6 October. SPE-26578-MS. http://dx.doi.org/10.2118/26578-MS.

Wardlaw, N.C. 1979. Pore Systems in Carbonate Rocks and Their Influence on Hydrocarbon Recovery Efficiency. In *Geology of Carbonate Porosity*, ed. Bebout D., Davies G., Moore C. H., and Scholle P. S., 1–24. AAPG course notes 11.

Williams, B.B., Gidley, J.L., Schechter, R.S. 1979. *Acidizing Fundamentals*, Vol. 6. Richardson, Texas: Henry L. Doherty Memorial Fund of AIME, SPE Monograph Series, Society of Petroleum Engineers of AIME.

Zenger, D.H. and Mazzullo, S.J. 1982. *Dolomitization*, Vol. 65. Stroudsburg: Hutchinson Ross Publishing Company.